POROSITY, PORE-SIZE DISTRIBUTION AND PORE SURFACE AREA OF THE APACHE LEAP TUFF NEAR SUPERIOR, ARIZONA USING MERCURY POROSIMETRY

by

Gerald Thomas Vogt

A Thesis Submitted to the Faculty of the

DEPARTMENT OF HYDROLOGY AND WATER RESOURCES

In Partial Fulfillment of the Requirements
For the Degree of

MASTER OF SCIENCE
WITH A MAJOR IN HYDROLOGY

In the Graduate College

THE UNIVERSITY OF ARIZONA

1 9 8 8

STATEMENT BY AUTHOR

This thesis has been submitted in partial fulfillment of requirements for an advanced degree at The University of Arizona and is deposited in the University Library to be made available to borrowers under rules of the Library.

Brief quotations from this thesis are allowable without special permission, provided that accurate acknowledgment of source is made. Requests for permission for extended quotation from or reproduction of this manuscript in whole or in part may be granted by the head of the major department or the Dean of the Graduate College when in his or her judgment the proposed use of the material is in the interests of scholarship. In all other instances, however, permission must be obtained from the author.

SIGNED: Gerald Thomas Vogt

APPROVAL BY THESIS DIRECTOR

This thesis has been approved on the date shown below:

D. D. EVANS
Professor of Hydrology and Water Resources

May 13, 1988
Date

With love, I dedicate

this thesis to

my parents

ACKNOWLEDGMENTS

This research was performed at the University of Arizona under the guidance of Dr. Daniel D. Evans. Support for this work was obtained from the Nuclear Regulatory Commission.

I wish to express my sincere gratitude to Dr. Evans for his support of my work. I would also like to thank Dr. Don Davis and Dr. Young Kim for their advice, assistance and critique of my research.

To Todd Rasmussen and Jim Blanford, I thank you for your insight and assistance. To Larry York, who helped me with porosimetry experiments, I thank you. To Priscilla Sheets, I thank you for your drafting support. To Robert Armstrong of the Department of Mining, I thank you for the use of your laboratory equipment.

To my cohorts in room 246D, thank you for your support and patience. I am very grateful to the Department of Hydrology for its expertise and guidance throughout my graduate training.

Finally, to my family, who supported me every step of the way, I express my love and gratitude.

TABLE OF CONTENTS

TABLE OF CONTENTS--Continued.

LIST OF ILLUSTRATIONS

LIST OF ILLUSTRATIONS--continued.

LIST OF ILLUSTRATIONS--continued.

LIST OF TABLES

LIST OF TABLES--continued.

ABSTRACT

Characterization and quantification of fluid flow is dependent upon the distribution, size and interconnectedness of pores in an unsaturated rock matrix. This study examines the use of mercury porosimetry in determining porosity, pore-size distribution and pore surface area of an unsaturated, slightly welded to densely welded tuff near Superior, Arizona. 121 samples of tuff were subjected to mercury intrusion pressures to 200 MPa. A bimodal pore-size distribution exists for all samples of slightly welded tuff with the larger pore size class mode diameter averaging 2.91 μm and the lower pore size class mode diameter averaging .07 μm. Interconnected porosity, pore surface area and bulk density averaged 14.62%, 3.46 m^2/gm and 2.13 gm/cm^3, respectively. On average, 52.73% of the porosity was accounted for by the large pore size class while 96.28% of the pore surface area was accounted for by the small pore size class. Samples of densely welded tuff exhibited a unimodal pore-size distribution with an average mode diameter of .035 μm.

CHAPTER 1

INTRODUCTION

The disposal of high-level nuclear waste into unsaturated, fractured, consolidated media has recently received congressional approval. The ability of the host rock to isolate high-level waste from the accessible environment is of paramount importance. The rock matrix near the repository has the potential to direct fluid movement away from the repository to the surrounding environment. Fluid flow and transport properties of the host rock must be thoroughly assessed before repository operation is realized.

Characterization and quantification of fluid flow is dependent upon the distribution, size and interconnectedness of pores in the rock matrix. The matrix porosity indicates the fluid holding capacity of the media while the pore-size distribution relates the fluid content as a function of the matrix water potential. Unsaturated hydraulic conductivity can be estimated from these relations. Pore size and porosity also give indications of pore surface area. Specific surface area measurements aid in sorption capacity estimates of the matrix by quantifying available exchange sites.

In response to requisite research, the University of Arizona has been contracted by the Nuclear Regulatory Commission to evaluate fluid flow and transport through fractured, unsaturated tuff. Of particular importance is the characterization of slightly welded tuff, similar to that found at the Nevada Test Site. A field site near Superior, Arizona

has been set up to study slightly welded to densely welded tuff. The Apache Leap study site is contained in slightly welded to non-welded ash-flow tuff, approximately 3 km east of the town of Superior which is located 50 miles east of Phoenix.

1.1 Rock Matrix Characterization

The unsaturated hydraulic conductivity and water holding capacity are dynamic properties of the rock matrix which respond to the level of stress present from temperature, loading and fluid availability. To further estimation methods for unsaturated hydraulic conductivity and water holding capacity, effective porosity and pore-size distribution of the medium should be known. In this study, mercury porosimetry was employed for the determination of porosity, pore-size distribution and pore surface area. Mercury porosimetry relies on capillary theory and the non-wetting property of mercury to determine porosity, pore-size distribution and pore surface area by forcing mercury into matrix samples under pressure. The instrument used in this study was capable of intrusion pressures up to 200 MPa. Physical data consisting of bulk and grain density can also be realized from this technique.

Samples are enclosed in a glass bulb attached to a capillary stem known as a penetrometer (see figure 1.1). The sealed glass bulb and stem are evacuated, filled with mercury and then subjected to incremental pressure increases. The mercury responds by intruding into smaller and smaller pores of the matrix sample. Mercury volume changes in the penetrometer stem are directly related to intrusion volume and

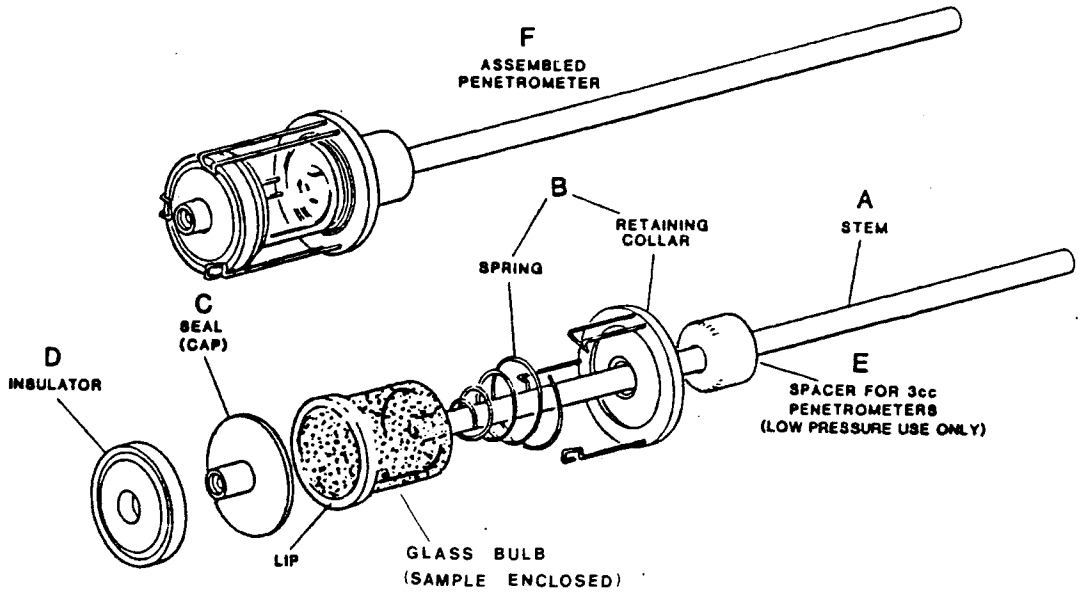

Figure 1.1. Penetrometer assembly showing glass bulb and stem.

pore size according to capillary theory. Theoretically, pore sizes down to 6 nm can be measured.

The intruded volume of mercury measures the interconnected pore spaces of the matrix sample which includes conductive and dead end pores. Pores > 6 nm in diameter were measured with the porosimeter used in this study. Effective porosity determination from the water saturation method measures all conductive and dead end pores. The difference between the measured porosity from the porosimeter and effective porosity from the saturation method is a function of the porosity percentage accounted for by pore sizes less than 6 nm in diameter in the matrix sample.

Incremental intrusion volumes are used to predict the pore-size distribution range from atmospheric pressure to 200 MPa. Pore geometries and arrangements can alter results predicted by capillary theory by restricting fluid flow into pores. The effect is to underestimate large pore sizes and overestimate small pore sizes. For this reason, mercury porosimetry does not produce true pore-size distribution curves. Pore sizes here are described by pore size classes and the mode of the diameter of the pore size class to minimize the pore geometry effects.

A typical pore-size distribution curve from the slightly welded Apache Leap tuff is shown in figure 1.2. Two pore size classes are evident from the plot of incremental pore volume versus pore diameter. The minimum incremental intrusion volume pore diameter was chosen as the cutoff between the two class sizes. The modes of each class size were chosen to describe the bimodal distribution.

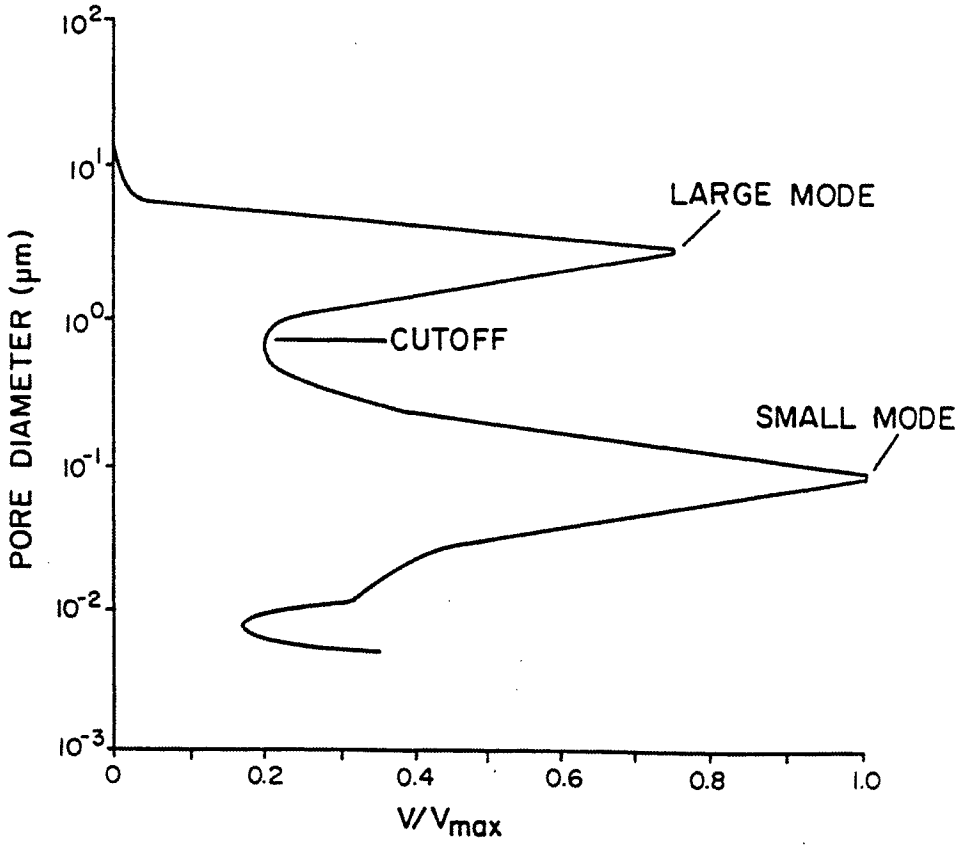

Figure 1.2. Pore-size distribution curve of slightly welded Apache Leap tuff sample. Plot is of pore diameter vs incremental intrusion. V = incremental intrusion. V_{max} = maximum incremental intrusion volume (cm^3/gm).

Porosity, pore-size distribution and pore surface area measurements were performed on 105 matrix samples obtained from 9 boreholes inclined at an angle of 45 degrees at the Apache Leap site. Sample locations were chosen at approximate 3 meter intervals along the boreholes away from visible fractures.

Geostatistical methods were used to determine the spatial variability of generated parameters along the boreholes and globally throughout the study site area.

1.2 Objectives and Scope

This paper presents the findings of the initial study of physical rock matrix properties from the Apache Leap study site. Fluid flow and transport properties of the rock matrix are also being investigated by others in the Department of Hydrology and Water Resources. The primary objective is to characterize the matrix for fluid flow. More specifically, the objectives of this study were to:

1) Determine porosity, pore-size distribution and pore surface area of the rock matrix using mercury porosimetry.

2) Determine the spatial variability of these properties along each borehole and globally throughout the study site location.

3) Compare different techniques to mercury porosimetry in the determination of bulk density and porosity of the rock matrix.

4) Correlate generated data sets by regression analysis to determine predictive capabilities of the analyzed parameters.

1.3 Other Related Work

In addition to mercury porosimetry studies of the rock matrix, research continues on related matrix and fracture characterization. According to Rasmussen and Evans (1986), bulk density and porosity of a rock sample can be determined using water saturation, gravimetric and gamma ray attenuation methods. Water saturation methods for porosity are being investigated in the laboratory and caliper measurements of rock volume, coupled with gravimetric analysis of sample weight are being used for bulk density determination.

Rahi (1986) describes the outflow method to determine unsaturated hydraulic conductivity, hydraulic diffusivity and moisture content. The outflow method produces moisture characteristic curves between .01 and .10 MPa suction. Research, in the laboratory, continues with the outflow method on matrix samples 5 cm long by 6.35 cm in diameter.

Klavetter and Peters (1987) present moisture release curves determined from thermocouple psychrometry. Research continues on 1 cm by 1 cm unsaturated rock cylinders for suctions greater than 1 MPa. Unsaturated pneumatic conductivity is being determined on the 5 cm by 6.35 cm cores mentioned above. The unsaturated pneumatic conductivity is determined using the measured air flow, cross-sectional area and core segment length in a sealed environment (Yeh et al., 1988).

Fracture orientation and characterization studies, along with methods to analyze flux and travel times in fracture-matrix systems are also being conducted. Groundwater recharge, infiltration and deep percolation are being studied at a site adjacent to the field site. Field data will be used to estimate boundary effects and fluxes over the

large-scale range of the hydrogeologic system when computer simulation models are run. Also, existing field and laboratory techniques are being scrutinized as to their applicability in the unsaturated fractured rock.

Past and present research results will be analyzed to aid in the characterization of the Apache Leap Tuff for matrix and fracture fluid flow and transport.

CHAPTER 2

GEOLOGY AND FIELD SITE

2.1 Description of Study Area

The town of Superior lies in the northeast corner of Pinal County Arizona. At an elevation of 910 meters, it is surrounded by the Superstition Mountains to the northwest and Pinal Mountains to the east. The Apache Leap is a 600 meter escarpment of ash flow tuff located just east of the city. Queen Creek and its tributaries act as a major drainage of the Apache Leap region. Queen Creek is a tributary to the Gila River which is the major drainage for central and eastern Arizona. U. S. Highway 60 is the major thoroughfare for the town of Superior. The highway passes east through Queen Creek Canyon to the top of the Apache Leap escarpment. Narrow canyons and pinnacles of weathered tuff are ubiquitous along the roadcut and representative of the region.

The Apache Leap Study Site is located on U. S. Forest Service property south of highway 60 approximately 3 kilometers east of the town of Superior (See figure 2.1). The study site was chosen as a field site investigative area for unsaturated fractured tuff. The study site area is contained in a much larger dacitic ash flow sheet extending areally for approximately 250 km^2.

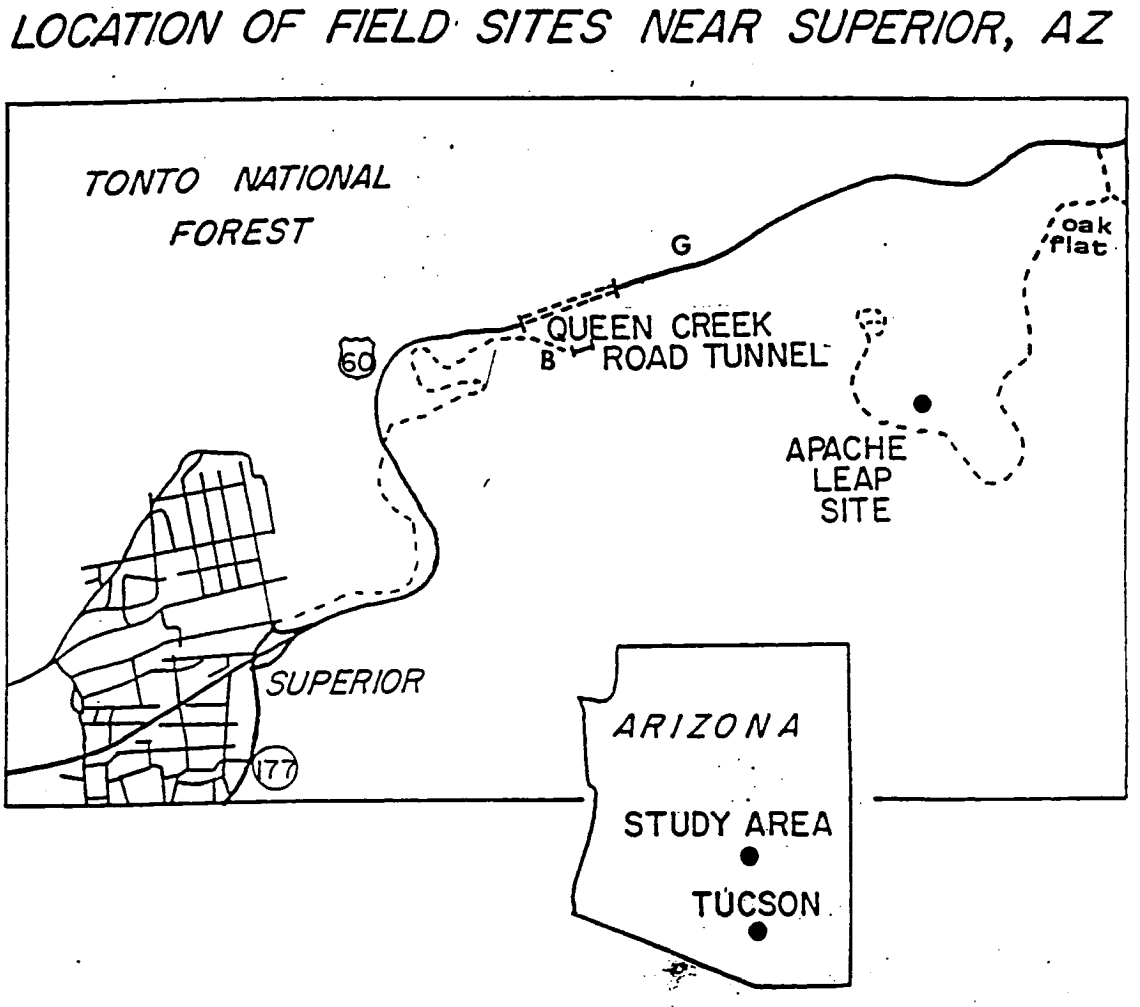

Figure 2.1. Location of field sites near Superior, Arizona. B = brown zone sampling location. G = gray zone sampling location.

The field site is located in slightly welded unsaturated, fractured tuff in the vicinity of Oak Flat. A significant amount of the upper surface of the deposit has been eroded. The average thickness near the study site is 100 m. The topography is marked by exposed bedrock surfaces forming valleys and canyons of moderate relief with little or no topsoil. The field site is a relatively flat 30 m by 50 m section of exposed tuff.

2.2 Geology

Extensive studies of the ash flow sheets near Superior have been performed by Peterson (1961, 1968). A synopsis of his work and findings is given next.

The Apache Leap tuff is composed of a number of ash flows that erupted rapidly enough in succession to form an ash flow sheet which generally cooled as a simple cooling unit. Local variability exists because of compound cooling effects. Most of the separate ash flows cannot be individually identified. Both welded and non-welded zones of tuff compose the deposit.

Based on chemical composition (described in figure 2.2), the rock is a quartz latite. Most of the literature refer to the rock as dacite because of large quartz and feldspar phenocrysts embedded in the groundmass. These phenocrysts appear to be distributed uniformly throughout the groundmass and account for 35 to 45 percent of the rock by volume. Plagioclase is the most dominant phenocryst mineral followed by quartz, biotite and sanidine. The major phenocrysts generally range

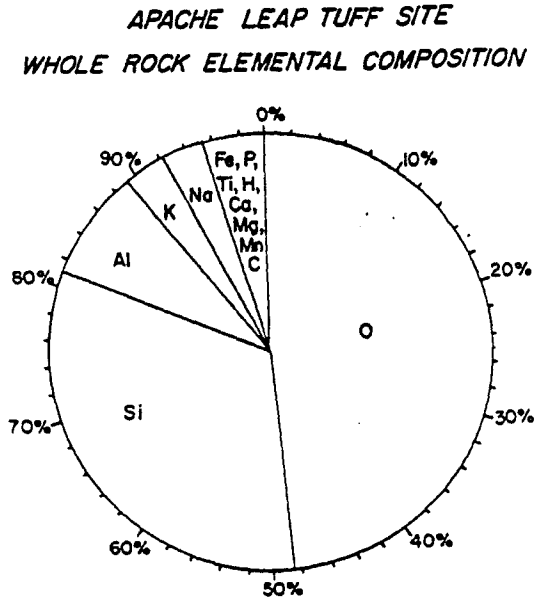

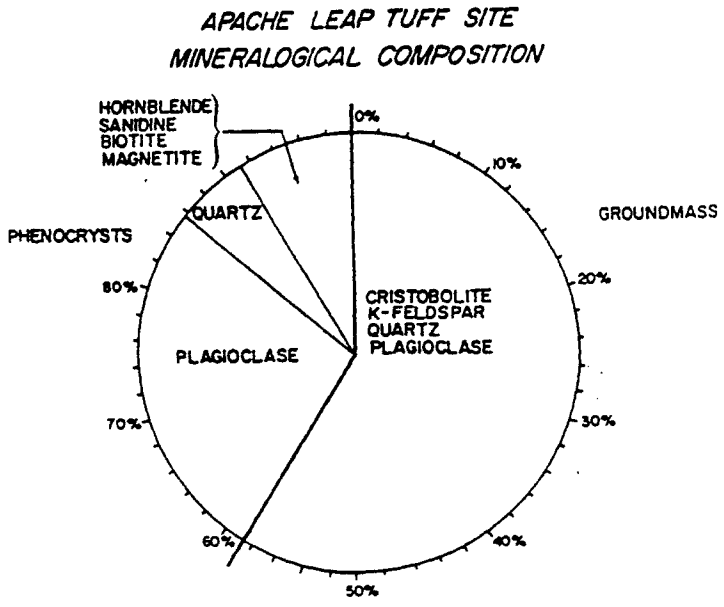

Figure 2.2. Elemental and mineralogical composition of Apache Leap Tuff (After Peterson, 1961).

in size from .5 mm to 1 mm in diameter with occasional appearance of a 3 mm size.

Pumice fragments have also been identified in local abundance in some parts of the deposit. Near the top of the deposit, they are equidimensional but become more flattened in the lower zones of the deposit. Most of the pumice inclusions carry the same phenocrysts with the same proportions as the matrix. The difference lies in the fact that unbroken phenocrysts appear in the pumice inclusions while the phenocrysts in the enclosing rock are broken.

Ash flow tuff results from the deposition, compaction and consolidation of a mobile, high-density suspension of hot glass shards, pumice and rock fragments known as nuee' ardents. A nuee' ardent is both a type of eruption and an agent of transport consisting of a basal avalanche and an overriding cloud of expanding gas and dust. The ash flow sheets originated as nuee' ardents. The magma degassed with enough explosive force to spread in all directions as a gas-charged avalanche. The ash-sized particles were carried as far as 30 kilometers by the basal avalanche.

The first material was quickly cooled on the pre-volcanic Paleozoic limestone surface and formed an insulating layer which prohibited rapid cooling of the subsequent flows. This insulating layer is described as the lower non-welded zone in figure 2.3. It promoted longer cooling and thus greater compaction and welding from the weight of the overburden. The vitrophyre represents a layer of rapid cooling and flattening, giving rise to a partly welded glass. Most of the vitrophyre is a densely welded tuff composed of black glass and the

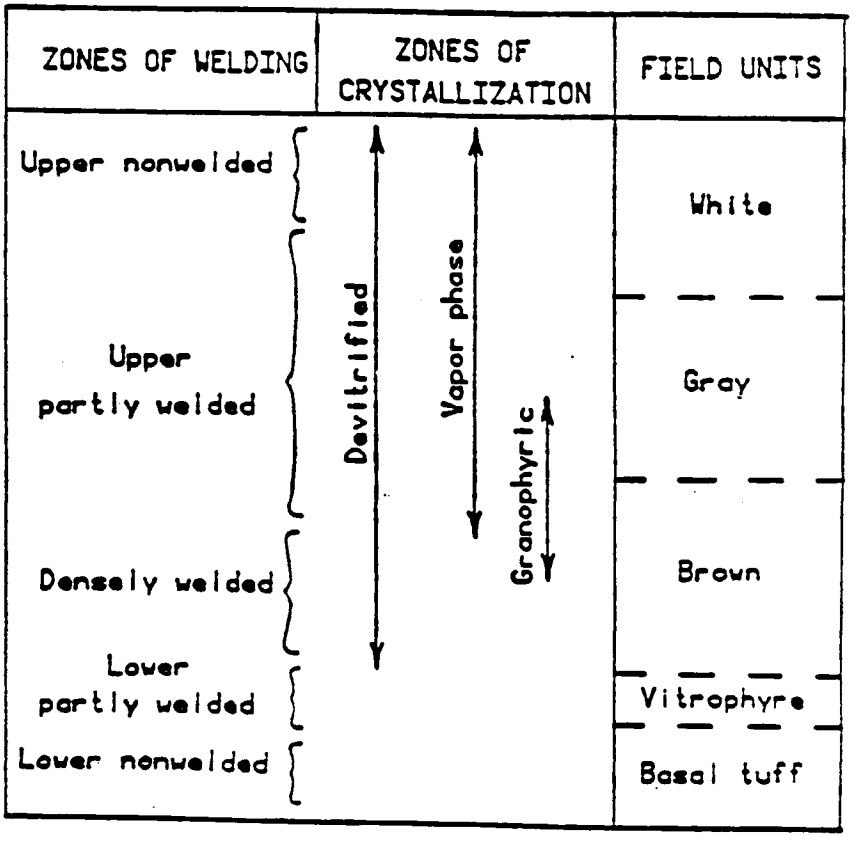

Figure 2.3. Physical characteristics of the Apache Leap Tuff (after Peterson, 1968).

normal distribution of phenocrysts. The vitrophyre ranges in thickness from 1 m to 25 meters.

The deposit shows three color zones described by the degree of welding in each layer. The brown unit cooled slower and the devitrified glass formed an aphanitic groundmass of densely welded material. The gray unit lies immediately above the densely welded brown unit and is characterized by less welding (more porosity) and more crystallization as the gases collected in the pore spaces. Near the top of the deposit, as the gases filled even more pores and the weight of the overburden decreased greatly, the particles remained undeformed and non-welded. Crystallization dominated this white unit because of the constant flow of gases up through the groundmass. The aphanatic groundmass of the white unit lacks oriented structures. Its maximum thickness is 250 meters but only averages 60 to 100 meters in most locations.

The age of the tuff deposit has been confirmed to be of Tertiary time. Dating techniques suggest a middle Miocene age, approximately 20 million years.

2.3 Borehole Description

Three sets of boreholes of varying lengths, each set in one vertical plane, are located at the study site (See figure 2.4). The X borehole set was drilled in September, 1985, while the Y and Z sets were drilled in November, 1986. All three sets were drilled at a 45 degree angle to the horizontal. Table 2.1 gives relevant information concerning the length of all boreholes. A vertical datum was established to a reference point located 14.14 m in the N37°E direction

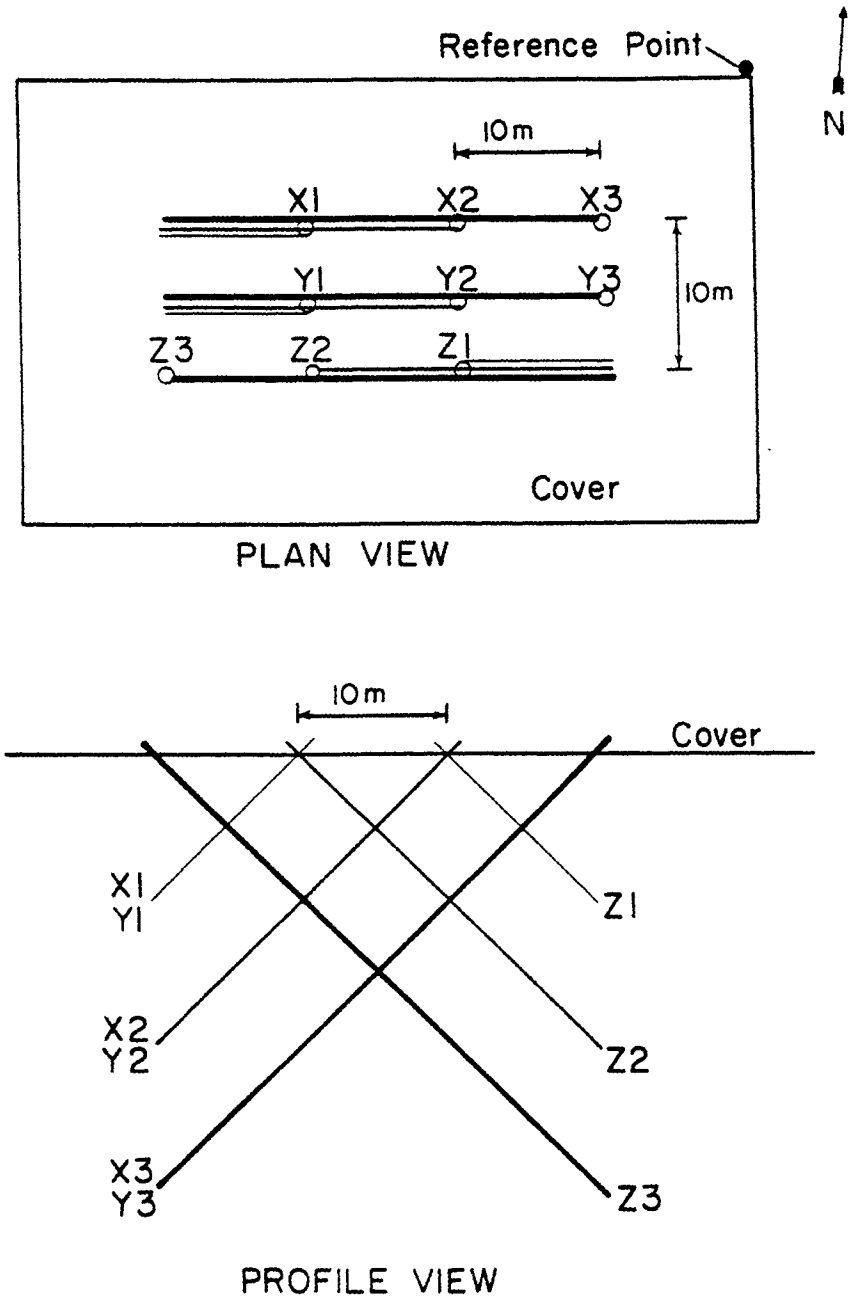

Figure 2.4. Borehole configuration at the Apache Leap study site showing inclined boreholes. Thicker lines indicate longer boreholes. All boreholes are nominally 10 cm in diameter.

from borehole X3. The borehole elevations are in reference to the lower lip of casing on borehole X1 which was given an arbitrary elevation of 100 m.

TABLE 2.1 Borehole lengths. (after Weber, 1986)

BOREHOLE	LENGTH (m)
X1	18.4
X2	32.6
X3	46.6
Y1	17.2
Y2	30.9
Y3	44.9
Z1	17.0
Z2	31.5
Z3	45.2

The X and Y sets of boreholes trend in a westerly direction with both X3 and Y3 being easternmost. The Z set trends in an easterly direction with Z3 being westernmost. The X series of boreholes are cased for 1.34 m below land surface while the Y and Z series are cased for 1.58 m below land surface to maintain the integrity of the borehole wall. The spacings are shown in figure 2.4.

Three dimensional fluid and transport monitoring is made possible by this particular borehole configuration. The drilling procedure used surface set HQ oversized diamond-core bits and a stabilizer equal to the borehole diameter to maintain straight axi-symmetric drilling. Cores with a diameter of 6.35 cm were obtained from the borehole. A scribing tool provided a mark on the core every 3.05 m. This was done to provide information on fracture location and orientation.

All core from the borehole drilling was logged. Weber (1986) gives a description of fractures and their orientation of the X set of boreholes. Fracture orientation and location data indicate steeply dipping fractures which are generally directed to the southwest and northwest. This is in good agreement with surface exposures of various surrounding outcrops near the study area.

CHAPTER 3

BACKGROUND

Mercury porosimetry is based on capillary theory governing fluid behavior. Previous studies have demonstrated its usefulness for a variety of situations. Data have been collected and analyzed relying on capillary and geostatistical theory, respectively.

3.1 Capillary Theory

The determination of the pore size distribution of porous media using mercury porosimetry is a well established practice. Ritter and Drake (1945) presented a paper fully devoted to mercury porosimetry, which forms the basis of all present studies.

Washburn (1921) mentioned the idea of forcing mercury into a porous material to obtain a pore size distribution. He drew upon the relation:

$$P = -2\,\beta(\cos\,\alpha)/\,r \qquad (3.1)$$

where P = pressure, β = surface tension, α = contact angle and r = pore radius, to determine the pressure required to force mercury into a pore of radius r. Mercury is a non-wetting liquid toward most substances with contact angle greater than 90 degrees. Therefore, it must be forced into cracks or pores by applying pressure. From equation 3.1, the required pressure is proportional to the surface tension of the mercury and the cosine of the contact angle of the mercury on the solid

pore wall. Assuming pores to be cylindrical capillaries, equation 3.1 is used for the determination of pore size with mercury porosimetry. Although this is not true in most naturally occurring porous media it has been widely accepted as the standard. Studies by Joyner et al. (1951) comparing mercury porosimetry to nitrogen desorption found good agreement between the two methods.

For all data in this study, a contact angle of 130 degrees was used for both intrusion and extrusion. A value of 485 dynes/cm was used for the surface tension of the mercury meniscus. These values were suggested by Micromeritcs Corporation (1986). A detailed description of the procedure used in this study is contained in Appendix A.

During mercury intrusion, as the pressure increases mercury is forced into smaller and smaller pores. Obviously the pores are not all interconnected and of equal radius. Figure 3.1 shows shapes of grouped pores. Because of pore heterogeneity and contact angle hysteresis, to be discussed later, mercury will not be forced into pore radii as predicted by equation 3.1. The group of pores in figure 3.1 do not act as a single capillary or bundle of capillaries but as individual "ink bottle" pores. With cylindrical constant radius pores, the governing radius remains constant for intrusion and extrusion and equation 3.1 applies. With ink bottle pores, the throat radius controls intrusion and the pore radius controls extrusion.

Given r_n, the narrow radius of a pore neck and r_w, the wide pore radius, it is seen that r_n is the governing radius during intrusion. As pressure increases mercury is forced into smaller pores. Figure 3.1.a shows a situation where this is not absolutely true. As the pressure is

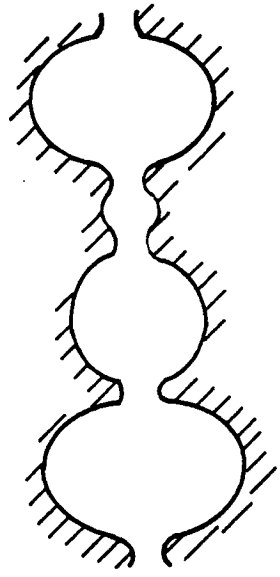

Figure 3.1. Grouped pores of varying radii.

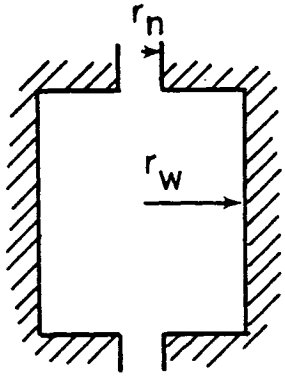

Figure 3.1.a

Pore with narrow throat radius and wide pore radius.

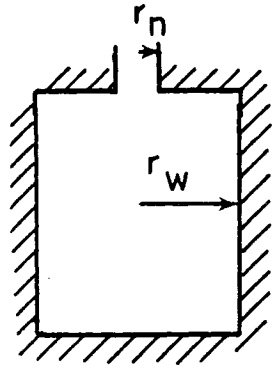

Figure 3.2.

Dead end pore with restricting throat.

increased up to some value P_n corresponding to r_n, the pore neck will be intruded with mercury. The intrusion will continue until all of the pore is flled because P_w, the pressure associated with a pore of radius r_w, has been exceeded.

The opposite occurs during extrusion. Some pressure P_{max} has been attained at the upper limit of intrusion and then the pressure is decreased to a value equal to P_n. The mercury in the pore will not leave the pore until a value of P_w is reached. If $P_n >> P_w$ and subsequently $r_w >> r_n$ then it is possible that mercury cohesive forces will be broken and a discontinuity in the mercury stream will result causing mercury to be trapped in the pore. This is termed volume hysteresis. Kloubek (1981) suggests no discontinuities will occur but that mercury will still be trapped in the pore.

Volume hysteresis may be a function of several factors including: 1)pore geometry; 2)pore roughness; 3) ink bottle effect; 4) surface tension variability; and 5) contact angle hysteresis. Contact angle hysteresis is defined as the change in angle of contact between intrusion and extrusion. Contact angle values vary according to the material being intruded. Kloubek (1981) and Good and Mikhail (1981) found values as high as 180 degrees for advancing (intruding) angles and values as low as 90 degrees for receding angles. The advancing angle is generally greater than the receding one.

Volume hysteresis can also arise due to the ink bottle effect. In the case of dead end pores as illustrated in figure 3.2, the smaller the ratio of r_n:r_w the larger the difference between intrusion and

extrusion pressures. If the ratio is low enough, according to Kloubek, mercury will remain trapped in the pore regardless of the neck size.

The initial intrusion/extrusion produces volume hysteresis. When subsequent pressure increase/decrease takes place, the curves are shaped differently (see figures 3.3 and 3.4). The newly shaped reintrusion curve defines local hysteresis. Kloubek (1981) stated that the local hysteresis was caused by mercury caps being formed on the already-filled pores. The change in volume of these caps is a function of their curvature. It is assumed that the mercury menisci do not move along the pore wall during reintrusion.

In comparing saturation/desaturation curves of water and mercury for different pore arrangements, certain similarities exist. For the simplified pore geometry of figure 3.5 when $r_n:r_w$ is sufficiently high, the behavior of water and mercury is shown in the figure. Mercury saturation is attained at some pressure P_n, while water saturation is attained at S_w, or near zero relative suction. In this ink bottle example, water will be drawn out of the pore when the threshold suction value, S_n, corresponding to r_n occurs. Theoretically, the pore will rewet upon reaching some suction value S_w.

This phenomenon is in direct comparison to the volume hysteresis mentioned earlier. The mercury intrusion curves are a better representation of water desorption than the extrusion curves. In the case of mercury intrusion, larger pores fill first under a low pressure. As the pressure is increased, smaller and smaller pores are filled with mercury until some maximum pressure is attained. The controlling radius upon intrusion is the size of the throat leading into a pore. With

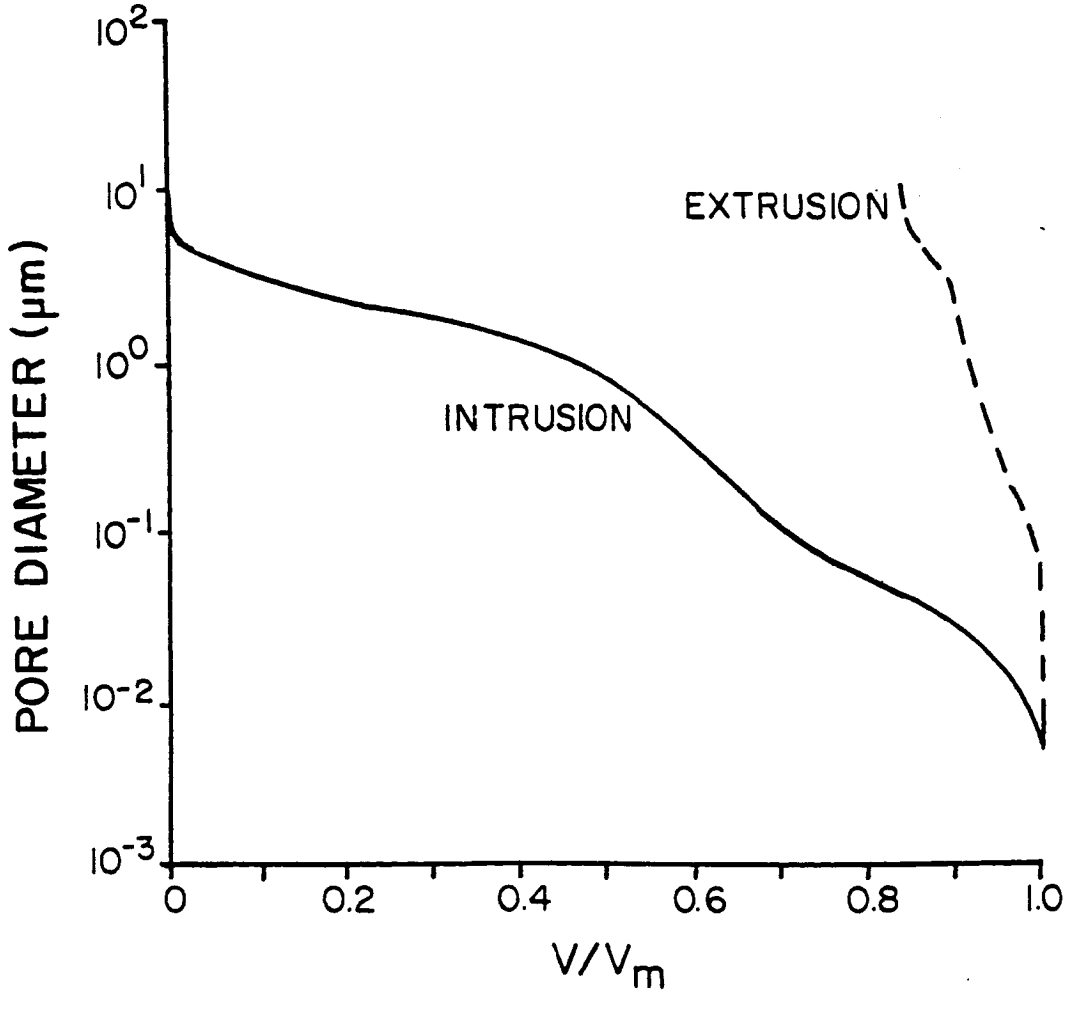

Figure 3.3. Initial intrusion/extrusion plot of pore diameter vs cummulative intruded volume of Hg (cm^3/gm). V_m = total volume intruded. V = cummulative intruded volume.

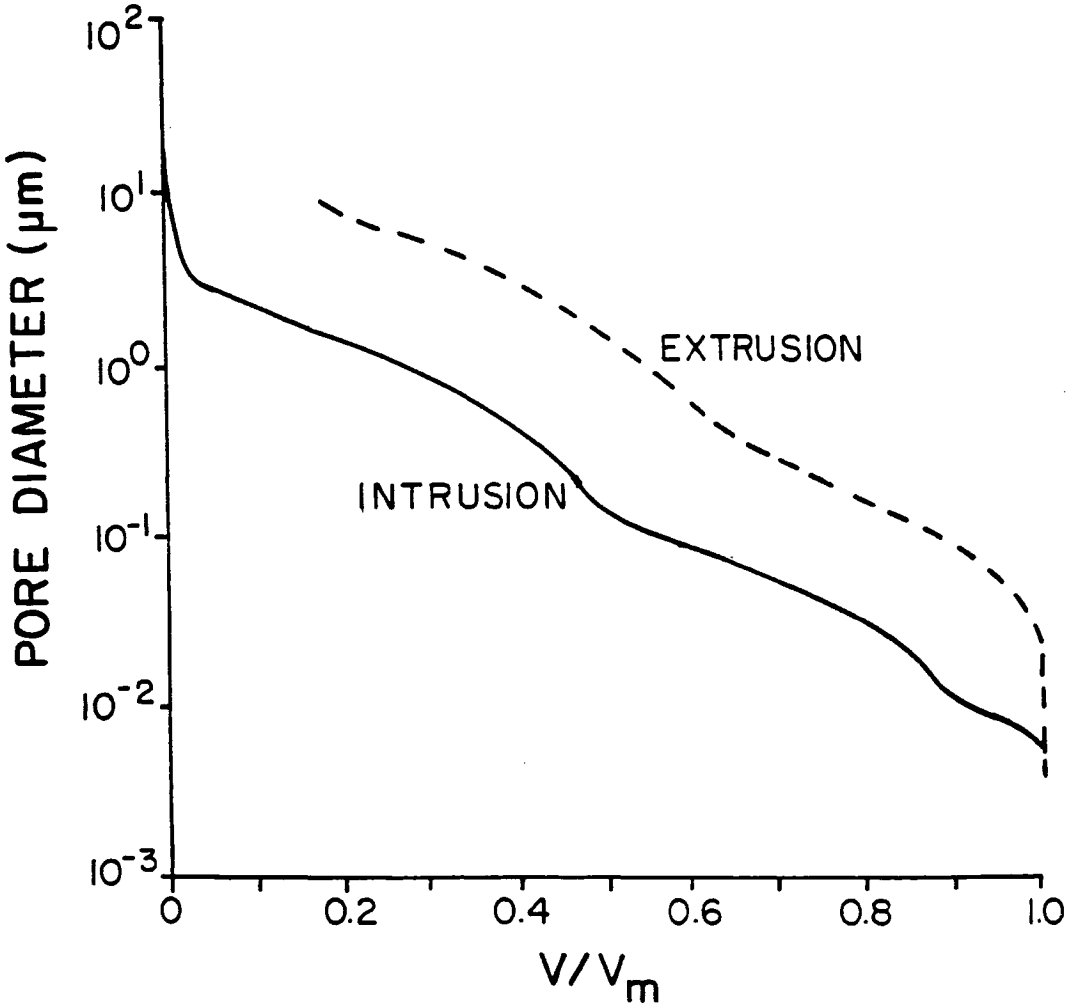

Figure 3.4. Second intrusion/extrusion plot of pore diameter vs cummulative intruded volume of Hg (cm^3/gm). V_m = total volume intruded. V = cummulative intruded volume.

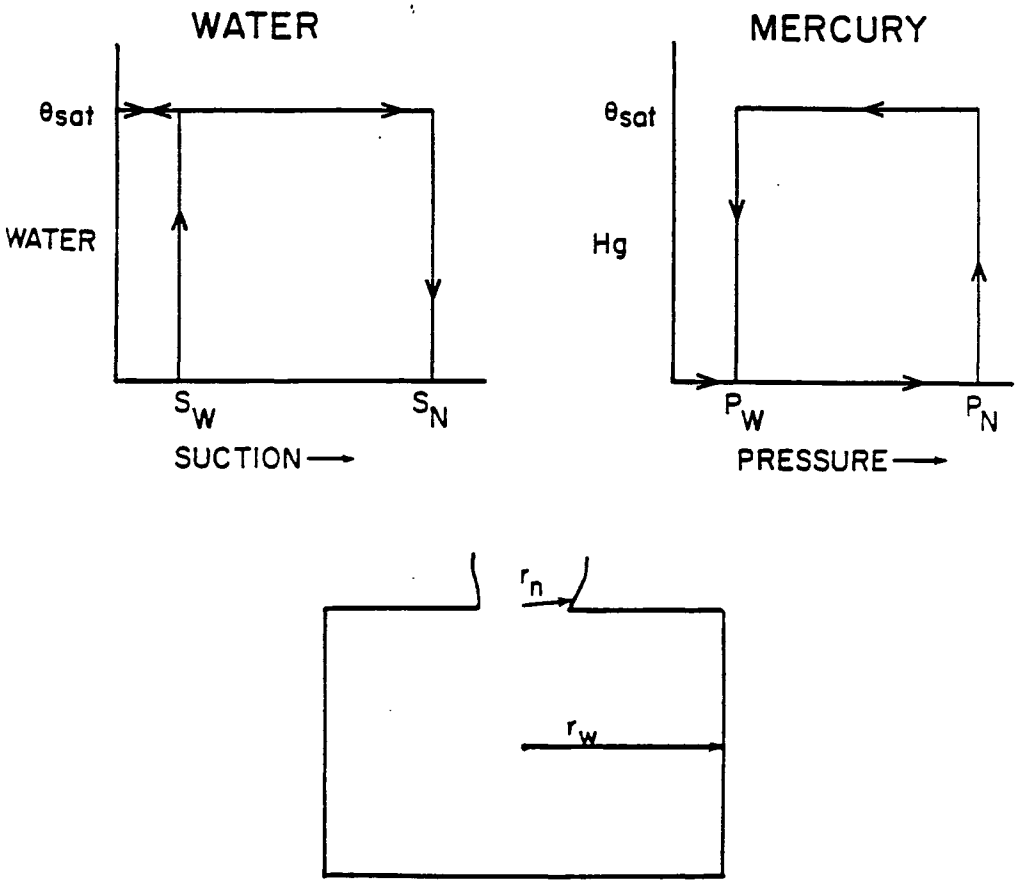

Figure 3.5. Dead end pore and theoretical behavior of water and mercury with pressure/suction increase and decrease.

water desorption, the large pores drain first under low suction or tension. As the suction increases, smaller and smaller pores are drained of water. The controlling radius in this case is again the throat size connecting pores. If a situation exists like figure 3.5, then the large pore will not drain until a suction value corresponding to the smaller throat radius is reached. For these reasons, mercury intrusion should be considered comparable to the water desaturation curves when comparing results between the two methods.

Pore surface area measurements can be obtained independently of the pore geometry assumptions by calculating the amount of work needed to force mercury into the pores. The work being defined as some maximum pressure, P, multiplied by the total change in volume ΔV. In the case of mercury intrusion on non-wetting surfaces, the work required to saturate an area Δa of pore surface is equal to (in differential form):

$$dw = \beta \cos \alpha \, da \qquad (3.2)$$

By equating work terms,

$$\beta \cos \alpha \, da = P \, dV \qquad (3.3)$$

and assuming constant β and $\cos \alpha$ and integrating yields:

$$A = -\int_{V_o}^{V_m} P \, dV \; / \; \beta \cos \alpha \qquad (3.4)$$

which reduces to

$$A = 3.262 \int_{V_o}^{V_m} P dV \qquad (3.5)$$

when β = 485 dynes/cm

$\cos \alpha$ = 130 degrees

P = average pressure in MPa over the increment V_o to V_m

A = surface area in m^2/gm

V_o = cummulative intruded pore volume at P_o in cm^3/gm

V_m = cummulative intruded pore volume at P_m in cm^3/gm

Rootare and Prenzlow (1967) found good agreement with mercury intrusion and gas adsorption techniques on materials with areas below 100 m^2/gm.

3.2 Previous Work

Since the mercury porosimetry study of Ritter and Drake (1945), mercury porosimetry has been widely used in industry. Its applications have varied from the study of pore structure and fluid distributions by Pickell et al. (1965) to a recent study by Klavetter and Peters (1987) regarding hydrologic properties of volcanic tuff.

Winslow and Lovell (1981) measured pore size distributions of a variety of construction materials including portland cement, compacted fine grained soils and shales using mercury intrusion. Whittemore (1981) used mercury porosimetry to obtain pore size distributions in ceramic processing research. Both raw materials and finished products were subjected to mercury porosimetry measurements to measure structure. Klar (1971) used porosimetry to study the changes in inter and intra particle porosity for copper powder as a function of compacting pressure.

A similar application of mercury porosimetry to this study was performed by Klavetter and Peters (1987). They compared mercury intrusion saturation curves to thermocouple psychrometer saturation curves from samples of welded and non-welded tuff. They found good agreement between the two methods for a small number of samples but

overall agreement was poor. A large variability was found in the mercury intrusion results. It should be pointed out that comparison of mercury intrusion was made with psychrometer saturation curves. Perhaps a more favorable result would have been attained if desaturation curves had been compared.

According to Klavetter and Peters (1987), the pore size distribution results using mercury intrusion of the welded and slightly welded tuffs qualitatively agreed with the results from scanning electron microscopy. They also found pore size distributions from mercury porosimetry results capable of measuring larger pore diameters more accurately than thermocouple psychrometry.

An excellent bibliography on mercury porosimetry was presented by Modry et al. (1981).

3.3 Geostatistical Theory

The geostatistics methodology began in the mining industry to estimate ore reserves. Matheron (1973) provided a theoretical basis by the formation of random functions. The method resembles the classical statistical approach but differs by assuming that adjoining samples are correlated spatially instead of being independent of each other. The appeal here is the recognition of the spatial relationship and its ability to be expressed in quantitative terms. This correlation can be expressed in terms of a function known as a variogram.

The following explanation draws upon literature by Kim (1981) and Warrick et al. (1986).

The mathematical basis for geostatistical application is known as the theory of regionalized variables. A variable is regionalized if it is distributed in space and exhibits some degree of spatial correlation. Examples of this include bulk density, porosity or the thickness of an ash flow sheet.

The main purposes of the regionalized variable (ReV) theory are to define the structural properties of the regionalized variable and to estimate the variable from sample data. Regionalized variables usually exhibit both local variations and broad regional trends.

An ReV is considered to be a unique realization of a certain random function, $Z(x)$. In practicality, we are limited to a single realization $z(x_i)$ of the random function $Z(x)$ at the position x_i. Spatial homogeneity is fulfilled under the general heading of the hypothesis of stationarity to allow for the single realization substitution. A random function is strictly stationary when its spatial law is constant over the entire sample space. For estimation purposes, the characteristics of this random function must be known. The characteristics can be determined from sample data if weak stationarity assumptions are fulfilled.

Weak stationarity exists if:

1. $E[Z(x)]$ exists.

where $Z(x)$ is a random function whose set of values $Z(x_1)$, $Z(x_2)$, $Z(x_3)$,. . ., $Z(x_n)$ at x_1, x_2, x_3,. . ., x_n defines a point or some support volume centered at x in space,

and

2. For any vector h, the variance of Z(x+h) - Z(x) exists and depends only on h.

Weak stationarity is also known as the intrinsic hypothesis. The intrinsic hypothesis does not fulfill second order stationarity assumptions, however. Second order stationarity exists when:

1. E[Z(x)] exists and does not depend on x.

2. For each pair of random variables, [Z(x), Z(x+h)] the covariance, C(h), exists and does not depend on x.

$$C(h) = E[Z(x)\ Z(x+h)] - m^2 \qquad (3.6)$$

where m = mean value or E[Z(x)]

The variogram function defines the spatial correlation of adjoining samples and only requires weak stationarity. This correlation is the structured aspect of ReV and also of the random function. The variogram $\gamma(h)$ is defined as:

$$\gamma(h) = 0.5\ \mathrm{Var}[Z(x) - Z(x+h)] \qquad (3.7)$$

where x is defined as above and h is some distance away from x. "Var" here is the variance. Assumming zero drift, E[Z(x+h)] = E[Z(x)] and equation 3.7 is equal to

$$2\gamma(h) = E[Z(x) - Z(x+h)]^2 \qquad (3.8)$$

An estimate of $\gamma(h)$ or $\gamma^*(h)$ is given by:

$$\gamma^*(h) = 0.5\ (1/n) \sum_{i=1}^{n} [Z(x_i) - Z(x_i+h)]^2 \qquad (3.9)$$

with n being the number of pairs separated by some distance h. This is a vector function of the distance h.

A typical variogram is given in figure 3.6. The lag distance, h, is the separation distance between sample pairs. The range, r, is

defined as the distance at which sample pairs are correlated. The value of $\gamma(r)$ is called the sill. If $h > r$, samples are no longer correlated. Sometimes the value of $\gamma(0)$ does not equal zero. This is termed the nugget value C_o. It is used to characterize the residual influence of all variabilities which have ranges much smaller than the available distances of observations. In general the nugget value should be small if proper sampling procedures have been followed.

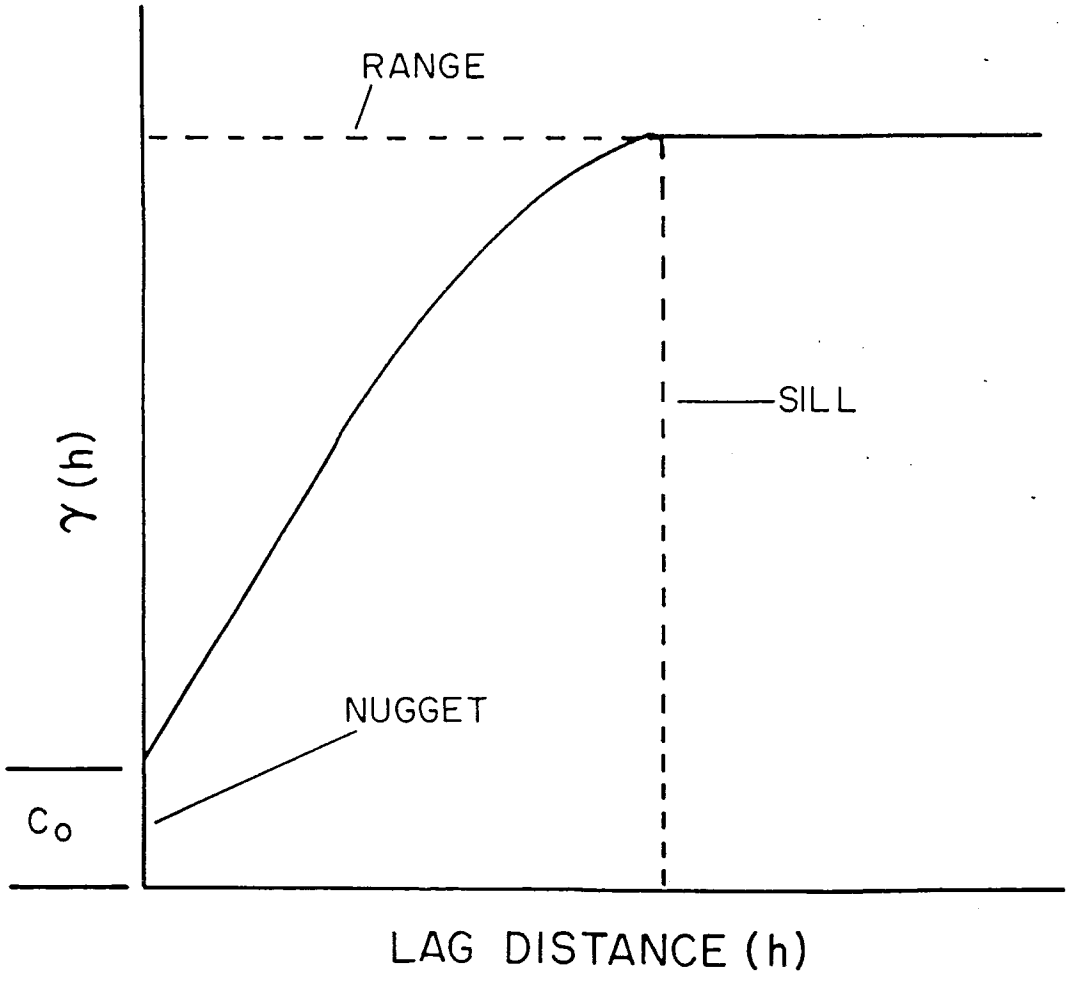

Figure 3.6. Semi-variogram showing sill, range, r, and nugget C_o.

CHAPTER 4

SAMPLE DESCRIPTION AND PROCEDURES

Samples were collected and analyzed according to the following information. General procedural guidelines were supplied by Micromeritics Corporation (1986).

4.1 Sample Description

Approximately 285 m of 6.35 cm diameter core resulted from the borehole drilling. Figure 4.1 shows the borehole arrangement and sample locations. A sampling scheme was implemented to test an equal number of samples from each borehole set. As a result of this scheme, 35 sample points were chosen for each set with seven samples originating from the shortest boreholes (X1, Y1 and Z1), 12 samples from each borehole X2, Y2 and Z2 and 16 samples from the longest boreholes (X3, Y3 and Z3). Sample points are given letter designations in figure 4.1.

Sample points in the top four meters of core were chosen at approximately 1 m intervals. This was done to better define any surface effects of the deposit. At points below four meters in all boreholes, samples were chosen at approximately 3 m intervals. Together 105 sample locations were chosen and cut from the original core. Sample locations were purposely chosen away from any visible fractures in the core, causing non-uniform spacing between sample points. A 10 cm length of core was cut for each sample location. The top 5 cm portion was used

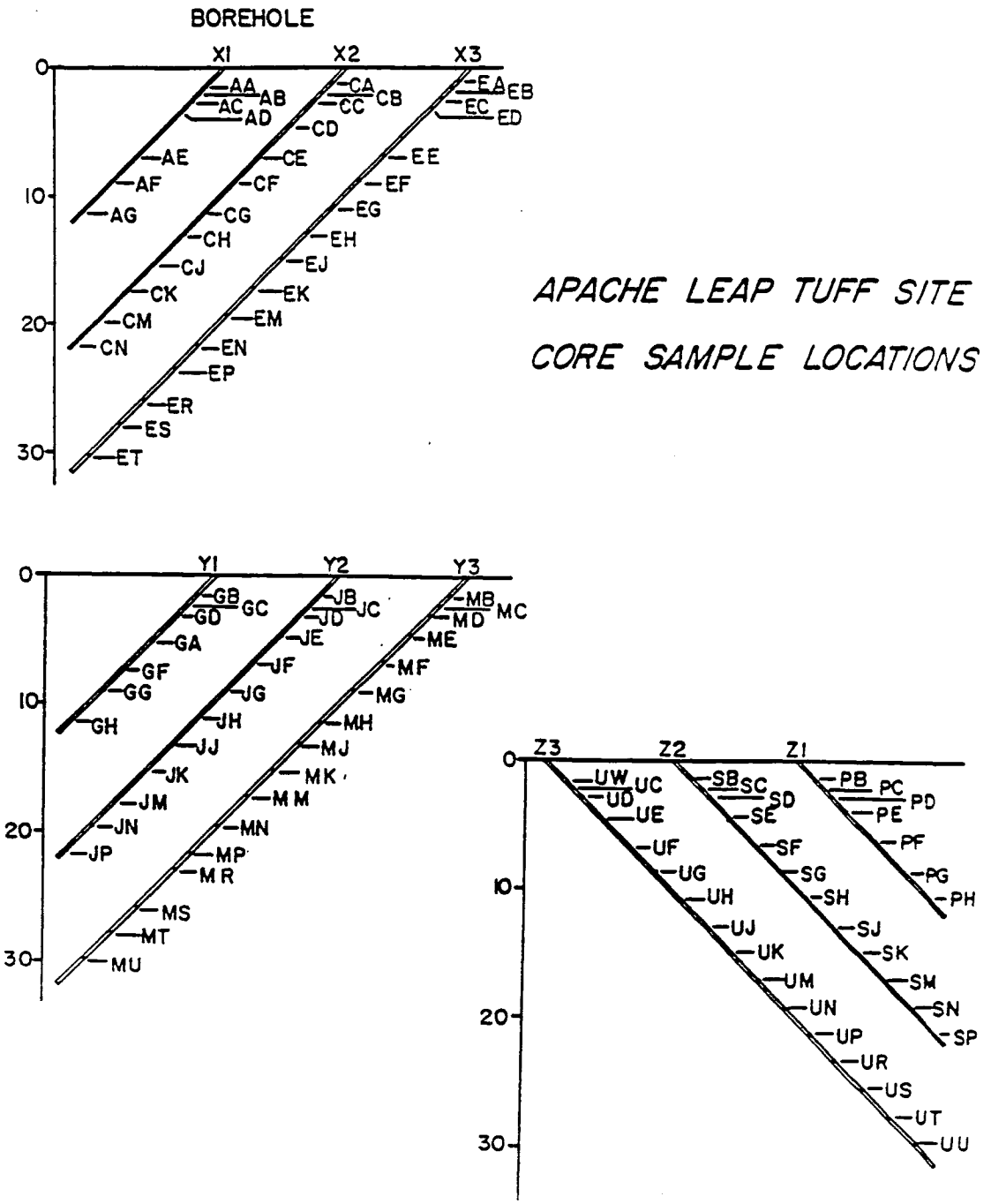

Figure 4.1. Apache Leap study site sample locations. Letter designations indicate sample points. 105 points total.

for another study involving air and water permeability and thermal conductivity. The next 2.5 cm portion was used for this study while the last 2.5 cm portion was used for psychrometry investigations. Figure 4.2 details the 10 cm core segment.

The 10 cm core samples were cut using a water cooled diamond radial arm rock saw. Maximum dimensions for samples in this study were 2.5 cm in diameter by 2.5 cm long. A diamond edged coring bit 2.54 cm in diameter was used to drill the samples out of the original core. All samples were sized from 2 cm to 2.5 cm long.

Once the samples were cut to proper dimensions they were dried at 105 degrees C until weight loss ceased. They were then placed in sealed containers until porosimetry measurements were performed.

4.2 Poresizer Description

The instrument used in this study was a Micromeritics Model 9310 Poresizer capable of intruding mercury up to 200 MPa. A Welch Scientific Model 1402 vacuum pump capable of 1×10^{-4} mm Hg was used in conjunction with the poresizer. An IBM PC computer linked the software supplied by Micromeritics to the poresizer.

The poresizer measures the volume of mercury intrusion and extrusion on an electrical capacitance basis. The volume of mercury forced into the pores of a sample by an applied pressure is measured by the change in electrical capacitance of a cylindrical coaxial capacitor formed by an outer metallic shield on the penetrometer stem and the inner column of mercury. As pressure is increased and mercury

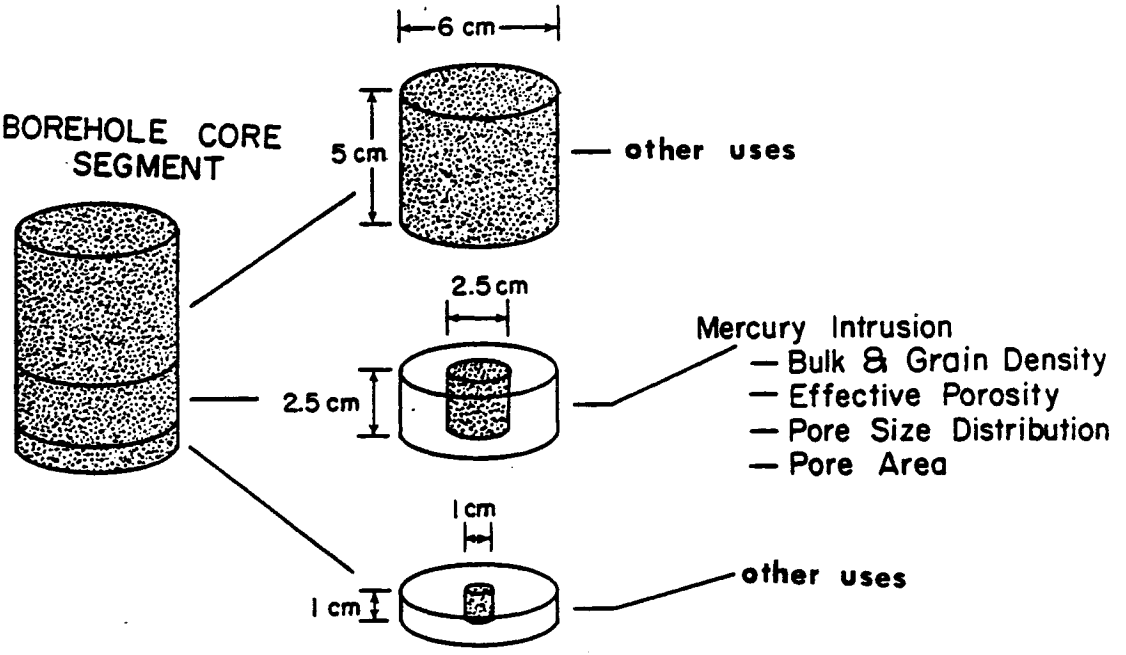

Figure 4.2. Ten cm borehole core segment and its uses.

is forced into the sample pores, the level of mercury falls in the penetrometer stem causing a linear decrease in electrical capacitance.

Figure 1.1 diagrams the type of penetrometer used. Each penetrometer has associated with it a calibration factor in units of microliters per picofarad. Capacitance changes are converted to volume changes by multiplying by the appropriate calibration factor. Both the inner and outer diameters of the penetrometer stem are carefully controlled to detect volume changes of well under one microliter. The glass stem of the penetrometer is made of metal-clad precision-bore borosilicate glass capillary tube which is fused to a chamber which contains the sample.

Samples are loaded into the glass chamber of the penetrometer, sealed and then evacuated to a vacuum near 50 μm of Hg. Mercury is loaded into the penetrometer through a capillary in the stem. As mercury flows into the penetrometer, it surrounds the sample and fills the capillary in the penetrometer stem. Low pressure mercury intrusion can be detected between 0 MPa and atmospheric pressure. In this study, pore size corresponding to below atmospheric pressure was not significant. Therefore, only high pressure intrusion/extrusion results are reported.

High pressure generation is accomplished in the poresizer with a ram driven by a ball screw which is driven by a gear motor. The high pressure system is filled with high pressure fluid (a mixture of synthetic oil and low-odor kerosene) which is pressurized by the ram. This fluid contacts the mercury capillary in the penetrometer stem and forces the mercury into the pores. A capacitance transducer connected

to the high pressure chamber via a gold-plated banana plug and conical insulator detects and measures the intrusion volume.

4.3 Procedure

A complete listing of the procedures used for mercury intrusion is given in Appendix A. A general description follows.

Once the samples were dried, weighed and loaded into the penetrometer they were evacuated and then surrounded by mercury. Samples in the penetrometer were subjected to a range of pressures from atmospheric to near 200 MPa. Pore sizes corresponding to pressures below atmospheric pressure were considered insignificant because initial intrusion commenced at pressures close to twice atmospheric. A listing of the pressure table used in this study is given in Table 4.1. Each sample was subjected to one intrusion/extrusion cycle per run. Two runs were performed on each sample. This was done for two reasons: 1) to better define the volume hysteresis effect of the various pore sizes; and 2) to quantitatively analyze the effect of pore size on trapping mercury. During the high pressure test, pressure equilibrium was established for ten seconds for each pressure point in table 4.1 before a reading was recorded. This allowed time for mercury equilibrium within the pores.

Intrusion/extrusion data were recorded and stored automatically on the PC. At the completion of each test, the results were stored on a data diskette. Direct parameter listings of total intrusion volume, pore area, median pore diameter, bulk density and skeletal density were stored. From this information, porosity was determined by multiplying

the total intrusion volume by the bulk density. Pore size distribution was determined by plotting the incremental pore volume versus pore diameter using equation 3.1.

TABLE 4.1 Pressure table used during automatic high pressure operation of Poresizer 9310. Only intrusion pressures are shown. Extrusion pressures are the same as intrusion values only in the reverse order i.e. from 163 MPa to .10 MPa. Pore diameter intruded is according to capillary theory and equation 3.1.

POROSIZER PRESSURE (MPa)	(psia)	PORE DIAMETER INTRUDED (μm)
.10	14.7	12.2
.13	18.9	9.52
.17	24.1	7.46
.21	30.8	5.84
.27	39.4	4.57
.35	50.4	3.57
.44	64.4	2.79
.57	82.6	2.18
.72	105	1.71
.93	135	1.33
1.19	172	1.05
1.52	221	.82
1.95	283	.64
2.48	360	.50
3.19	462	.39
4.07	590	.31
5.20	754	.24
6.64	963	.19
8.49	1231	.15
10.8	1574	.11
13.9	2018	.09
17.8	2580	.07
22.7	3300	.05
29.1	4220	.04
37.2	5390	.03
47.6	6910	.026
60.9	8830	.02
77.9	11300	.016
100	14500	.012
127	18450	.0098
163	23600	.0076
187	27200	.0066

CHAPTER 5

RESULTS AND DISCUSSION

A total of nine parameters for each of 105 sample points have been generated. The parameters are:

1) Porosity (Porosity)
2) Bulk Density (BULK)
3) Pore Area (PAREA)
4) Mode Diameter of Large Pore Size Class (LPD)
5) Mode Diameter of Small Pore Size Class (SPD)
6) Percentage of Total Porosity from Large Pore Size Class (LPDPER)
7) Percentage of Total Porosity from Small Pore Size Class (SPDPER)
8) Percentage of Total Pore Area from Large Pore Size Class (LPSAPER)
9) Percentage of Total Pore Area from Small Pore Size Class (SPSAPER)

In addition, pore-size distribution curves, represented by plotting incremental intrusion volume versus pore diameter and incremental surface area curves, represented by plotting incremental surface area versus pore diameter, were also generated. A typical pore-size distribution curve is given in figure 5.1.a. Figure 5.1.b shows an incremental surface area plot for the same sample.

In this study, all of the study site samples tested (those from X, Y or Z boreholes), exhibited a bimodal distribution with respect to pore size. For ease of identification the mode of each distribution was chosen as the descriptor. Pore size classes were divided at the pore diameter where the minimum incremental intrusion between modes occurred. Two pore size classes emerged from this division, large and small. The range of each class varies with each sample. Although a true pore-size

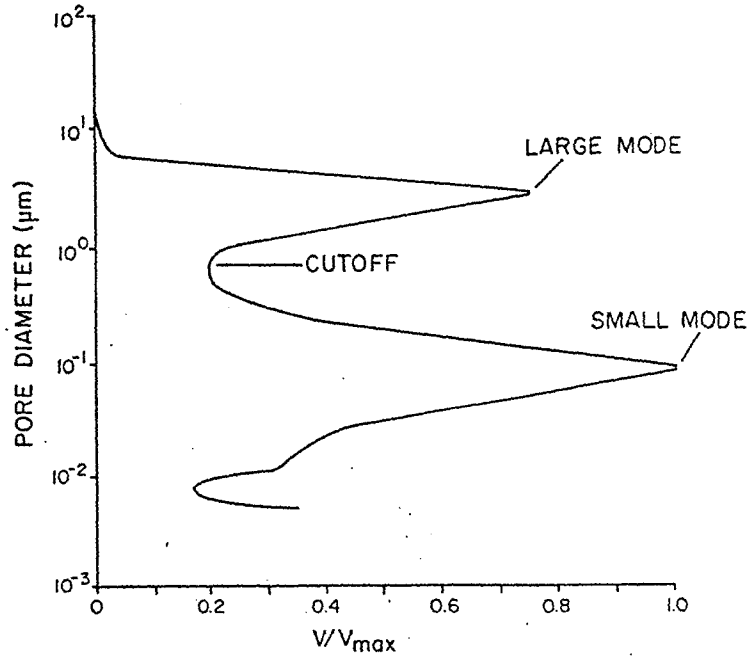

Figure 5.1.a Pore-size distribution curve of sample CC. Plot is of pore diameter vs incremental intrusion. V= incremental intrusion V_{max} = maximum incremental intrusion volume (cm^3/gm).

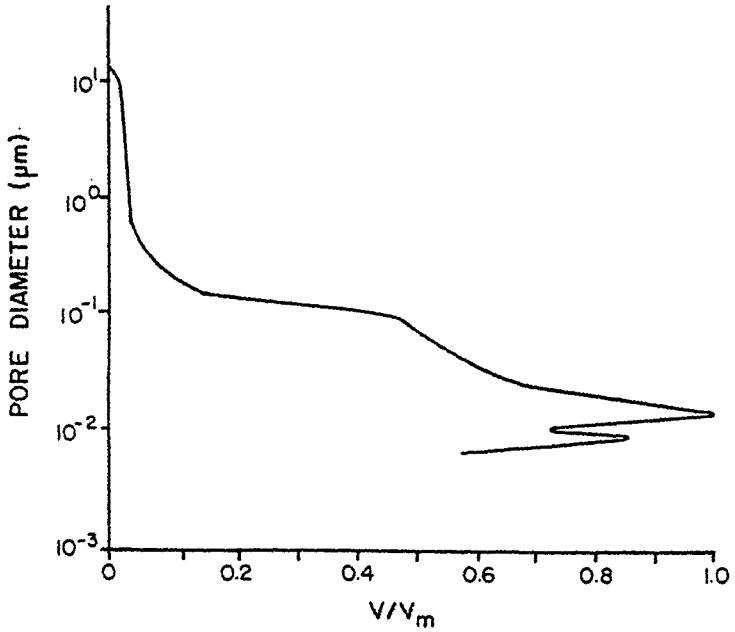

Figure 5.1.b Plot of pore diameter vs incremental surface area for sample CC. V = incremental surface area. V_m = maximum incremental surface area (m^2/gm).

distribution is not given here, one can get an idea of the pore size range by looking at the two modes and the percentage of porosity and surface area from each pore size class. Numbers 4) and 5) above represent the mode of the individual class size. Numbers 6) and 7) represent the percentage of total porosity attributed to the respective pore size division. Numbers 8) and 9) represent the percentage of pore area attributable to each pore size class.

All of the data generated in this study is found in Appendix B. Relevant data will be presented in tabular and graphical form throughout the discussion. Regression statistics can also be found in Appendix B. Calibration results for the porosimeter are found in Appendix C. The porosimeter was checked for intrusion volume accuracy every 50 sample measurements. Manufacturer supplied silica-alumina pellets with a known pore volume and surface area were the calibration standard.

5.1 Porosity

Porosity determinations based on mercury porosimetry are limited to the maximum attainable pressure applied by the poresizer. The maximum pressure attained in this study was 200 MPa. According to equation 3.1, a pore diameter of 6 nm can be intruded at this pressure. Figures 5.2 to 5.4 show porosity of each borehole sample. The axis of the borehole represents the mean porosity value for each individual borehole. Table 5.1 gives a summary of the porosity statistics.

The porosity results represent measurable interconnected porosity of the tuff samples to a pore size of 6 nm. Interconnected porosity accounts for both dead end pores and liquid conducting pores. These

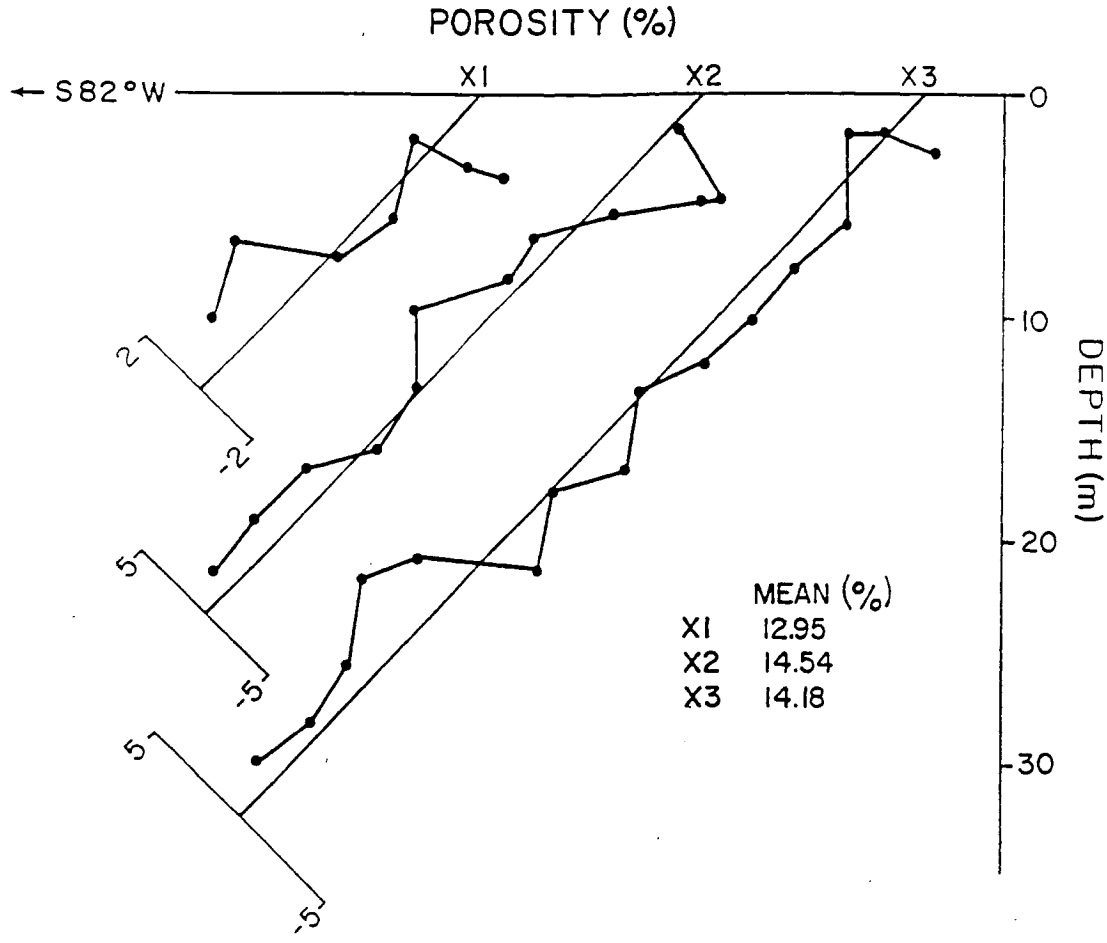

Figure 5.2. Porosity results from X borehole series. Borehole axes represent mean values. Plotted points represent difference from mean.

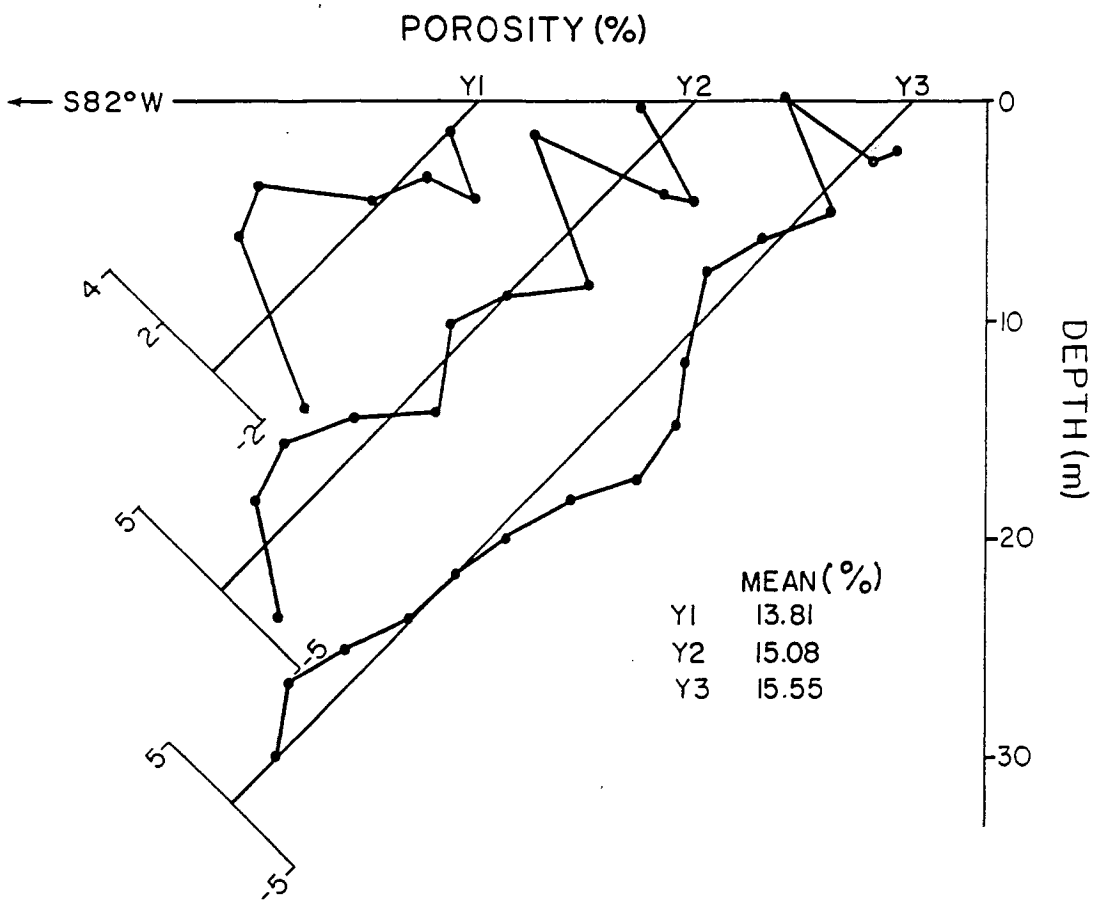

Figure 5.3. Porosity results from Y borehole series. Borehole axes represent mean values. Plotted points represent difference from mean.

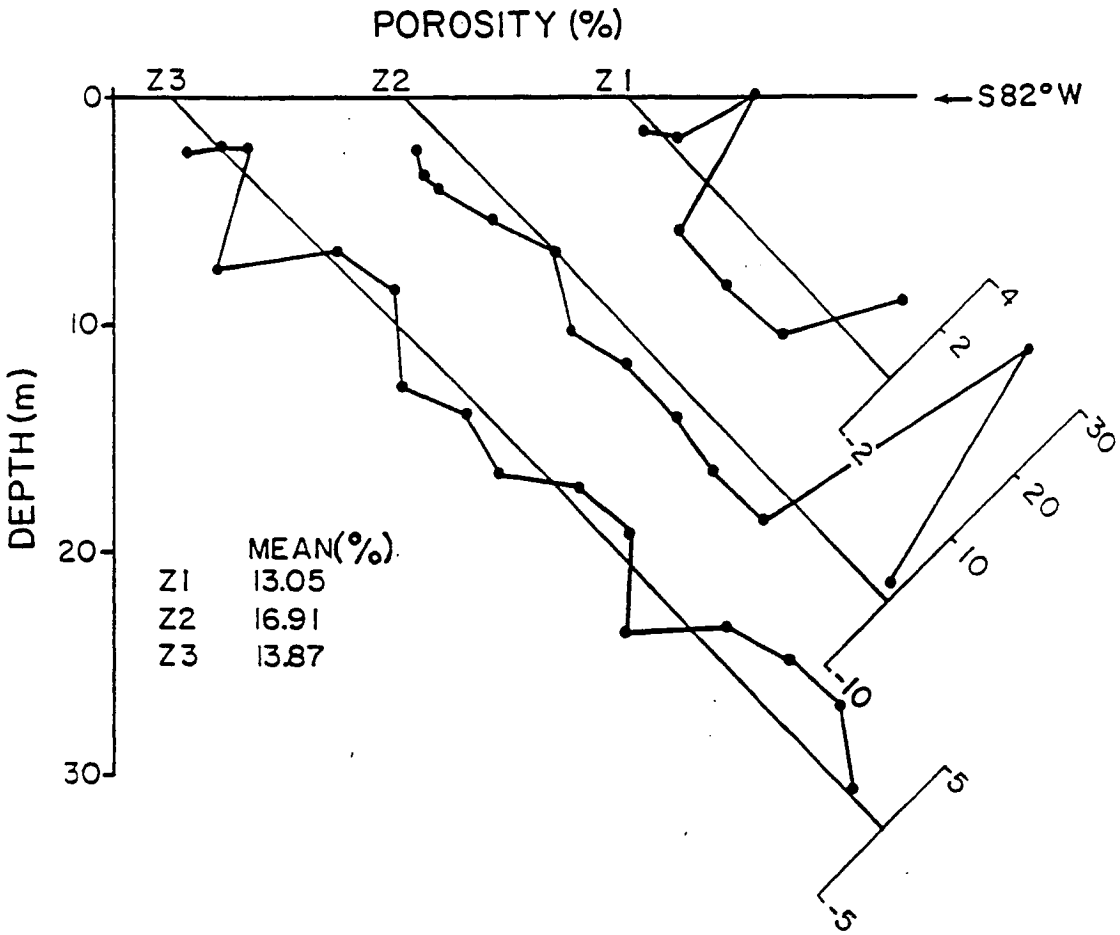

Figure 5.4. Porosity results from Z borehole series. Borehole axes represent mean values. Plotted points represent difference from mean.

values are from first run intrusion results. In some instances, a small volume of mercury was intruded into new pores during the second intrusion run. This amount never amounted to over two percent of the total porsity. It is questionable whether this newly intruded mercury actually measured matrix porosity or just some breakdown or destruction of the microporosity of the sample. For this reason, only first run porosity is considered.

TABLE 5.1 Statistical summary of porosity results. Mean values in % of measured porosity. Total number of samples equals 105.

BOREHOLE	MEAN	VARIANCE	COEF. OF SKEW	COEF. OF VARIATION
X1	12.95	1.99	.13	.11
X2	14.54	5.61	-.99	.16
X3	14.18	2.38	.55	.11
ALL X	14.06	3.56	-.17	.13
Y1	13.81	3.87	.24	.14
Y2	15.08	4.78	.18	.14
Y3	15.55	4.94	.86	.14
ALL Y	15.04	4.71	.51	.14
Z1	13.05	2.73	.74	.13
Z2	16.91	96.73	3.25	.58
Z3	13.89	4.39	-.66	.15
ALL Z	14.75	35.28	4.99	.40
ALL DATA	14.62	14.67	6.15	.26

Klavetter and Peters (1987) determined porosity on samples of tuff from Yucca Mountain in Nevada and concluded that pressures in excess of 345 MPa must be employed to measure interconnected porosity. The porosity values here will be less than actual porosity. Because of sample variation, an estimated difference between actual porosity and measured porosity is not available. Later in this discussion the mercury intrusion porosity results will be compared to water saturation

method results. The comparison will give a quantification to the pore space < 6 nm.

Tables B5.1 - 13 (in Appendix B) contain statistical data on individual boreholes, the X, Y and Z series boreholes and all borehole data. Included are correlation coefficients, covariance and cross-product results from regression of each parameter versus every other parameter, including elevation.

Figure 5.2 shows the variation of porosity with depth along the X boreholes. X1 shows the strongest correlation with elevation at -.78. The correlation coefficient suggests porosity is increasing with depth along the borehole. Grouping all of the X boreholes, results in a correlation with elevation of -.56. Although this is not a strong linear regression coefficient it does suggest an increasing porosity trend with depth. A decreased porosity near the surface of the deposit is likely due to chemical and physical weathering of the formation. The probable increased crystallization of minerals in fractures and pores certainly could affect the porosities of the samples. Surveying the regression statistics from all of the data in table B5.13 shows a minor correlation between depth and porosty of -0.26. This suggests the X borehole set possibly can be accounted for by local variation and not totally representative of the study site.

A more interesting result is obtained when regressing the porosity percentage from the large pore size class (LPDPER) versus elevation. Table 5.2 gives a synopsis of the information. More of the porosity is accounted for by the large pore size class with depth along the boreholes. A scattergram plot of the porosity percentage from the

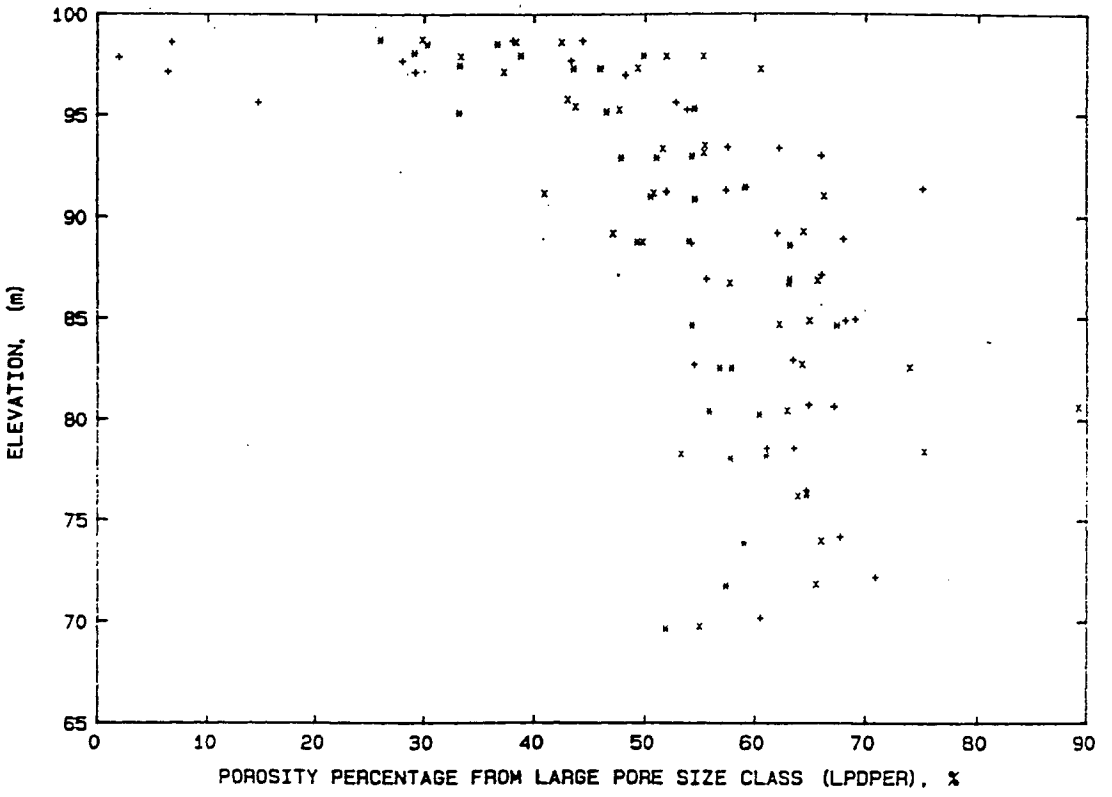

Figure 5.5. Scattergram plot of elevation vs percentage of porosity accounted for by the large pore size class (LPDPER). X series data plotted with '*'; Y series with '+'; and Z series with 'x'.

large pore size class (LPDPER) versus elevation is contained in figure 5.5. Samples from the X, Y and Z series are represented by *, + and x, respectively. The volume of larger pores increases with depth. Again, surface effects may play a part in this phenomenon. Two separate regressions were performed on the data in figure 5.5. A regression coefficient of -.59 resulted when elevation was regressed against LPDPER considering only data between 90 and 100 m in elevation. A regression of data from 65 to 90 m in elevation produced a -.11 regression coefficient. These coefficients suggest a definite surface effect on the large pore size class porosity percentage. As the deposit cooled, gas filled pores in local abundance toward the top of the deposit causing larger pore sizes.

TABLE 5.2 Sample statistics for percentage of porosity from the large pore size class (LPDPER). Correlation coefficient is of elevation versus LPDPER. Mean values are in percent of measured porosity. Total number of samples equals 105.

BOREHOLE	MEAN	VARIANCE	COEF. OF SKEW	CORRELATION COEF.
X1	45.16	53.34	-1.11	-.459
X2	52.98	157.6	-.89	-.783
X3	51.87	118.7	-1.49	-.687
ALL X	50.91	121.5	-.79	-.687
Y1	56.95	161.6	.31	-.922
Y2	49.29	299.0	-.94	-.757
Y3	51.85	572.5	-1.56	-.726
ALL Y	51.99	385.5	-1.40	-.638
Z1	44.89	160.2	.42	-.954
Z2	57.82	227.9	.65	-.779
Z3	57.96	70.9	-.03	-.565
ALL Z	55.29	161.2	.21	-.656
ALL DATA	52.74	221.9	-1.09	-.628

Near the surface of the deposit the ash flow cooled quickly releasing its trapped gas, allowing for smaller particle crystallization and less porosity. The trapped gas increased with depth up to a certain point allowing for larger pore sizes but not greater porosity. Slightly more than 50% of the porosity is accounted for by the large pores when considering all sample points.

5.2 Pore-Size Distribution

One major advantage to mercury porosimetry is the relative ease and time required to obtain a pore-size distribution. Figures 5.6 to 5.11 show the modes of the large and small pore size classes along the borehole axes.

Overall, no strong correlation exists between the modes of the bimodal distributions and any of the other parameters. Individual borehole results can be found in tables B5.1 - 12. The mode diameter of the small poresize class (SPD) exhibits a strong positive correlation with elevation in the X and Z series boreholes, .743 and .699, respectively but shows almost no correlation in boreholes Y2 and Y3. For most data, except Y2 and Y3, the mode diameter for the small pore size class decreases with depth which correlates with the occurrence of larger pore sizes with depth discussed earlier. Table 5.3 describes the sample statistics of the distributions.

The relatively small variance for both parameters indicates that most samples are grouped near the mean and that the deposit is fairly homogeneous with respect to the individual pore size classes.

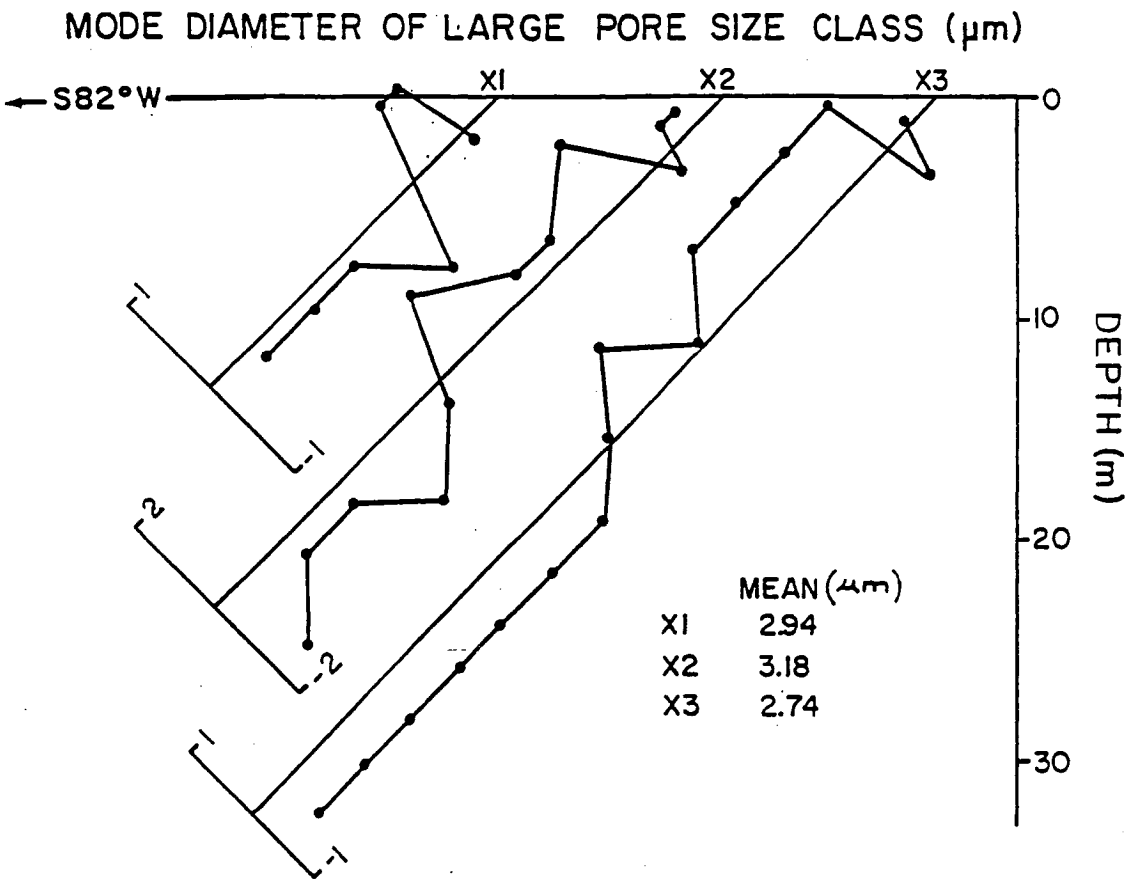

Figure 5.6. X series borehole plots of mode diameter of large pore size class for each sample point. Borehole axes represent mean values. Plotted points represent difference from mean.

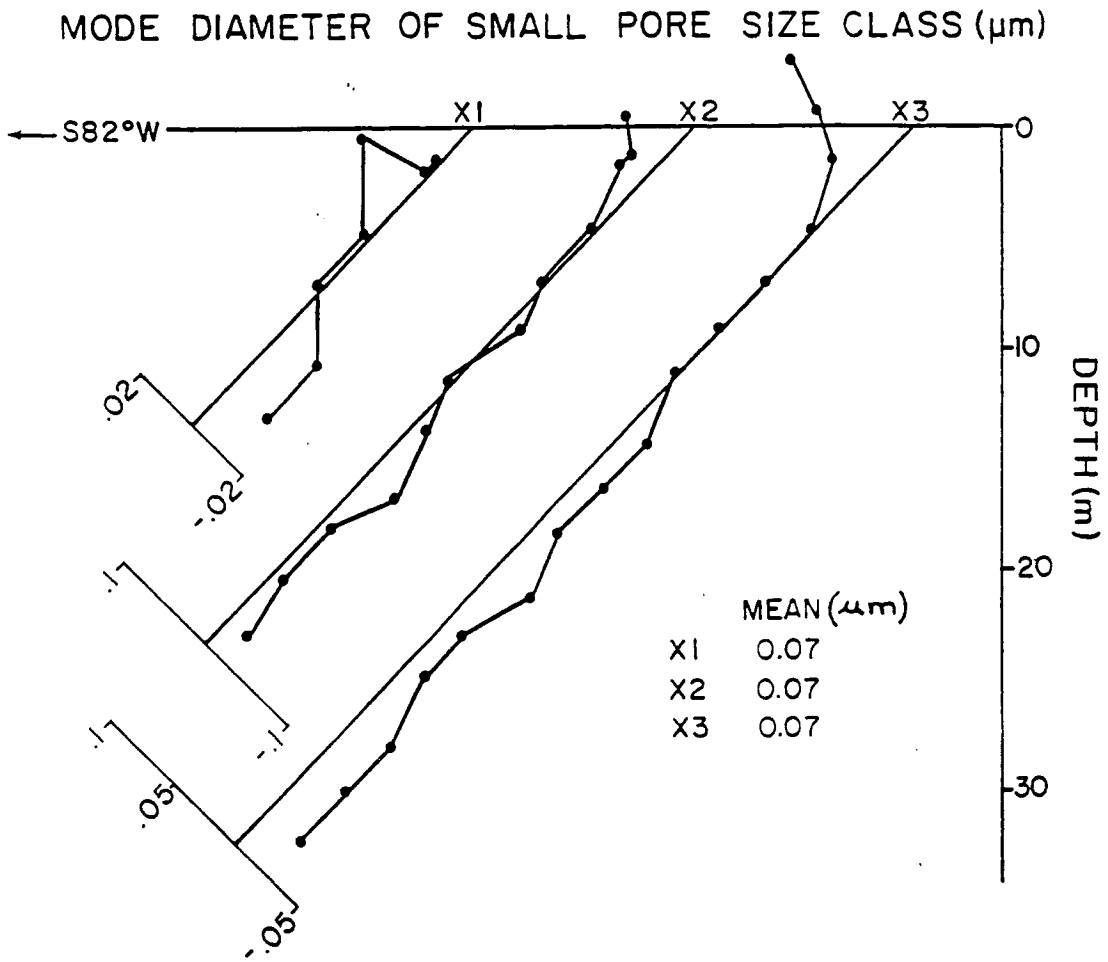

Figure 5.7. X series borehole plots of mode diameter of small pore size class for each sample point. Borehole axes represent mean values. Plotted points represent difference from mean.

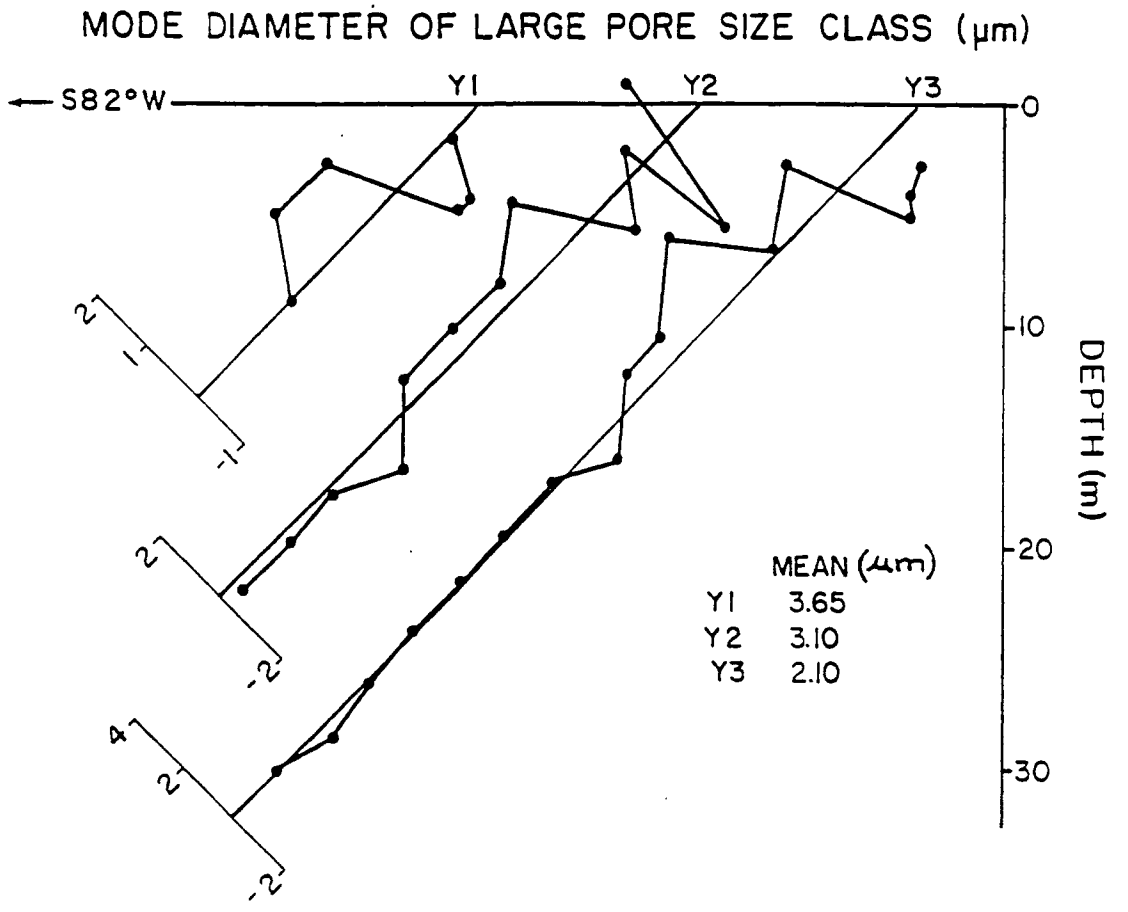

Figure 5.8. Y series borehole plots of mode diameter of large pore size class for each sample point. Borehole axes represent mean values. Plotted points represent difference from mean.

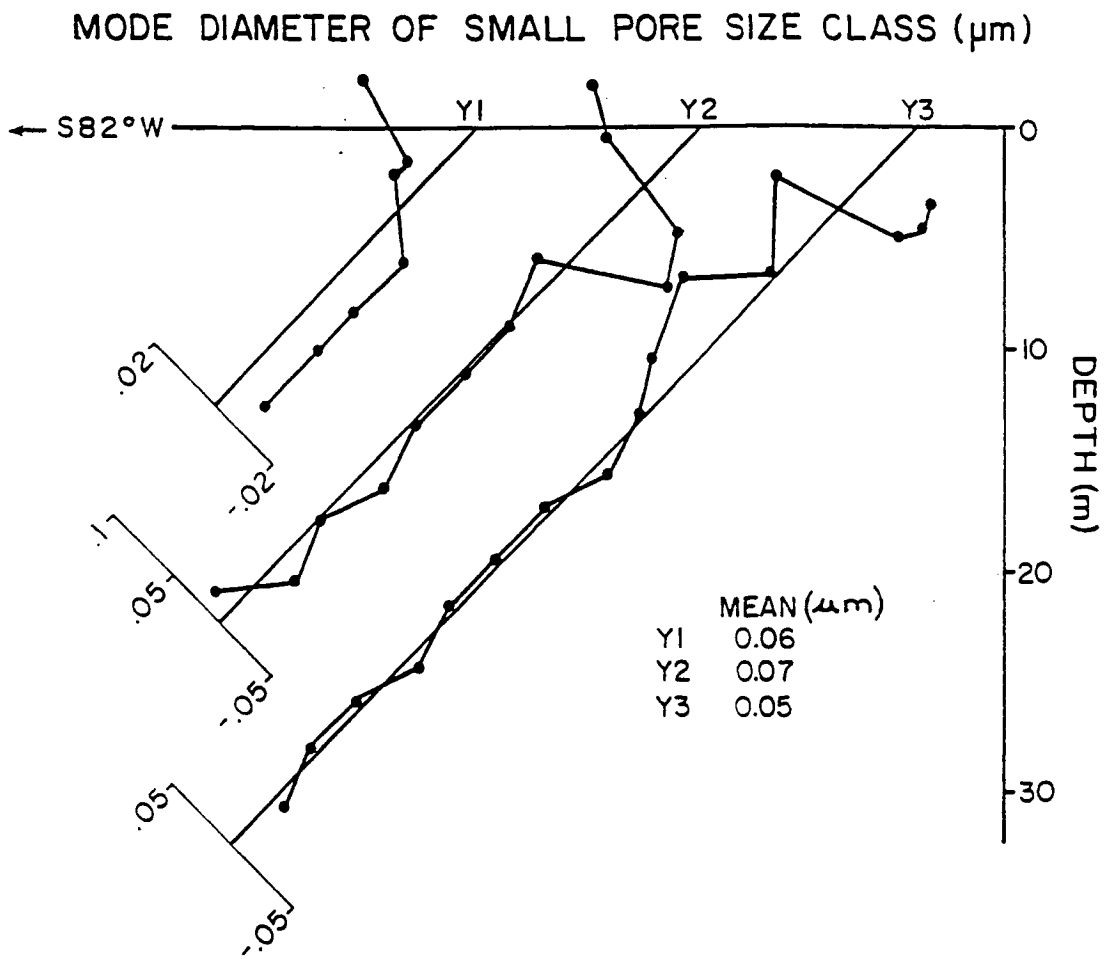

Figure 5.9. Y series borehole plots of mode diameter of small pore size class for each sample point. Borehole axes represent mean values. Plotted points represent difference from mean.

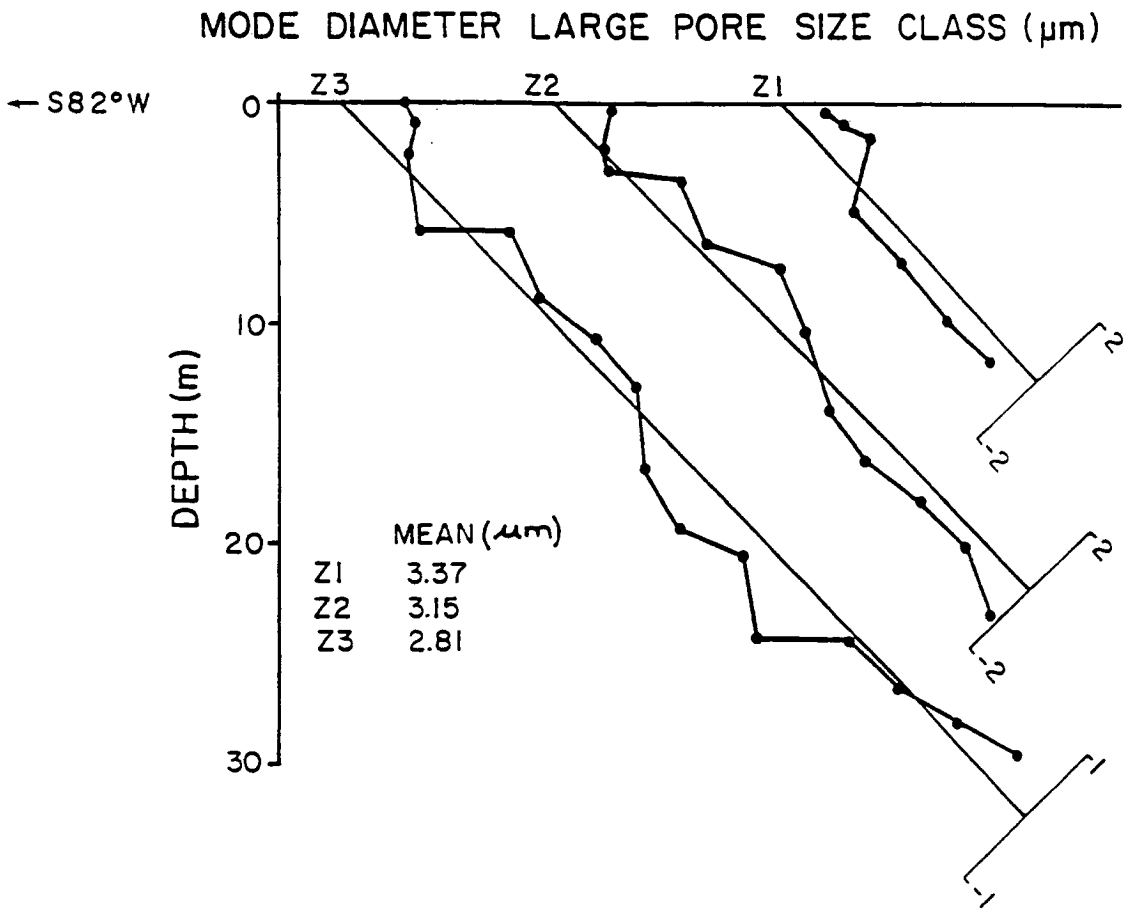

Figure 5.10. Z series borehole plots of mode diameter of large pore size class for each sample point. Borehole axes represent mean values. Plotted points represent difference from mean.

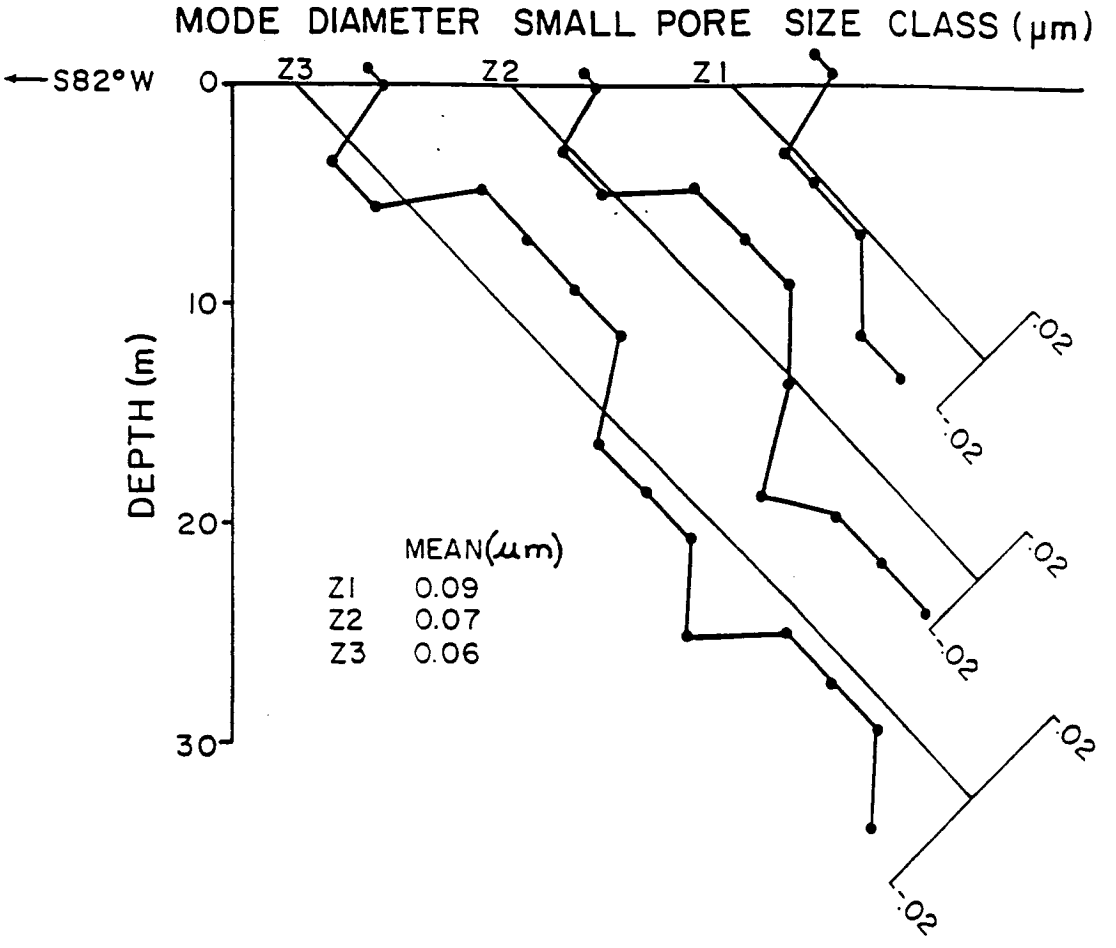

Figure 5.11. Z series borehole plots of mode diameter of small pore size class for each sample point. Borehole axes represent mean values. Plotted points represent difference from mean.

Coefficient of variation data also support the homogeneity of the pore size classes.

The pore-size distribution generated from the porosimeter is a function of several conditions. The main factors in determining the actual distribution and size of pores are the pore geometry and pore arrangement. Take, for example, the pore arrangement shown in figure 5.12. If capillary theory is strictly adhered to, the pore size corresponding to r_w would not be registered until a pressure corresponding to r_n was reached. At this time, the throats with radius r_n, and pore with radius r_w, would be filled. The corresponding

TABLE 5.3 Sample Statistics for mode diameter of large pore size class (LPD) and mode diameter of small pore size class (SPD). Mean values in units of μm. Total number of samples equals 105.

BOREHOLE	MEAN		VARIANCE		COEF. OF SKEW		COEF. OF VAR.	
	LPD	SPD	LPD	SPD	LPD	SPD	LPD	SPD
X1	2.94	.07	.25	.0001	.19	.61	.17	.17
X2	3.18	.07	.86	.001	-.09	.75	.29	.34
X3	2.74	.07	.40	.001	.50	1.80	.23	.43
ALL X	2.94	.07	.54	.001	.38	1.51	.25	.36
Y1	3.65	.06	.53	.0002	.27	1.34	.20	.20
Y2	3.10	.07	1.14	.001	-.56	.46	.34	.48
Y3	2.10	.05	1.23	.001	.26	-.11	.53	.46
ALL Y	2.75	.06	1.41	.001	-.27	.66	.43	.46
Z1	3.37	.09	.14	.0003	-1.23	.28	.11	.19
Z2	3.15	.07	.72	.0003	.62	-.30	.27	.24
Z3	2.81	.06	.75	.0001	.39	-.09	.31	.17
ALL Z	3.03	.07	.64	.0004	.14	.69	.26	.27
ALL DATA	2.91	.07	.86	.001	-.24	.75	.32	.36

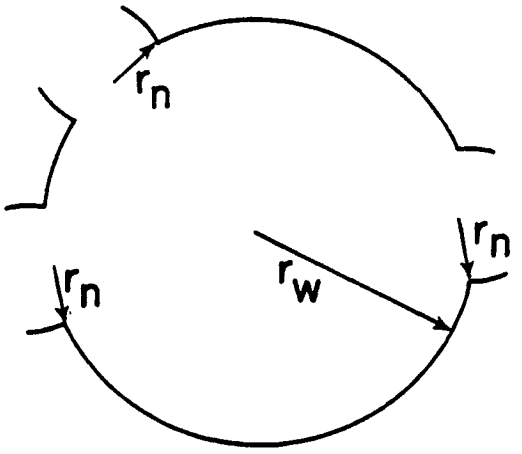

Figure 5.12. Pore with wide radius, r_w, and throats with narrow radius, rn.

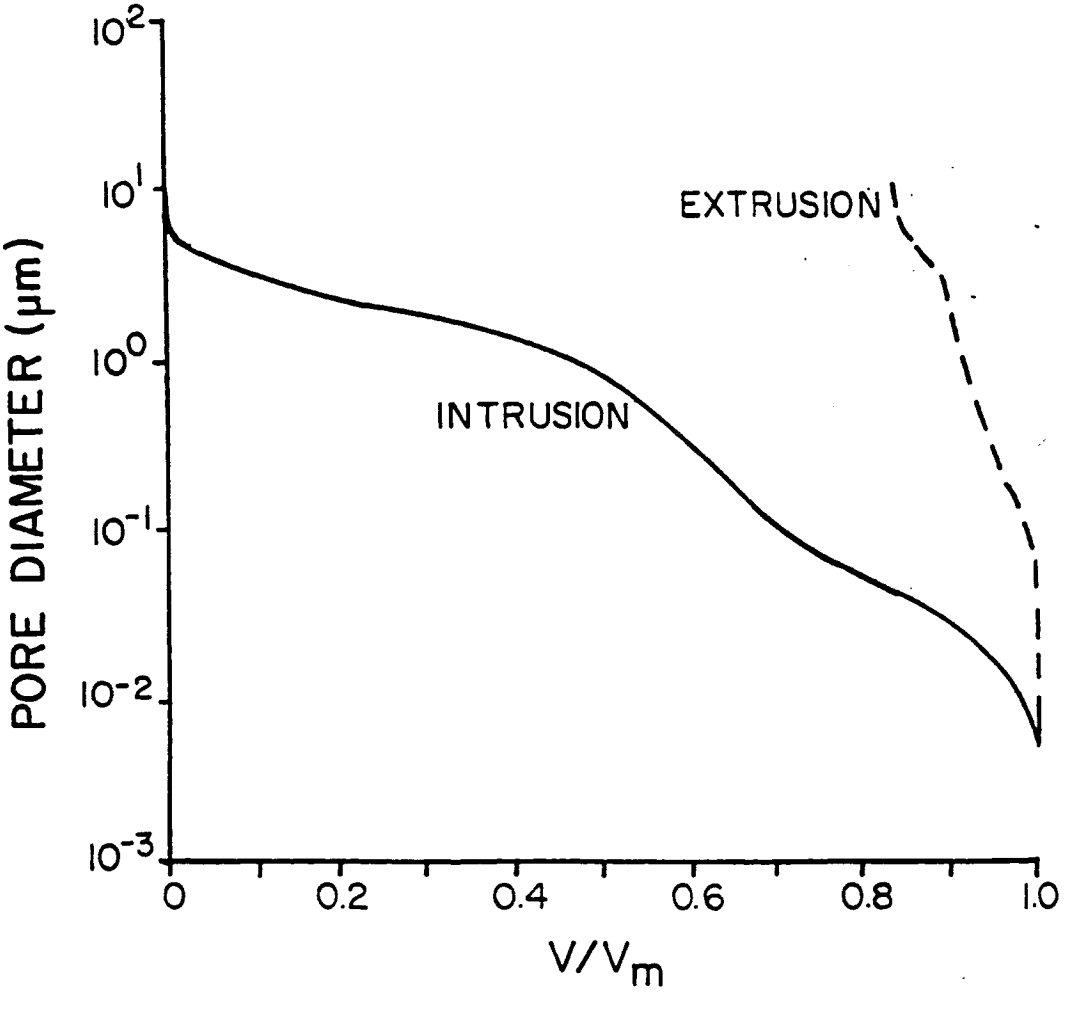

Figure 5.13. Initial intrusion/extrusion plot of pore diameter vs cummulative intruded volume of Hg (cm^3/gm). V_m = total volume intruded. V = cummulative intruded volume.

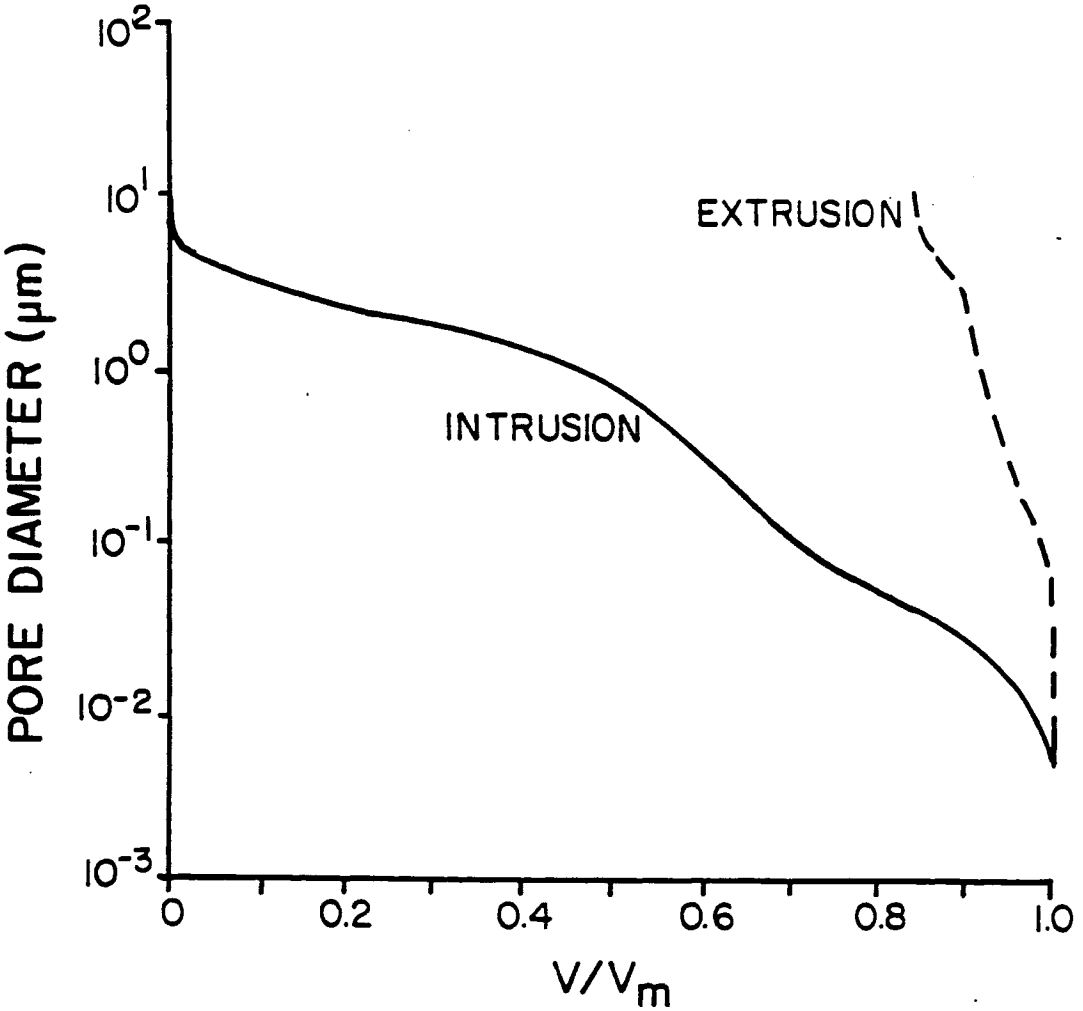

Figure 5.14. Second intrusion/extrusion plot of pore diameter vs cummulative intruded volume of Hg (cm^3/gm). V_m = total volume intruded. V = cummulative intruded volume.

intrusion volume would apply to the smaller pore size, when actually a portion of the intruded mercury volume should have been credited to the larger pore size. This was termed volume hysteresis in Chapter Three.

This phenomenon probably occurs at every range of pressures over the intrusion/extrusion cycle. The pore size distributions generated are more of a cummulative distribution such that measured pore sizes not less than a certain size are measured at each pressure increment. For this reason the results here are tabulated as pore size classes and modes of these classes instead of absolute pore-size distributions.

De Boer (1958) gave an explanation on shapes of capillaries by studying the types of hysteresis loops generated from various pore structures. Figures 5.13 and 5.14 show typical first run and second run intrusion/extrusion curves from the non-welded tuff samples studied here. Figure 5.15 shows five types of hysteresis loops as described by de Boer. The type E hysteresis loop is characterized by a sloping adsorption branch and steep desorption branch at intermediate pressures. Capillary shapes which attribute to type E hysteresis are shown in figure 5.16. Type E hysteresis can be compared to the first run intrusion/extrusion cycle of figure 5.13. Although each sample displays a certain amount of heterogeneity, it is hypothesized that capillary structures with similar response to the ones pictured in figure 5.16 exist in the microstructure of the non-welded tuff samples.

The type A hysteresis loop compares favorably to the second run curves of figure 5.14. De Boer describes type A loops as cylindrically shaped capillaries which are open at both ends. Adhering to the local hysteresis theory of Chapter three and the conclusion of Kloubek (1981),

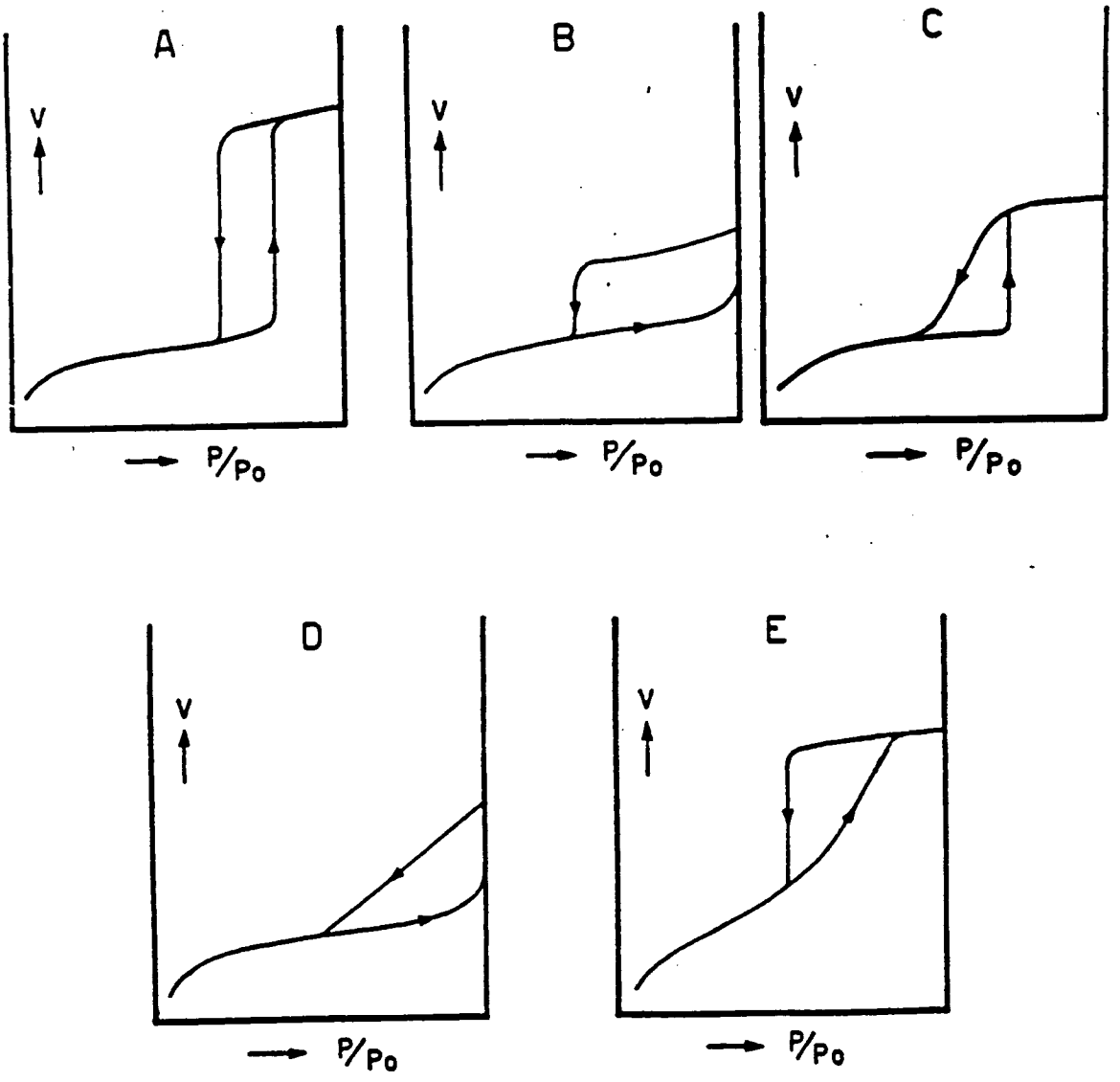

Figure 5.15. Five types of hysteresis loops describing different pore arrangements (After De Boer, 1958).

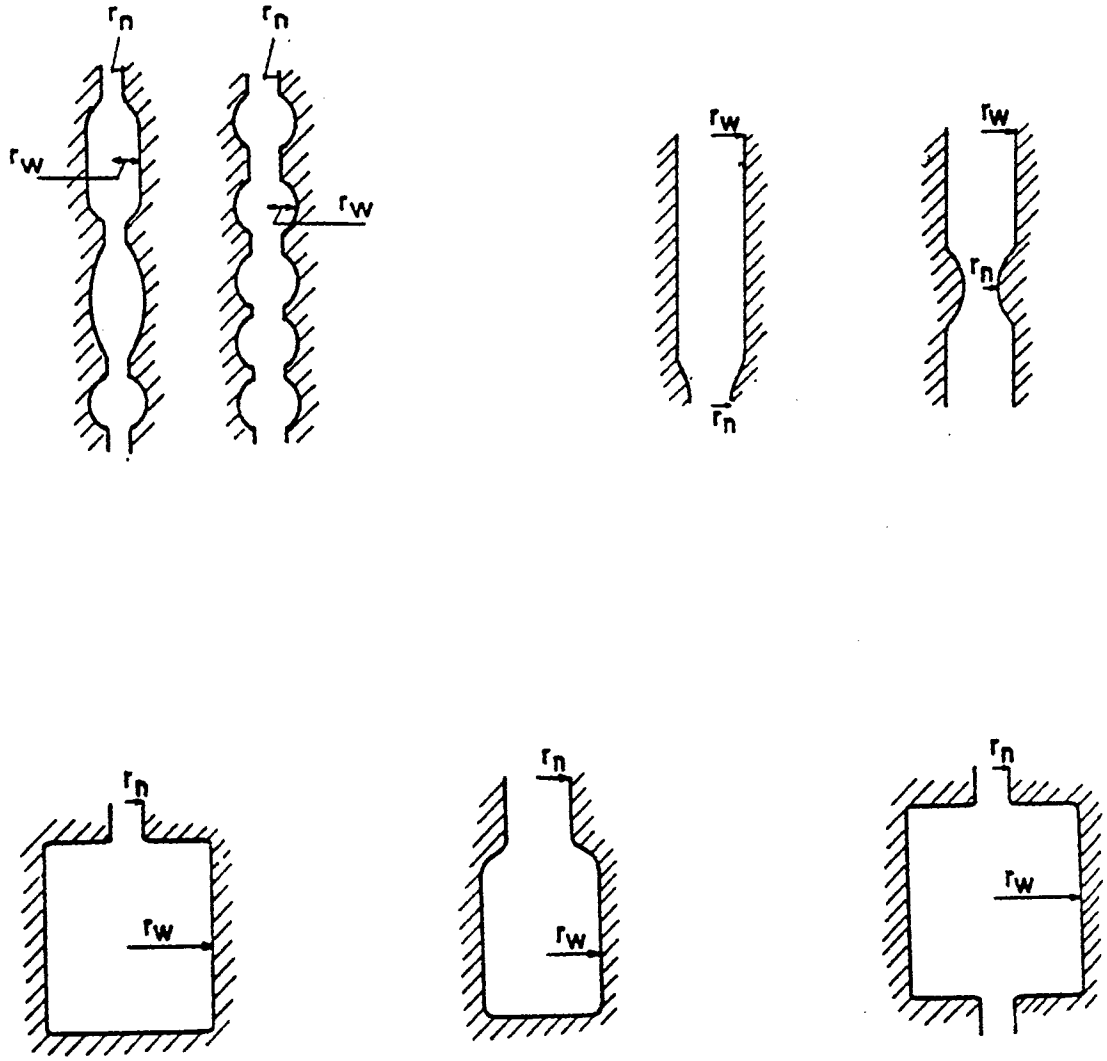

Figure 5.16. Capillary shapes which describe type E hysteresis (After De Boer, 1958).

that mercury caps are being formed on already filled pores, suggests one explanation for the different curve shape of the second run. The comparison of the first run curve to the second run curve gives an indication as to which pore sizes are trapping mercury. If the intrusion/extrusion was completely reversible, one would expect the curves to be identical, less machine variability and structural degradation of the sample. Between 70 and 95% of the intruded mercury is trapped inside the pores after the initial run. When comparing the initial run to the second, from figures 5.13 and 5.14, it appears that pores in the large to medium size range are trapping most of the mercury. Perhaps this pore size class is most abundantly surrounded by pores or throats of smaller radius.

TABLE 5.4 Summary statistics for pore surface area (PAREA) in m^2/gm and surface area percentage attributable to the large pore size class (LPSAPER) in %.

BOREHOLE	MEAN		VARIANCE		COEF. OF SKEW		COEF. OF VAR	
	PAREA	LPSAPER	PAREA	LPSAPER	PAREA	LPSAPER	PAREA	LPSAPER
X1	3.18	2.50	.04	.31	1.74	1.04	.07	.22
X2	3.29	3.37	.33	3.95	2.40	.16	.17	.59
X3	3.05	3.13	.18	1.41	.80	-.23	.14	.38
ALL X	3.16	3.09	.20	2.06	1.87	.46	.14	.46
Y1	3.07	3.27	.18	5.67	-.05	.90	.14	.73
Y2	4.39	3.16	14.37	3.56	3.20	.28	.86	.60
Y3	4.84	4.95	19.71	8.45	2.02	-.52	.91	.59
ALL Y	4.33	4.00	13.83	6.67	2.66	.17	.86	.64
Z1	3.11	2.39	.46	2.86	.45	.92	.22	.71
Z2	2.96	4.26	.25	4.24	.10	.58	.17	.48
Z3	2.76	4.01	.15	2.97	-.59	.15	.14	.43
ALL Z	2.90	3.77	.25	3.69	.39	.38	.17	.51
ALL DATA	3.47	3.72	5.06	4.49	4.83	.63	.65	.57

This phenomenon may only be a function of the type of slightly welded tuff studied here. Further study into this area could lead to quantification of mercury-trapping pore sizes. Further study into actual pore geometries and arrangements could be advanced with the use of scanning electron microscopy.

5.3 Pore Surface Area

The surface area of pores encountered in all samples was calculated using equation 3.5. The work required to force mercury into pore spaces is independent of any geometry assumption for pore structure (Rootare and Prenzlow, 1967). Pore area statistics are given in table 5.4.

The pore surface area variation of all sample data is given in figures 5.17 to 5.19. The pore surface area ranged from 1.96 m^2/gm in sample UP (see figure 5.19) to 16.2 m^2/gm in sample JE (see figure 5.18). The mean pore area for all samples is 3.47 m^2/gm. In comparison, according to Hillel (1980), a typical kaolinite clay mineral has a specific surface of 5-20 m^2/gm. Rootare and Prenzlow (1967) determined the surface area of 20 different powders using mercury porosimetry and found good agreement with nitrogen adsorption. Calcium cynamide, flourspar and fly ash all have surface areas comparable to the Apache Leap Tuff.

A pocket of high porosity and high surface area is located near the surface of boreholes Y2 and Y3. Gas trapped from the cooling ash flow probably accumulated in this region causing larger porosities and pore surface areas. Figure 5.20 presents a typical plot of pore size and pore area distribution. Figure 5.20 combines the plots in figures

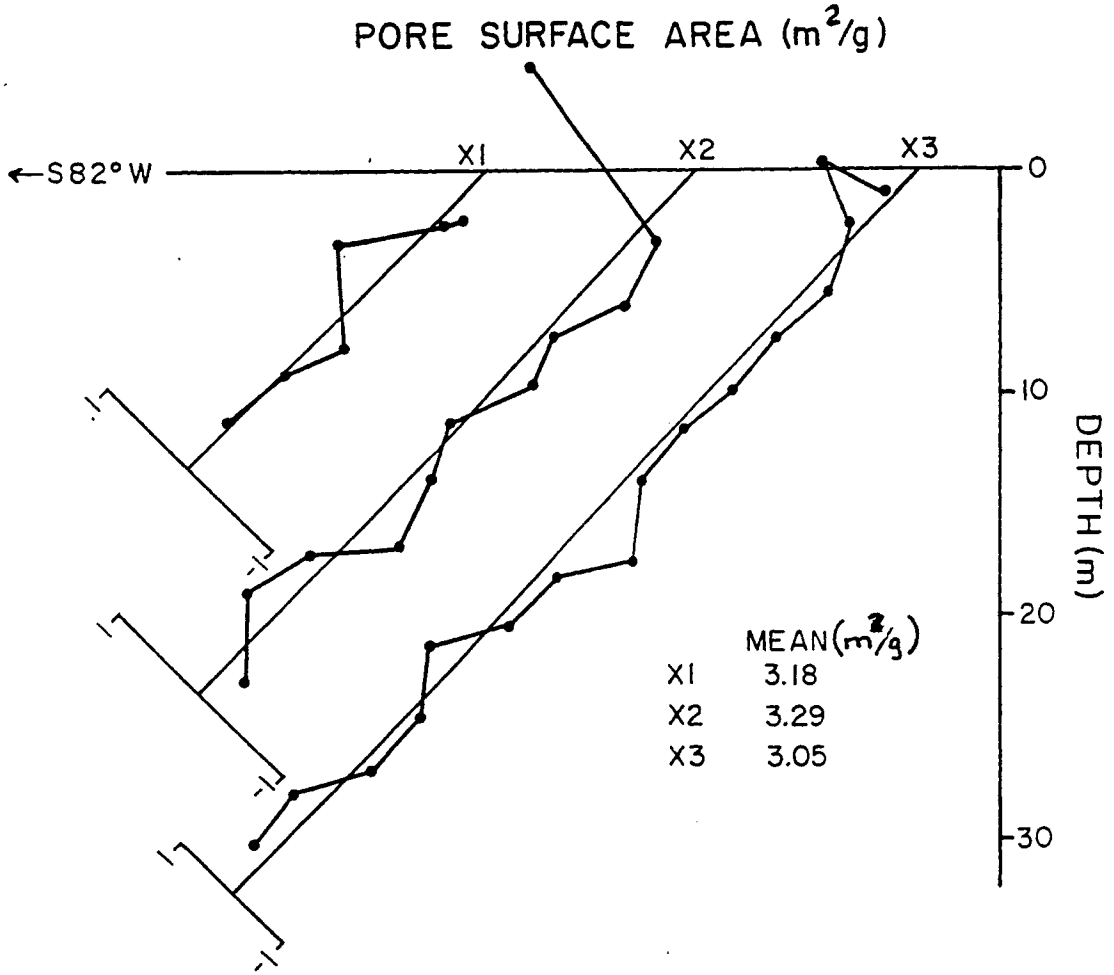

Figure 5.17. Pore surface area results from X borehole series. Borehole axes represent mean values. Plotted points represent difference from mean.

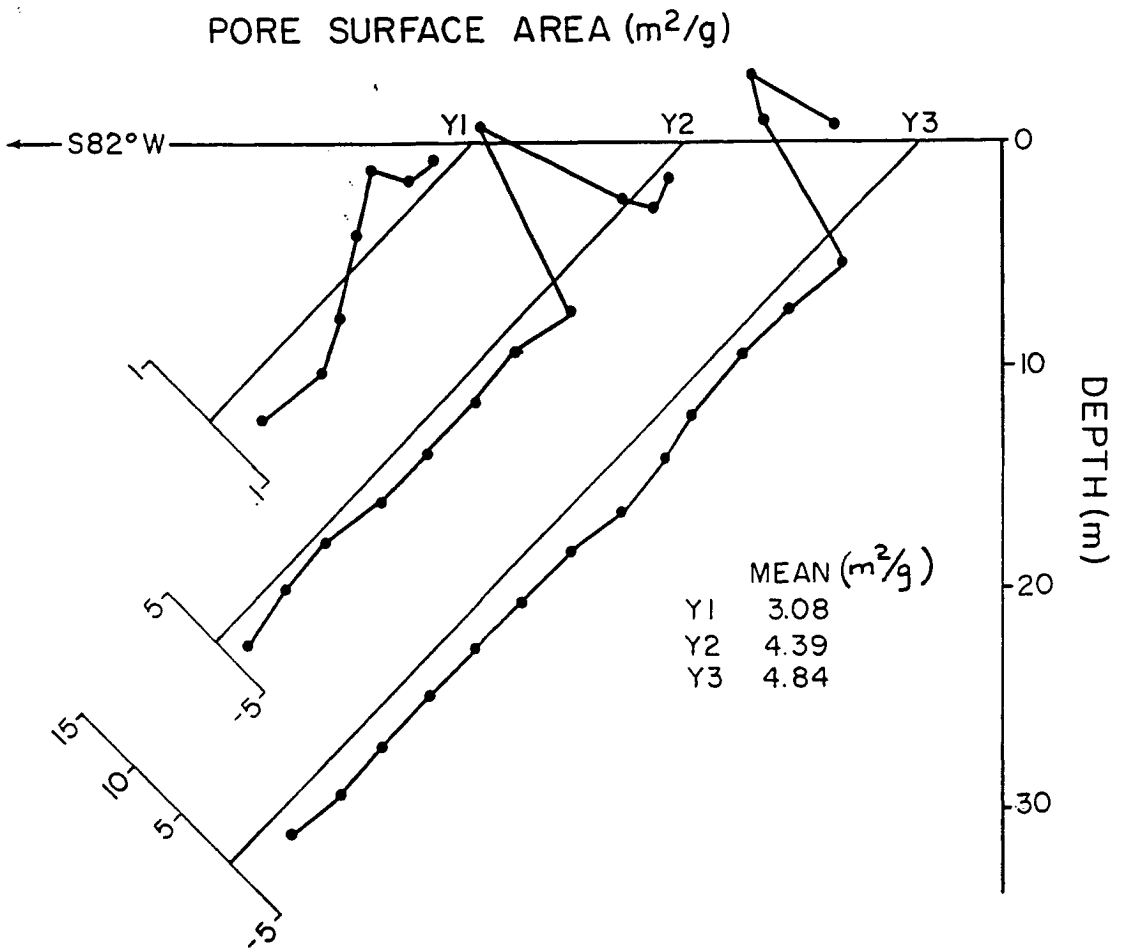

Figure 5.18. Pore surface area results from Y borehole series. Borehole axes represent mean values. Plotted points represent difference from mean.

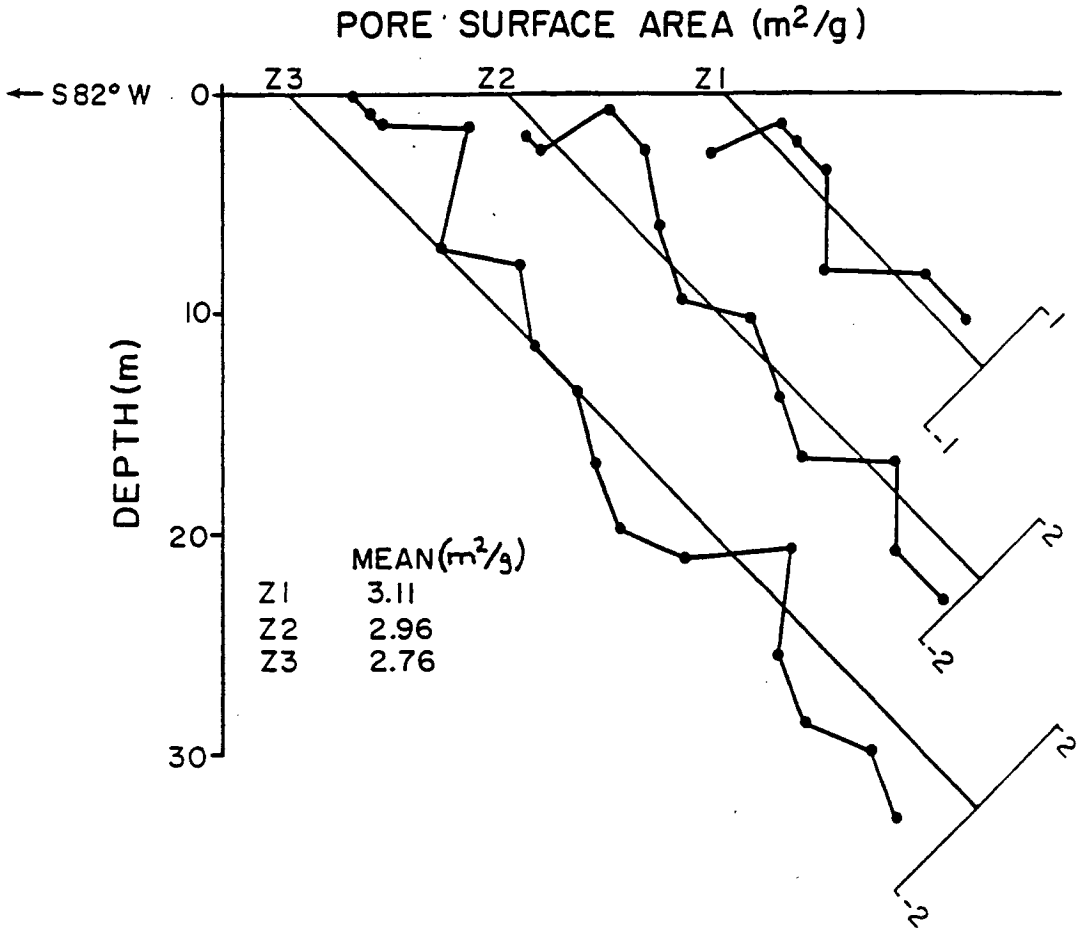

Figure 5.19. Pore surface area results from Z borehole series. Borehole axes represent mean values. Plotted points represent difference from mean.

5.1.a and 5.1.b. The bimodal pore size distribution is clearly apparent as is the unimodal pore area distribution. As expected, the pore area is skewed to the smaller pore sizes (positive skew). From table 5.4, when considering all data, only 3.72% of the pore surface area is accounted for by the large pore size class (upper modal distribution). The pore surface area gives an indication of the potential wetted area of rock at different fluid potentials. It is evident from the results that a large negative potential must exist to thoroughly dry the abundance of surface area contained in the tuff samples. The limitations of the poresizer prevented study of pores sized below 6 nm but it is expected that an even larger percentage of surface area accounted for by the smaller pore size class exists.

The strongest linear correlation of any of the parameters studied when considering all data exists between the porosity accounted for by the large pore size class and the pore surface area accounted for by the large pore size class. The correlation coefficient is 0.841 along with a positive covariance of 26.5. This suggests that a higher than average porosity percentage from the large pore size class is most likely paired with a higher than average surface area percentage from the large pore size class. In short, more large pores produce greater surface area percentage from the large pores. A scattergram plot of porosity percentage from the large pore size class (LPDPER) versus the surface area percentage from the large pore size class (LPSAPER) is shown in figure 5.21.

Generally, more surface area from the large pore size class exists with depth along the boreholes. This is in agreement with the

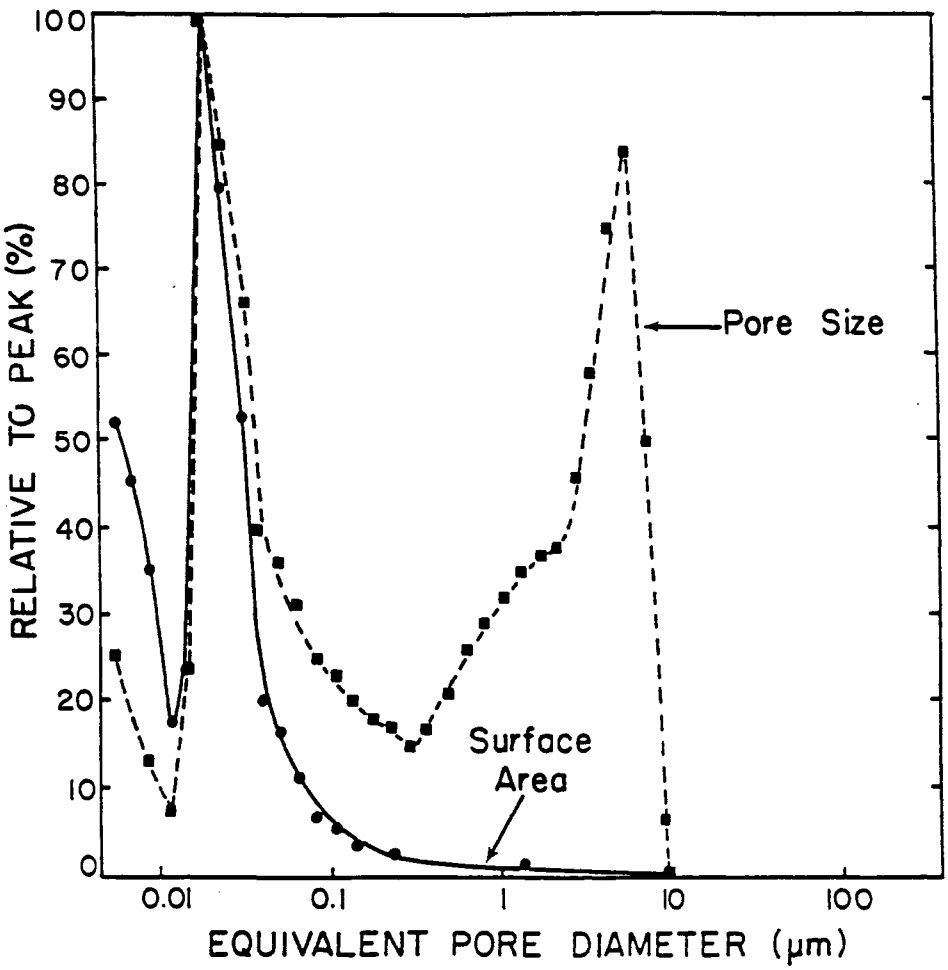

Figure 5.20. Plot of relative pore surface area and pore-size distribution vs pore diameter.

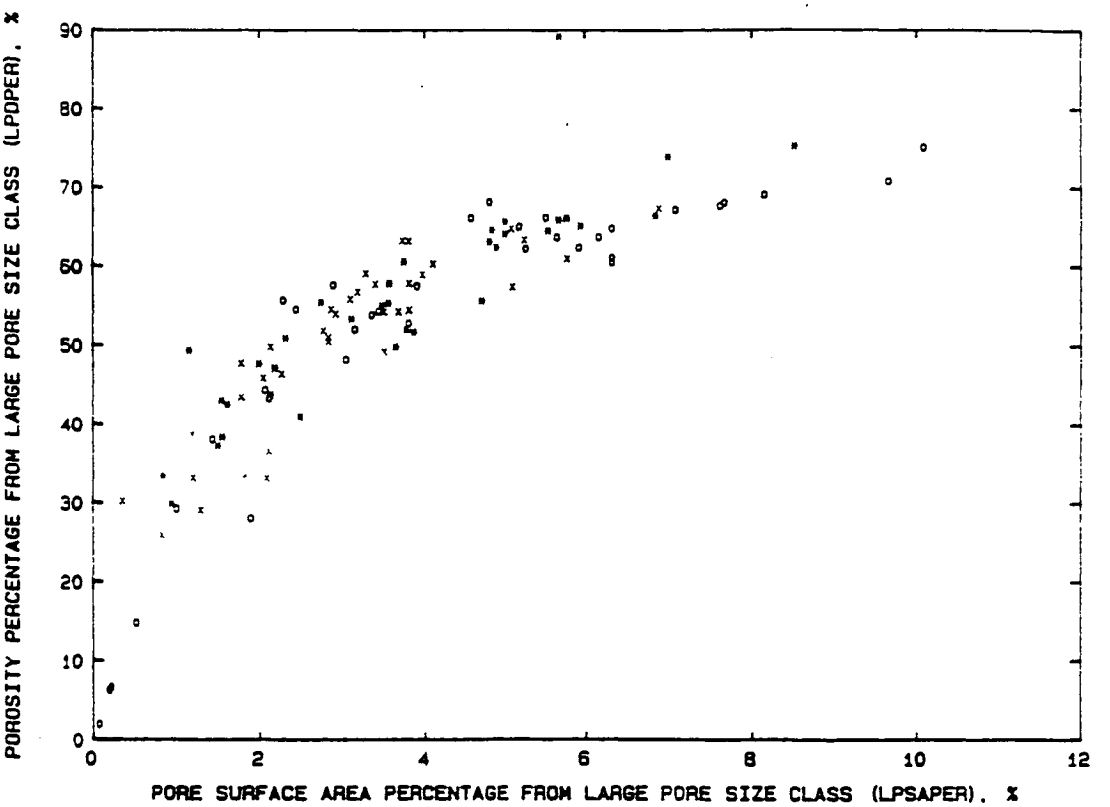

Figure 5.21. Scattergram plot of porosity percentage from large pore size class (LPDPER) vs pore surface area percentage from large pore size class (LPSAPER). X series data denoted by 'x'; Y series by 'o'; Z series by '*'.

porosity percentage increasing with depth. All of this data can be related to the moisture characteristic curve of the rock matrix. By applying capillary theory to the data on pore size distribution and using the surface area measurements, predictions as to the shape of the curve can be generated.

Mercury porosimetry determinations of surface area and porosity do not directly correspond to water availability estimates. Most of the surface area here is accounted for by small pore sizes. During mercury intrusion, mercury is forced into smaller and smaller pores. The intrusion is only a function of the pressure applied because of the non-wetting nature of mercury to most surfaces. Water, on the other hand, is held in pores by capillary tension and also around matrix particles by adhesion (see figure 5.22). A pore size distribution generated by water desaturation accounts for total removal of water, both from capillary wedges and from particle surfaces.

For this reason, the pore size distribution generated from mercury porosimetry may underestimate the water availability at a certain pressure/suction value. With a high percentage of surface area avialable from small pores, water is most likely held in greater tension but may benefit from less tortuosity in the small pore size domain. Depending on the arrangement of large and small pores, the water conducting properties of the tuff matrix could be enhanced (large pores grouped together, small pores grouped together) or hindered (pores interspersed creating a large tortuosity effect in transmission of water).

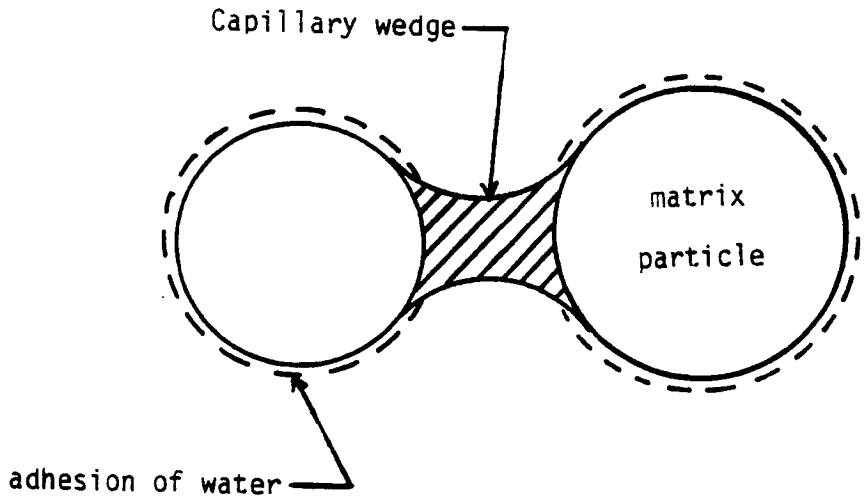

Figure 5.22. Capillary wedge and adhesion of water on matrix particle.

5.4 Spatial Variability

Recalling information presented in Chapter 3; the variogram is the arithmetic mean of the squared differences between two experimental measures Z(x) and Z(x+h) at any two points separated by the vector h. Within a certain locality, the variability between these two points is only dependent on the distance h and not on location x. A variogram (or as used here, a semi-variogram), is a tool for analyzing the spatial distribution of variables.

On average, the difference between two points or sample volumes increases as the distance between them increases. The variogram can be considered an estimation variance, that is, the variance of the error committed when the value at a point x, is estimated by a value at point (x+h). According to Journel and Huijbregts (1978) the quality of estimation depends on four factors. They are:

1) The relative distances between what is to be estimated and the information used to estimate it.

2) The size and geometry of what is to be estimated.

3) The quantity and spatial arrangement of the estimating information.

4) The degree of continuity of the phenomenon under study, which is conveyed by its characteristic semi-variogram.

Semi-variograms have been constructed for the seven parameters studied here. The variability between points Z(x) and Z(x+h) is due to several factors, each on a nested range of scales. The scales vary from sampling errors ($h \sim 0$), to the petrographic level ($h < 1$ cm) to the stratification level (h=100 m) to the province level ($h > 1$ km). All of

these scales may be acting simultaneously at all levels of h, causing data variability. It is often difficult to characterize even a single structural scale. The micro-variabilities, those at a distance less than the minimum sampling distance, are represented on the semi-variogram by a discontinuity or "nugget" at the origin.

The semi-variograms generated are contained in figures 5.23-5.29. All sample data (105 points) were used in construction of the graphs. The three dimensional variogram program GAM3D (Geomath, 1987) was utilized for this purpose. VPLOT2 (Geomath, 1987), a program designed to plot both experimental and theoretical variograms, was used to match theoretical data to experimental data. All variograms are global in the sense that they are not directional. The class size employed varied between 2.5 and 4 meters. None of the data sets were transformed.

If the semi-variogram exhibits a sill value, which is the point where the curve becomes more or less stable, the lag distance where it occurs is called the range. The sill value is simply the a priori variance of the random function $Z(x)$. The range or zone of influence defines the maximum distance at which the data are correlated.

Spherical variogram models were fit to the experimental data in figures 5.23, 5.24 and 5.26 representing BULK, porosity and LPD, respectively. The porosity value for sample SN of 47.58 was replaced by the mean value of 14.8% when generating figure 5.24. It is obvious from the data that an instrument malfunction or physical impairment of the sample occurred during the porosimetry experiment because the porosity percentage was greater than twice the maximum percentage obtained from

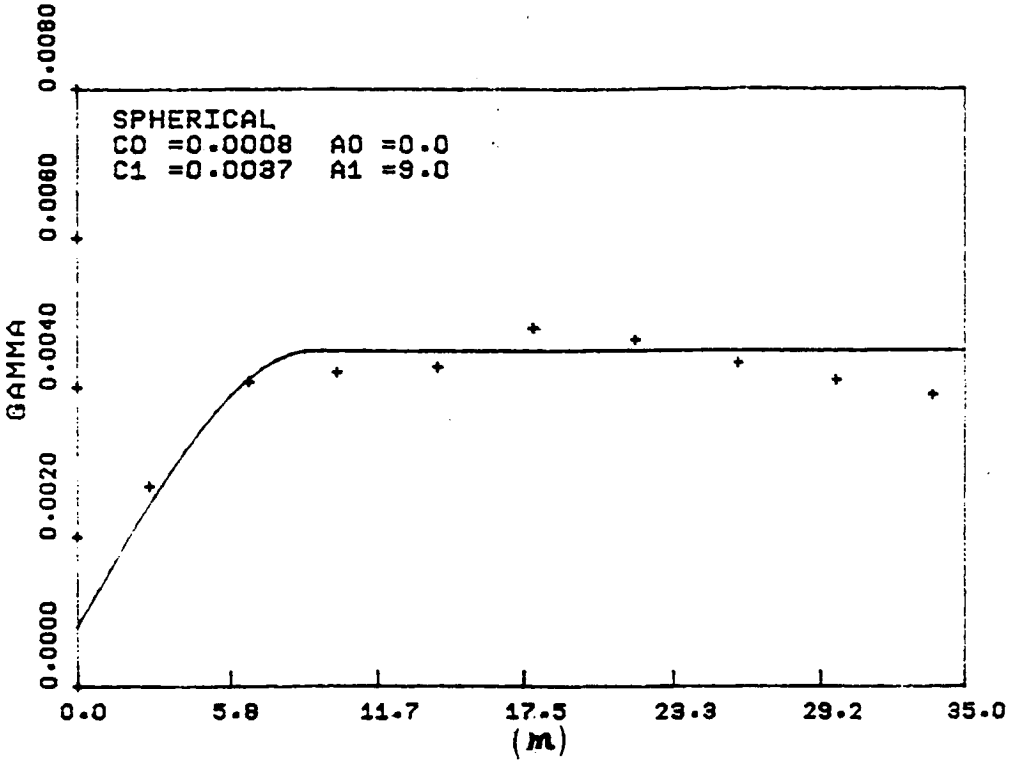

DIRECTION = 0. WINDOW = 90. MEAN = 2.130
CLASS SIZE = 4.00 VARIANCE = 0.0043
LOGARITHMS - NO NO. OF SAMPLES = 105

Figure 5.23. Semi-variogram of bulk density results.

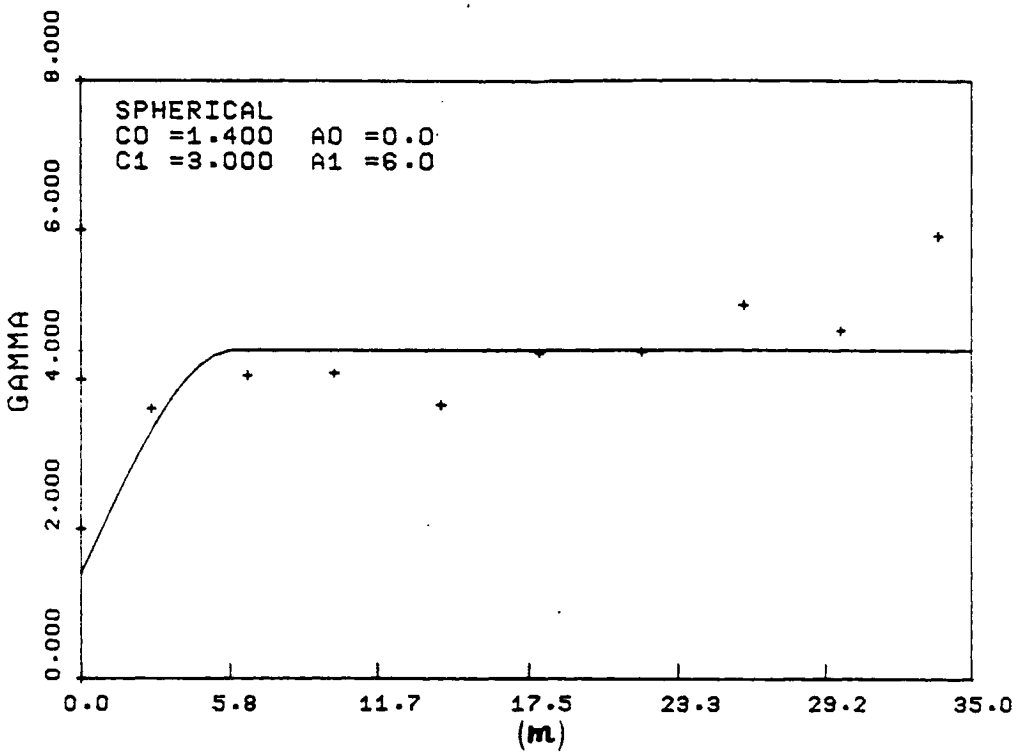

DIRECTION = 0. WINDOW = 90. MEAN = 14.300
CLASS SIZE = 4.00 VARIANCE = 4.2400
LOGARITHMS - NO NO. OF SAMPLES = 105

Figure 5.24. Semi-variogram of porosity results.

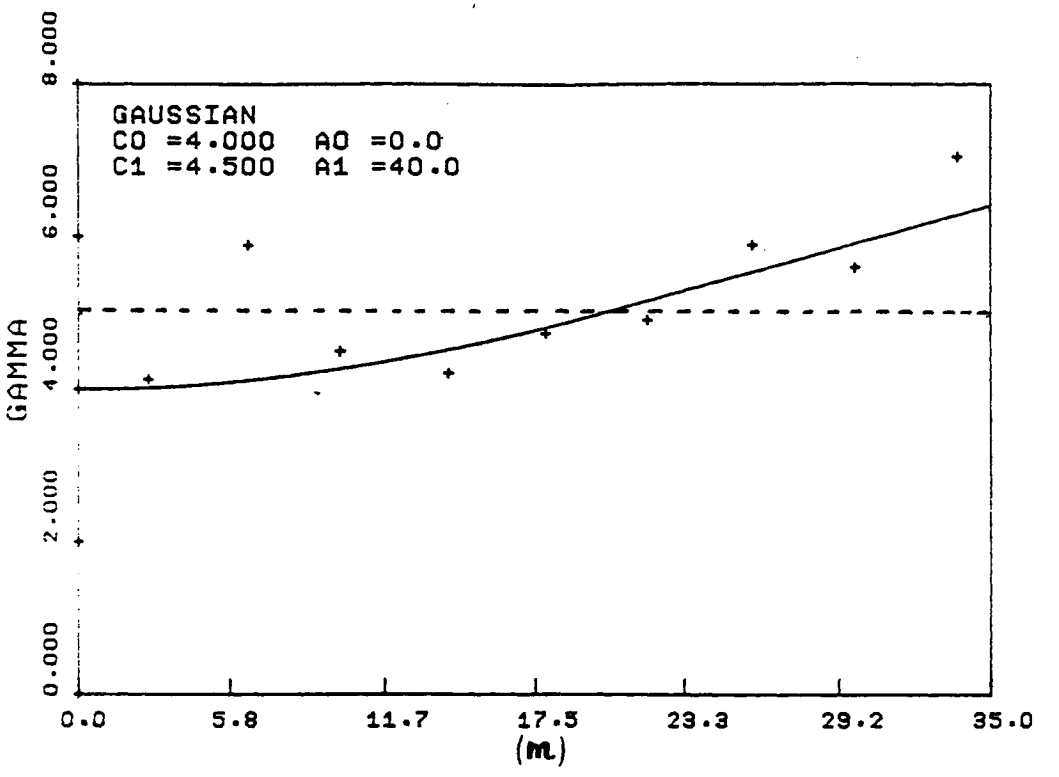

DIRECTION = 0. WINDOW = 90. MEAN = 3.470
CLASS SIZE = 4.00 VARIANCE = 5.0600
LOGARITHMS - NO NO. OF SAMPLES = 105

Figure 5.25. Semi-variogram of pore surface area results. Dotted line represents pure nugget effect (random variogram--no correlation).

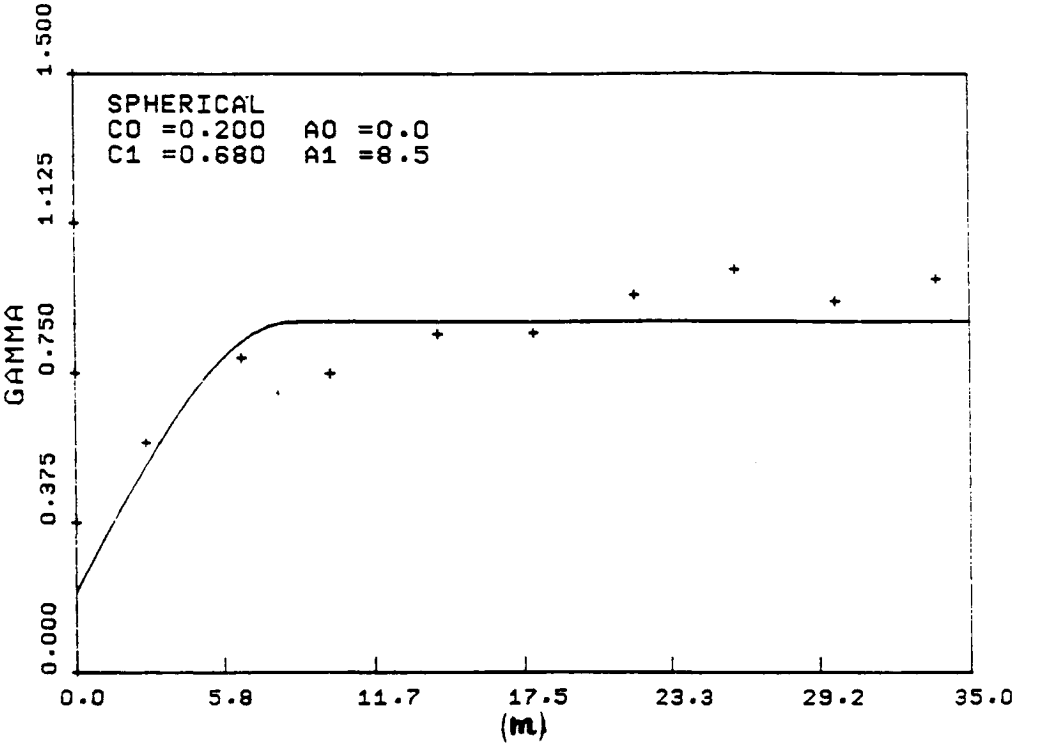

DIRECTION = 0. WINDOW = 90. MEAN = 2.910
CLASS SIZE = 4.00 VARIANCE = 0.8630
LOGARITHMS - NO NO. OF SAMPLES = 105

Figure 5.26. Semi-variogram of mode diameter of large pore size class results.

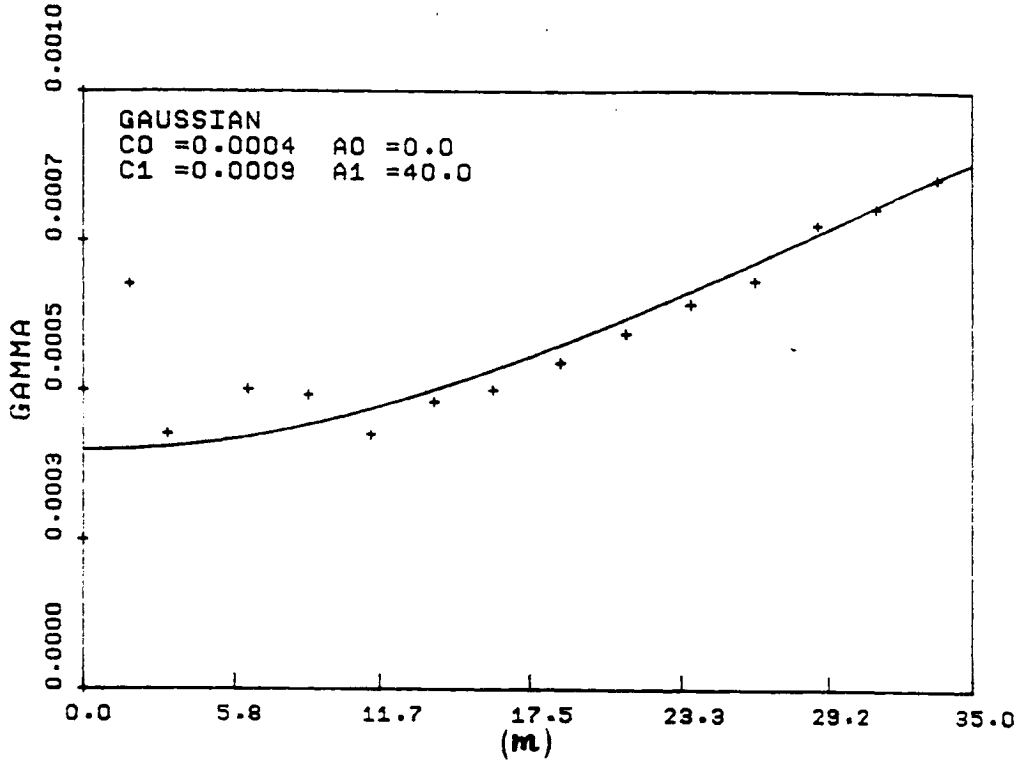

DIRECTION = 0. WINDOW = 90. MEAN = 0.066
CLASS SIZE = 2.50 VARIANCE = 0.0006
LOGARITHMS - NO NO. OF SAMPLES = 105

Figure 5.27. Semi-variogram of mode diameter of small pore size class results.

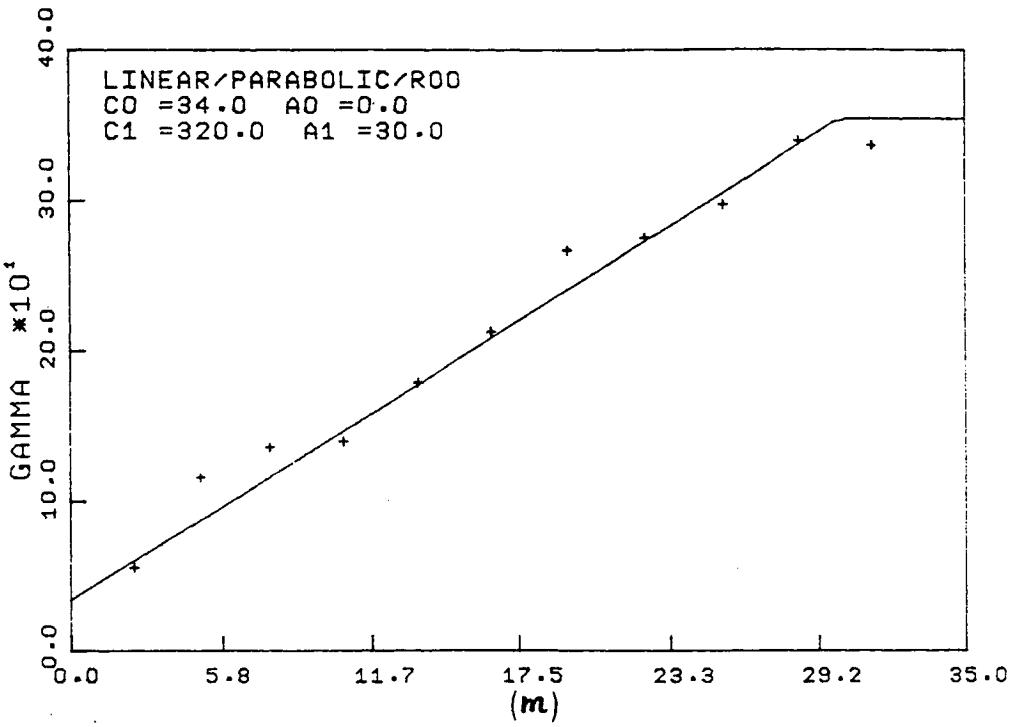

DIRECTION = 0. WINDOW = 90. MEAN = 52.700
CLASS SIZE = 3.00 VARIANCE = 222.0000
LOGARITHMS - NO NO. OF SAMPLES = 105

Figure 5.28. Semi-variogram of porosity percentage from large pore size class results (LPDPER).

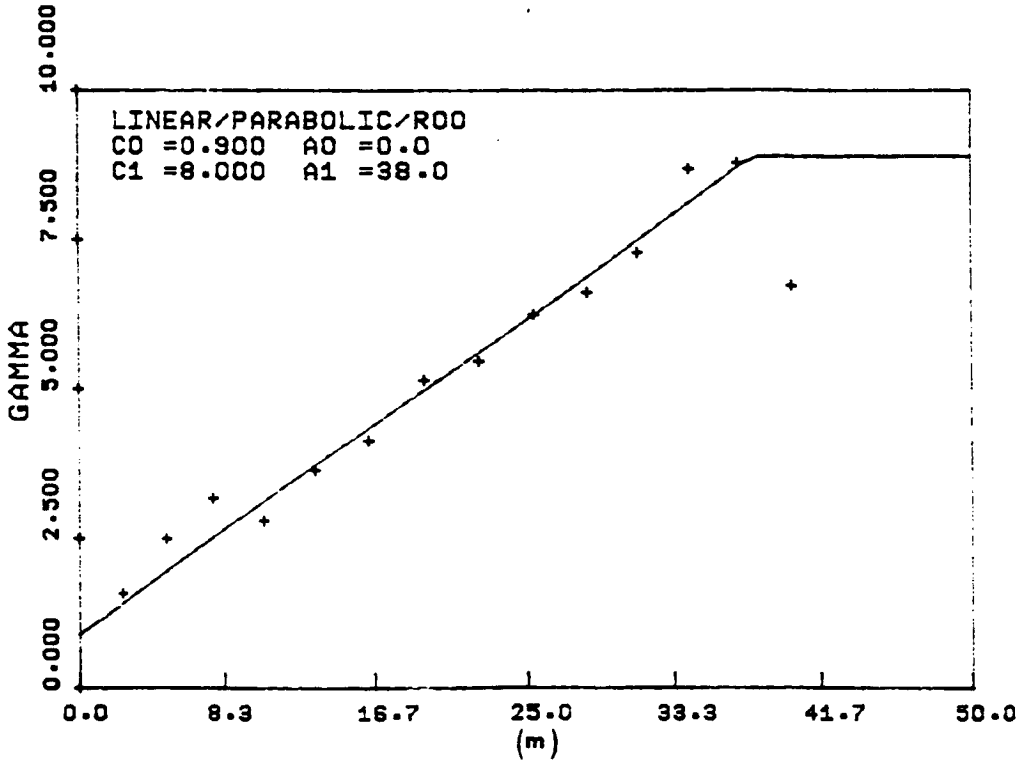

DIRECTION = 0. WINDOW = 90. MEAN = 3.710
CLASS SIZE = 3.00 VARIANCE = 4.4800
LOGARITHMS - NO NO. OF SAMPLES = 105

Figure 5.29. Semi-variogram of pore surface area percentage from large pore size class (LPSAPER).

any of the other samples. The nugget, range and sill of these three semi-variograms are presented in table 5.5. These three parameters in particular show very good structure of the study site deposit. The local range of influence varies between 6 and 8.75 m. This is not the range of influence for these parameters for the whole deposit but just for the study site area. Kim (personal communication 1988) has shown a range of influence for porosity structure in the horizontal direction of several kilometers for similar material from the Nevada Test Site. Notice the good agreement between the sample variance and the sill values of the semi-variograms. Usually the sample variance is used as a first approximation for the sill. In this case the variance is a "best" approximation.

The nugget effect is very minimal for the bulk density values. This suggests both a strong sampling procedure and minimal scale effects. The higher nugget values for both porosity and LPD are probably a function of the testing technique and the tuffaceous material. Porosity variations of over 1% may well be accounted for by core cutting and sample cutting from the cores. The porosity percentage could certainly vary by 1.5% across the face of the 6 cm diameter core

TABLE 5.5 Semi-variogram results from figures 5.23, 5.24 and 5.26.

SAMPLE PARAMETER	NUGGET	RANGE (m)	SILL	VARIANCE
BULK	.0008	8.75	.0045	.0043
POROSITY	1.4	6.0	4.40	4.24
LPD	.2	8.2	.88	.86

because of the composition of the tuff. The nugget of 0.2 for the mode diameter of the large pore size class is relatively small. The histogram results are plotted on a logarithmic scale and a variation of one bar width on the histogram results in a diameter difference of greater than 0.2 for the upper pore size class.

Gaussian models were fit to the PAREA and SPD data sets shown in figures 5.25 and 5.27. The effective range of a gaussian model is the square root of 3 times its range (Geomath, 1987). The effective range for each figure is approximately 11 meters. The nugget for pore area is relatively high. The higher range and scale effect may play a significant role in producing a high nugget for PAREA. A larger range of sampling may reduce the appparent discontinuity at the origin. The PAREA semi-variogram may also represent an absence of spatial correlation or pure nugget effect represented by the dotted line on figure 5.25. With this interpretation, spatial independence exists at all scales presented and the best estimator at any point in the deposit is the mean value. The SPD semi-variogram is subject to the same restrictions as the LPD only to a higher degree because of the greater relative difference in histogram bar widths.

Linear models best estimated the LPDPER and LPSAPER data in figures 5.28 and 5.29. Linear models do not exhibit sill values so the models were constructed with an estimated sill value. A close inspection of these figures shows a fairly high degree of correlation between the shapes of the two data sets. The correlation is supported by the 0.841 correlation coefficient generated from the regression of

figure 5.21. High nugget values reflect the variability of the deposit with respect to the bimodal distribution of pore size.

Overall, a definite structure exists in the tuffaceous deposit. This data may be helpfull in determining sampling schemes for further study into tuffaceous deposits being considered for high level nuclear waste repositories.

5.5 Comparison With Other Methods

Porosity is related to bulk density and grain density by equation 5.1.

$$\text{Porosity} = 1 - (\text{bulk density}/\text{grain density}) \qquad (5.1)$$

Porosity and bulk density were determined on the Apache Leap Tuff core by two different methods, mercury porosimetry and water saturation in

TABLE 5.6 Comparison of methods to determine bulk density, porosity, and grain density. M.P. = Mercury Porosimetry. SAT = Water Saturation. Sample size for M.P. = 2.5 cm diameter by 2.5 cm long. Sample size for SAT = 6 cm diameter by 5 cm long.

	BULK DENSITY (gm/cm^3)		EFFECTIVE POROSITY (%)		GRAIN DENSITY (gm/cm^3)	
	M.P.	SAT	M.P.	SAT	M.P.	SAT
MAXIMUM	2.25	2.20	47.58	25.77	4.11	2.68
MINIMUM	1.94	1.86	9.18	14.49	2.21	2.34
MEAN	2.13	2.10	14.62	17.67	2.50	2.55
MEDIAN	2.14	2.12	14.31	17.39	2.51	2.56
COEF OF VAR	.03	.03	.26	.12	.07	.02

the case of porosity and mercury porosimetry and physical measuring and weighing in the case of bulk density. The data are found in Appendix B. Figures 5.30 - 5.32 show bulk density variation along the boreholes. Table 5.6 gives a synopsis of all data. Figure 4.1 shows a breakdown of a typical 10 cm length of core and the lengths of each tested section.

In comparing the results from different methods, mercury intrusion is in good agreement with the physically determined bulk density values. Both methods have a coefficient of variation of 0.03. When comparing mercury intrusion to water saturation to measure porosity, the mean porosity is near 18% less than the value determined from water saturation. This difference can be accounted for by the maximum pressure applied during intrusion. Commercial porosimeters are available which intrude mercury to a maximum pressure of 410 MPa. Porosity determinations with these instruments would approach total porosity. The variation in sample size between the two methods may also account for some of the difference. Therefore, mercury intrusion is a valid procedure in determining porosity as long as its limitations are considered.

The difference in grain density is accounted for by the porosity difference and equation 5.1. The maximum grain density of 4.11 gm/cm^3 from sample SN is not a true indication of grain density. A porosity value of 47.58 generated from the intrusion results is in error, causing the large grain density value. Evaluating the original data output shows a porosimeter malfunction for this sample run.

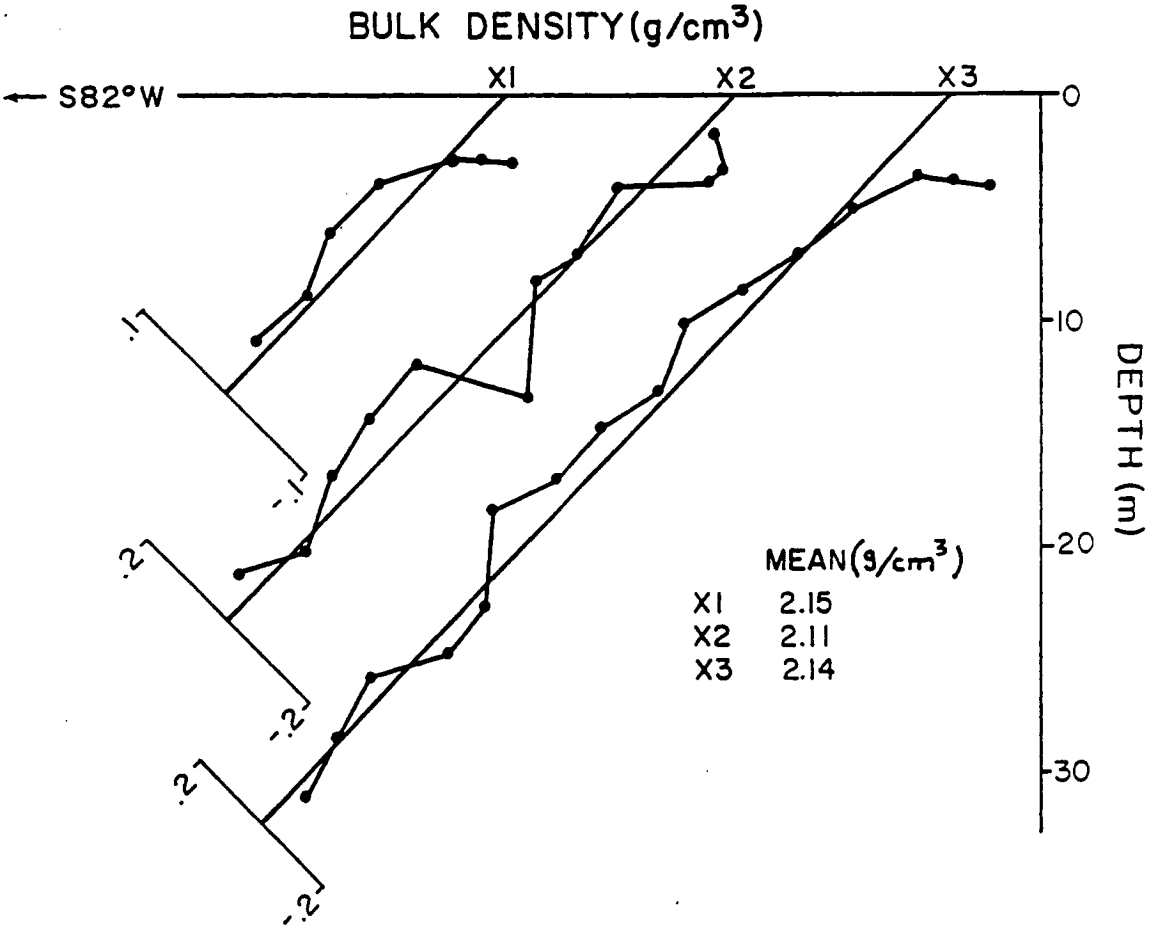

Figure 5.30. Bulk density results from X series boreholes. Borehole axes represent mean values. Plotted points represent difference from mean.

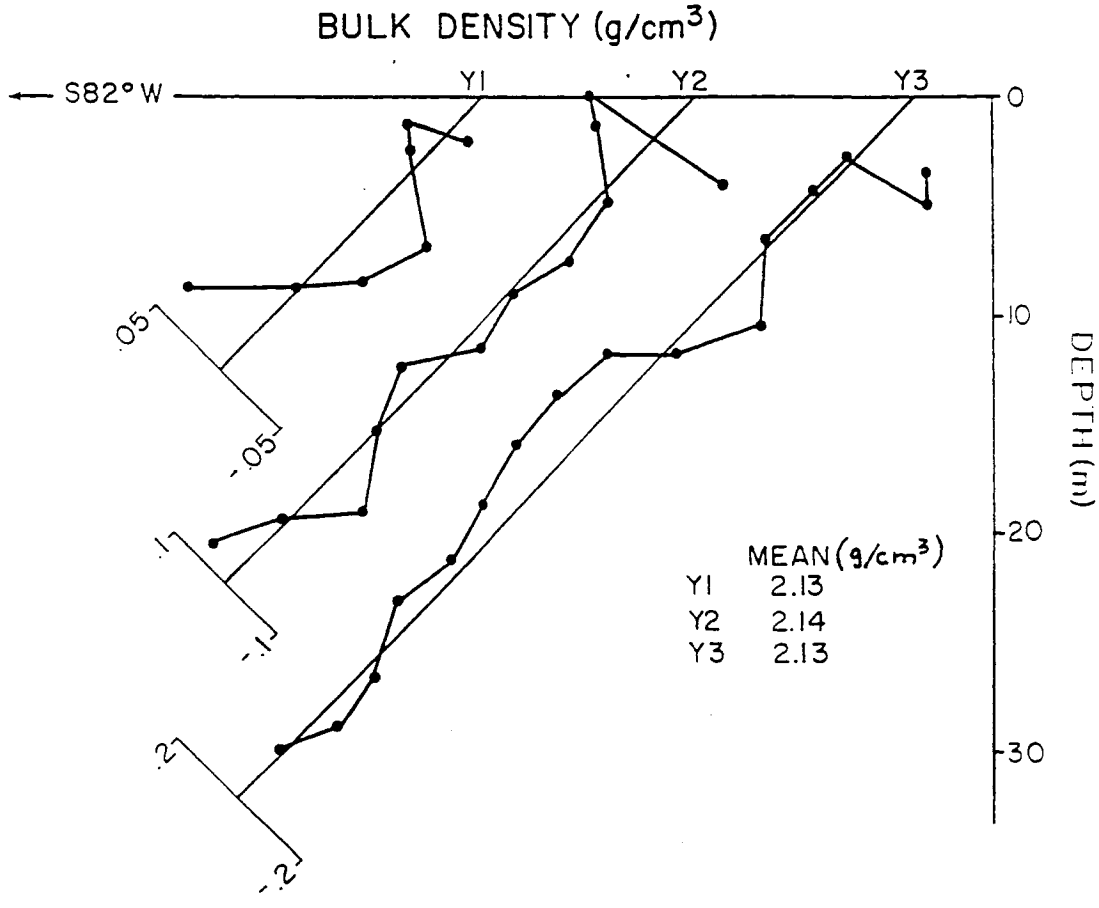

Figure 5.31. Bulk density results from Y series boreholes. Borehole axes represent mean values. Plotted points represent difference from mean.

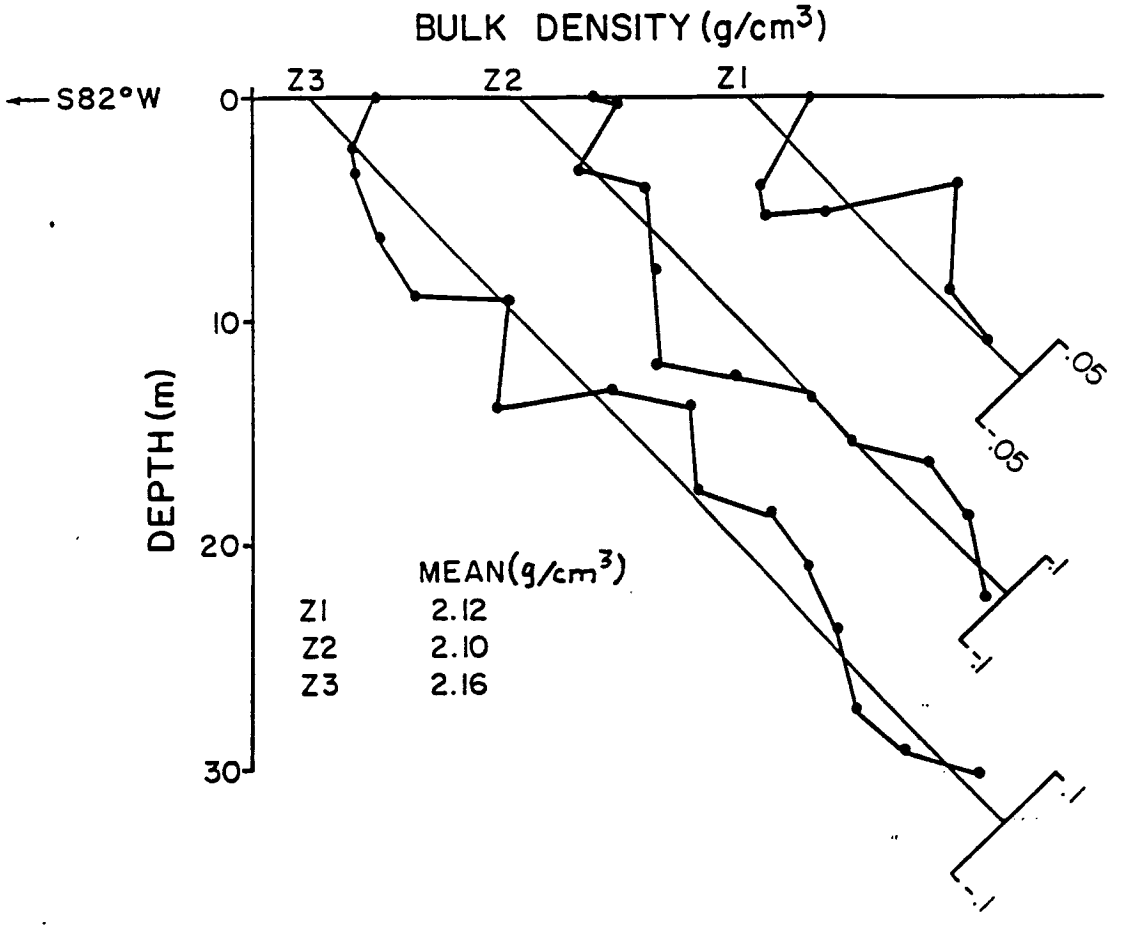

Figure 5.32. Bulk density results from Z series boreholes. Borehole axes represent mean values. Plotted points represent difference from mean.

5.6 Comparison With General Trend of the Area

To get an indication of rock properties outside of the study site location, 8 samples were obtained along the roadside of the Magma Mine Road between US Highway 60 and the study site. Sample locations were chosen at approximate 30 m elevation intervals. A modified chain saw equipped with a 15 cm diamond coring bit 2.9 cm in diameter was used to drill out each sample. In an attempt to minimize surface effects, the outside 5 cm of core was cut off and discarded.

The roadside samples were gathered and analyzed for 2 reasons. They are: 1) For a general comparison with the study site location; and 2) To act as an indicator for any blatent heterogeneity present in the deposit. A statistical summary of results appears in table 5.7. All sample means from the 8 roadside samples are within 2 standard deviations of the study site means. A t-test (Miller and Freund, 1977) was performed on the sample means for each of the variables from the study site and the roadside. A significant difference occurred between the two means for the variables PAREA and LPSAPER. When comparing the

TABLE 5.7 Summary statistics From Magma Mine Road samples. Number of samples = 8.

SAMPLE PARAMETER	MEAN	VARIANCE	SKEW	COEF OF VARIATION
BULK (gm/cm^3)	2.15	.005	1.45	.03
POROSITY (%)	14.98	7.54	-.49	.18
PAREA (m^2/gm)	2.521	.42	-.06	.26
LPD (um)	2.64	.47	.41	.26
SPD (um)	.096	.004	1.92	.67
LPDPER (%)	62.86	373	-.74	.31
LPSAPER (%)	6.21	10.4	-.07	.52

coefficient of variation between the two data sets, only the SPD variation is significantly higher than the study site sample data set. The coefficient of variation is perhaps the only variable that can be compared because of the drastic difference in the number of sample points for each set.

Because of the minimal number of samples from the roadside data set it is difficult to confidently present any data trends. All sample parameters were regressed against each other and certain trends emerged. Two trends or corrleations that were most important were those of pore surface area, PAREA, versus the porosity percentage from the large pore size class, LPDPER, and LPDPER versus the surface area percentage from the large pore size class, LPSAPER. These two correlations showed the strongest linearity, -.69 and .84, respectively, from the study site samples. Data from the roadside samples produced correlation coefficients of -.77 and .96 for PAREA versus LPDPER and LPDPER versus LPSAPER, respectively. This analysis supports the homogeneity of the tuffaceous deposit.

Samples were also obtained from 8 other locations near the study site representing the gray zone (moderately welded) and the brown zone (densely welded) of the Apache Leap Tuff (See figure 2.3). Gray zone samples were drilled along the roadcut of US Highway 60 in Queen Creek Canyon above the new highway tunnel on the north side of the road. Brown zone samples were drilled out of the exposed bedrock just west of the tunnel of old US Highway 60 (see figure 2.1). The coring device mentioned above was used for this purpose.

A statistical summary is given in table 5.8. The upper pore size class is absent from the data results obtained by mercury porosimetry from the 2 lower tuffaceous units. This results in reduced porosity and greater bulk density. Pore surface area is increased as more of the porosity is accounted for by the pore sizes of less than 1 micrometer. Porosities ranged from 5.4% to 8.7% for the moderately welded to densely welded samples. The greater degree of compaction and degassing of the deposit as it cooled played a major role in the decreased porosities.

TABLE 5.8 Summary statistics for brown (densely welded) and gray (moderately welded) zones of Apache Leap Tuff. Four samples per data set. Upper set is from the gray, lower brown.

SAMPLE PARAMETER	MEAN	VARIANCE	SKEW	COEF OF VARIATION
BULK (gm/cm^3)	2.45	.0004	-.02	.009
POROSITY (%)	5.91	.171	-.78	.07
PAREA (m^2/gm)	3.31	.10	.17	.09
SPD (%)	.047	.0003	1.52	.34
BULK (gm/cm^3)	2.33	.0004	.53	.009
POROSITY (%)	7.22	1.72	.16	.18
PAREA (m^2/gm)	6.60	2.19	.62	.22
SPD (%)	.024	.0002	.86	.58

CHAPTER 6

CONCLUSIONS

Mercury porosimetry methods were utilized to determine porosity, bulk density, pore-size distribution and pore surface area of over 120 samples of slightly welded to densely welded volcanic tuff. Conclusions generated from the statistical data analysis, follow.

1) The mean and standard deviation of the nine parameters studied are:

- Interconnected porosity to 6 nm pore diameter (Porosity)
  mean = 14.62% st. dev. = 3.83%

- Bulk density (BULK)
  mean = 2.13 gm/cm^3 st. dev. = .063 gm/cm^3

- Pore surface area (PAREA)
  mean = 3.46 m^2/gm st. dev. = 2.24 m^2/gm

- Mode diameter of large pore size class (LPD)
  mean = 2.91 μm st. dev. = .93 μm

- Mode diameter of small pore size class (SPD)
  mean = .07 μm st. dev. = .024 μm

- Percentage of measured porosity from large pore size class (LPDPER)
  mean = 52.73% st. dev. = 14.9%

- Percentage of measured porosity from small pore size class (SPDPER)
  mean = 47.27% st. dev. = 14.7%

- Percentage of pore area from large pore size class (LPSAPER)
  mean = 3.72% st. dev. = 2.12%

- Percentage of pore area from small pore size class (SPSAPER)
  mean = 96.28% st. dev. = 1.93%

2) A bimodal pore-size distribution exists for samples of slightly welded tuff of the Apache Leap study site. The distributions are described in terms of the modes of the pore diameters from each pore size class, upper (large) and lower (small).

3) Porosity results from mercury porosimetry are in relative terms 18% lower than the saturation method compared here.

4) The lower pore size class accounted for most of the surface area of the pores which averaged 3.47 m^2/gm. The range of percentage of surface area accounted for by the lower pore size class varied from 89.91% to 99.93%.

5) Sample parameters of bulk density, porosity and mode diameter of the upper pore size class showed the strongest structural trends in the analysis of spatial variability. The local range of influence for these 3 parameters varied between 6 and 9 m. The range of influence in the study site location for pore area is approximately 11 meters. The range of influence here should not be confused with the range of influence of the entire tuffaceous deposit which could be as high as several kilometers.

6) Overall, more porosity was accounted for by the upper pore size class as the distance from the land surface increased. A similar correlation exists for the pore area percentage accounted for by the upper pore size class.

7) The best linear correlation exhibited between two parameters was found between the porosity percentage from the upper pore size class and pore area percentage of the large pore size class. The correlation coefficient was 0.841.

8) Samples of the moderately welded to densely welded tuff exhibited a near log-normal distribution with respect to pore size with the mode diameter averaging 0.035 μm.

9) Mercury porosimetry measurements in excess of 200 MPa applied pressure are needed to fully determine porosity of the tuff samples. Pore diameters less than 6 nm were not measured by the poresizer because of instrument limitations. A significant percentage of total porosity exists below the 6 nm range for the slightly to densely welded tuff samples studied here. A quantitative measure of the percentage of total porosity less than 6 nm is accounted for by the comparison of mercury porosimetry results to water saturation results.

10) Porosimetry results agree strongly with physical measurement results in terms of bulk density determinations.

11) Mercury porosimetry may underestimate the water content at high suction values because of the adhesion layer effect of water on matrix particles.

12) Mercury intrusion results compare more favorably to water desaturation curves when considering the functional pressure relationships of the matrix geometry. In short, large pores are intruded with mercury before smaller pores. This compares directly with larger pores emptying first when a suction is present in terms of water desaturation.

APPENDIX A

MERCURY INTRUSION PROCEDURES

Contained in this appendix is a complete step-by-step procedural guide to mercury porosimetry as it applies to this study. Original procedures and guidelines were supplied by Micromeritics Corporation (1986).

DIRECTIONS FOR MERCURY INTRUSION

1. Make sure core sample is cut to proper specifications (26 mm diam. x 26 mm long **maximum**).

2. Oven dry samples until further weight loss is negligible. This is usually a minimum of 48 hours.

3. Place oven dry samples into small aluminum containers, mark with id number, and seal.

4. When ready for intrusion test, remove the sample from the aluminum container, weigh it, and record the weight.

5. Using the proper penetrometer (see page 3-4 of manual) lightly grease the ground joint of the penetrometer cap with Apiezon grease.

6. Place sample into penetrometer cup, cap it and seal with appropriate spring assembly.

7. Reweigh sample and penetrometer assembly and record the weight.

8. Repeat steps 4 through 7 using a different penetrometer and sample if analyzing two samples at once.

9. Install the penetrometers into the right and left preparation ports on the front of the poresizer 9310. To do this, remove the capacitance detector, turn the port counterclockwise to loosen, and remove the dummy rod. Install the assembled penetrometer (lightly greased with vacuum grease on the capillary end of the rod) and tighten the port.

10. Make sure either a dummy rod or penetrometer fills both ports before evacuating the system.

11. At this point load the poresizer program into the IBM PC. Put the Micromeritics Program disc into drive A and the Data disc in drive B. It will respond with a prompt to turn on the poresizer. Do this by engaging the switch on the front of the poresizer. A prompt will appear asking if a pen plotter will be used. Respond with a carriage return (CR). The menu table will now appear on the screen.

12. Press the "EVACUATE SLOW" button and the "LOW PSIA" button on the front of the poresizer. Note the atmospheric pressure reading on the poresizer. Turn on the vacuum pump. When the pressure drops below 0.5 psia, push the "um Hg" button and the "FAST EVACUATE SAMPLE" button.

13. The pressure should drop rather rapidly to between 500 and 700 microns. To test for leaks in the evacuation system, depress the "EVACUATE SAMPLE" buttons and watch the pressure reading. If it increases rapidly there is a leak in the system. The leak is probably around the penetrometer stem where it seats into the preparation port. Move the penetrometer back and forth and see if the leak subsides. (the penetrometer should not move more than 1 cm in and out.) Press the "FAST EVACUATE SAMPLE" button again and see if the pressure starts decreasing. The optimal vacuum is near 50 μm.

14. When the "best" vacuum is reached, press the "MERCURY FILL" switch. You have to manually hold the switch in for mercury to fill into the penetrometers. Hold the "MERCURY FILL" switch in until the red "UP" light comes on.

15. Release the fill button. Release the "FAST EVACUATE SAMPLE" button. Shift the pressure reading back to low psia by pressing the "LOW PRESSURE PSIA" button.

16. Momentarily press the "ADJUST LOW PRESSURE" button until the pressure is between 0.5 and 1.5 psia.

17. **IMPORTANT:** Press the "EVACUATE RESERVOIR" button. The pump will return to its normal operating sound in 20 to 30 seconds. This step is important because the mercury needs to be released from the "up" position. It is paramount that the reservoir is at the same potential as the rest of the system or a mercury leak could occur. **DO NOT RELEASE THE "EVACUATE RESERVOIR" BUTTON.**

18. Hold the "MERCURY DRAIN" button in until the green "down" indicator illuminates on the front panel. Release the "MERCURY DRAIN" button. Now release the "EVACUATE RESERVOIR" button. You can shut off the vacuum pump at this stage.

19. Depress the "ADJUST LOW PRESSURE" button until the pressure reaches atmospheric.

20. The low pressure/sample preparation run is now complete. Remove the penetrometers and reweigh them.

NOTE

While the vacuum pump is evacuating the sample(s) you can be entering data for the run. Below is a listing of what you will see appear on the screen. Follow the step by step procedure as given in the example below.

LISTINGS FROM MICROMERITICS PROGRAM

Quotation marks indicate a keyboard entry (do not enter the quotation marks). Bold face type indicates a comment on a particular section of the program.

9 3 1 0 P R O G R A M M E N U

(1) LOW PRESSURE OPERATION

(2) MANUAL HIGH PRESSURE OPERATION

(3) AUTOMATIC HIGH PRESSURE OPERATION

(4) PRESSURE TABLE EDIT

(5) RATE SEQUENCE EDIT

(6) PRINTER REPORT

(7) PEN PLOT

(8) STORE SAMPLE DATA

(9) RETRIEVE SAMPLE DATA

(10) RETURN TO DOS MONITOR

ENTER NUMBER FOR DESIRED SELECTION AND PRESS <RETURN>: "1"

- -

FINISHED WITH ALL PREVIOUS SAMPLES (Y/N)

Make sure previous sample data is stored. If it is, then <CR>.

- -

WILL A SAMPLE BE RUN IN THE LEFT LOW PRESSURE PORT (Y/N/RETURN=Y)

"<CR>"

ENTER SAMPLE INFORMATION FOR LEFT PORT PENETROMETER

(1) ENTER SAMPLE I.D. MAX 35 CHAR. "X-2 GC-2 5.5-6.0 No.1"

(2) ENTER SUBMITTED I.D. MAX 35 CHAR. "GTV"

(3) ENTER DATE OF ANALYSIS MAX 10 CHAR. "AUG 1 87"

(4) ENTER TIME OF ANALYSIS MAX 10 CHAR. "1200"

(5) ENTER PENETROMETER NO. "4"

(6) ENTER PENETROMETER CONST. (uL/pF) DEFAULT=10.79 "33.13"

(7) ENTER PEN VOL. (cc) DEFAULT=5.0 "18.226"

(8) ENTER PEN STEM VOL. (cc) DEFAULT=0.412 "3.226"

(9) ENTER HEAD CORRECTION FACTOR DEFAULT=4.68 "4.45"

(10) ENTER SAMPLE WEIGHT (g) DEFAULT=1.0 "25.67"

(11) ENTER SAMPLE+PEN WEIGHT (g) DEFAULT=2.0 "97.76"

(12) ENTER CONTACT ANGLE (degrees) DEFAULT=130 "<CR>"

(13) ENTER SURFACE TENSION (dynes/cm) DEFAULT=485 "<CR>"

(14) ENTER Hg DENSITY (g/cc) DEFAULT=13.5335 "<CR>"

(15) REPORT IN RADIUS OR DIAMETER (R/D) DEFAULT=D "<CR>"

---

(1) SAMPLE I.D. =X-2 GC-2 5.5-6.0 No.1

(2) SUBMITTER I.D. =GTV

(3) DATE =AUG 1 87

(4) TIME =1200

(5) PEN. NO. =4

(6) PEN. CONST. =33.13

(7) PEN. VOL. =18.226

(8) PEN. STEM VOL. =3.226

(9) HEAD CORR. FACTOR =4.45

(10) SAMPLE WEIGHT =25.67

(11) SAMPLE+PENETROMETER WEIGHT =97.76

(12) CONTACT ANGLE =130

(13) SURFACE TENSION = 485

(14) Hg DENSITY =13.5335

(15) REPORT IN DIAMETER

ALL OK (Y/N/RETURN=Y) **If yes, then <CR>**

DO YOU WANT A PRINTER REPORT TO BE AUTOMATICALLY PRINTED AFTER THE HIGH PRESSURE RUN IS COMPLETED (Y/N) "N"

- -

WILL A SAMPLE BE RUN IN THE RIGHT LOW PRESSURE PORT (Y/N/RETURN=Y) "N"

- -

INSTRUCTIONS FOR LOW PRESSURE RUN

1. INSTALL ASSEMBLED PENETROMETER(S) AND/OR DUMMY ROD(S) IN BOTH PORTS.

2. DEPRESS EVACUATE SAMPLE SLOW AND LOW PSIA PRESSURE TRANSDUCER BUTTONS.

3. TURN ON POWER SWITCH FOR VACUUM PUMP.

4. WHEN PRESSURE DROPS TO 1 PSIA (SEE MANUAL IF RUNNING A POWDER), RELEASE EVACUATE SAMPLE SLOW BUTTON AND DEPRESS EVACUATE SAMPLE MED and um PRESSURE TRANSDUCER BUTTONS.

5. BEWARE OF SAMPLE FLUIDIZATION.

6. WHEN PRESSURE DROPS TO 250 um, RELEASE MED EVACUATE SAMPLE BUTTON AND DEPRESS FAST EVACUATE BUTTON.

7. INSTALL CAPACITANCE DETECTORS OVER PENETROMETER ASSEMBLIES.

8. WHEN PRESSURE DROPS TO 50 um (OR HAS EQUILIBRATED AT SOME LOWER PRESSURE), DEPRESS Hg FILL BUTTON MOMENTARILY. IF LOSS OF VACUUM, ALLOW LONGER EVACUATION, OTHERWISE HOLD UNTIL Hg UP LIGHT IS ON. IF LIGHT GOES OUT, DEPRESS Hg FILL BUTTON UNTIL LIGHT COMES ON AGAIN.

9. PRESS 'SPACE-BAR' TO CONTINUE.

10. TURN OFF EVACUATE FAST SAMPLE BUTTON AND CHANGE FROM um TO LOW PSIA PRESSURE TRANSDUCER.

11. MOMENTARILY PRESS ADJUST LOW PRESSURE BUTTON UNTIL PRESSURE IS BETWEEN 0.5 AND 1.5 PSIA.

12. DEPRESS EVACUATE RESERVOIR BUTTON AND WAIT 20 TO 30 SECONDS OR UNTIL SOUND FROM VACUUM PUMP RETURNS TO NORMAL. DO NOT RELEASE THE EVACUATE RESERVOIR BUTTON.

13. PRESS 'SPACE-BAR' TO CONTINUE.

TAKE BASE LOW PRESSURE AND INTRUSION READINGS AS FOLLOWS:

1. DEPRESS MERCURY DRAIN BUTTON UNTIL MERCURY DOWN LIGHT COMES ON.

2. RELEASE EVACUATE RESERVOIR BUTTON AND MERCURY DRAIN BUTTON.

3. TO TAKE BASE LOW PRESSURE AND CAPACITANCE READINGS, PRESS 'SPACE-BAR'.

4. IF THE DATA IS OK, PRESS 'RETURN'.

5. LEFT PENETROMETER LOCATION BUTTON AND RIGHT PENETROMETER LOCATION BUTTON ARE IGNORED AND CAN BE IN ANY POSITION.

WAIT APPROXIMATELY 10 SECONDS FOR READINGS

LOW PRESSURE =13.1 PSI

LEFT CAPACITANCE = 112.34 pF

RIGHT CAPACITANCE = 111.87 pF

ALL OK (Y/N/RETURN=Y/SPACE=ANOTHER BASE READING) "<CR>"

POINT NO.	PRESSURE (PSIA)	LEFT CAPACITANCE (pF)	RIGHT CAPACITANCE (pF)
1	13	112.34	111.87

- -

'SPACE-BAR' = TAKE ANOTHER READING 'F9' = STOP DATA COLLECTION

"Press F9"

1. RETURN THE SYSTEM TO ATMOSPHERIC PRESSURE BY LIGHTLY TAPPING THE SLOW EVACUATION BUTTON UNTIL A PRESSURE BETWEEN 13.5 - 14.0 PSIA IS REACHED.

2. THE LOW PRESSURE RUN IS NOW COMPLETE. REMOVE THE PENETROMETER(S) AND REWEIGH IT (THEM).

3. PRESS 'SPACE-BAR' TO CONTINUE

ENTER LEFT PEN+SAM+Hg WEIGHT (g) DEFAULT=3.0 "165.78"

LEFT PEN+SAM+Hg WEIGHT = 165.78 G

ALL OK (Y/N/RETURN=Y) "<CR>" if all is OK

HIGH PRESSURE RUN

IMPORTANT

Before running the high pressure test make sure the hydraulic ram in the high pressure chamber is at its lowest limit. You can check this by pressing the scan down switch near the lower left corner of the poresizer. Press the switch to down and wait for the motor to stop running. Now bring the switch back to the neutral position. Now start the high pressure run.

The following is a step-by-step review of the high pressure run program.

9 3 1 0 P R O G R A M M E N U

(1) LOW PRESSURE OPERATION

(2) MANUAL HIGH PRESSURE OPERATION

(3) AUTOMATIC HIGH PRESSURE OPERATION

(4) PRESSURE TABLE EDIT

(5) RATE SEQUENCE EDIT

(6) PRINTER REPORT

(7) PEN PLOT

(8) STORE SAMPLE DATA

(9) RETRIEVE SAMPLE DATA

(10) RETURN TO DOS MONITOR

ENTER NUMBER FOR DESIRED SELECTION AND PRESS <RETURN>: "3"

PREPARING TO RUN LEFT PENETROMETER IN HIGH PRESSURE SYSTEM

ENTER NUMBER OF PRESSURE TABLE TO BE USED (1-9/DEFAULT=1): "2"

PRESS F9 TO TERMINATE

DO YOU WISH TO EQUILIBRATE AT PRESSURE POINTS (Y/N/RETURN=Y): "Y"

ENTER EQUILIBRATION TIME (SEC) DEFAULT=10:

PRESS 'F9' TO TERMINATE "<CR>"

ADJUST 'SET ATM PRESSURE' ON 9310 UNTIL THE DISPLAY SHOWS 13-14 PSIA FOR THE HIGH PRESSURE TRANSDUCER WITH THE HIGH PRESSURE CHAMBER VENTED TO ATMOSPHERIC PRESSURE. THEN PRESS 'RETURN' TO RECORD OFFSET OR 'F9' TO TERMINATE:

WAIT APPROX 10 SECONDS

CLOSE VENT VALVE AND PRESS 'RETURN' TO START HIGH PRESSURE RUN, 'F9' TO TERMINATE RUN:

When the high pressure run is complete, store the data as follows:

9 3 1 0 P R O G R A M M E N U

(1) LOW PRESSURE OPERATION

(2) MANUAL HIGH PRESSURE OPERATION

(3) AUTOMATIC HIGH PRESSURE OPERATION

(4) PRESSURE TABLE EDIT

(5) RATE SEQUENCE EDIT

(6) PRINTER REPORT

(7) PEN PLOT

(8) STORE SAMPLE DATA

(9) RETRIEVE SAMPLE DATA

(10) RETURN TO DOS MONITOR

ENTER NUMBER FOR DESIRED SELECTION AND PRESS <RETURN>: "8"

SECOND HIGH PRESSURE RUN

Run two high pressure tests per sample. Upon completion of the initial high pressure run and sample data storage, the main menu will again appear. In order to start the second high pressure run go through the same computer procedure as for the first run, i.e. enter the sample data for the low pressure operation, etc.

The only change in the sample data will be in the sample id-where this will be run No.2 and in the sample time. Enter the identical values from the first run.

When it comes time to set atmospheric pressure before the high pressure run, remember two things: (1) run the hydraulic ram motor down by manually pressing the "SCAN DOWN" button, and (2) open the vent valve on the top of the high pressure chamber.

Go through the same procedure after the second high pressure run as after the first high pressure run, i.e. store the sample data, etc.

It is now time for clean-up. Open the vent valve on the high pressure chamber to expose the system to atmospheric pressure. Unscrew the high pressure chamber and let the oil drip from the penetrometer for a few minutes.

SAFETY

Put on the safety goggles, rubber gloves, and surgeon's mask. Set the used mercury container on the platform of the poresizer and put the funnel into the container. Remove the penetrometer from the high pressure chamber and hold over the funnel with stem down into funnel tube. Carefully remove the penetrometer assembly by unlatching the spring and removing. Set this aside on a paper towel along with the black cap of the assembly. Next, while holding the penetrometer cup inside the funnel, gently slide the stainless steel cap off the penetrometer cup. Most of the mercury should drain out of the capillary into the container. Now lift the penetrometer out of the funnel and put a finger over the capillary and invert the cup over the funnel, dumping

the sample and remaining mercury into the funnel. Tap the penetrometer cup on the side of the funnel to dislodge any remaining mercury and then set aside on a paper towel.

It is important to remember to properly discard any contaminated towelling, gloves, etc. in special receptacles for the hazardous waste division to pickup. The intruded core samples should be treated the same way.

TROUBLE SHOOTING

The poresizer manual is fairly thorough in diagnosing procedural problems but does not detail diagnosing equipment problems.

1. The biggest problem most likely encountered will be with the vacuum system. Do the best possible job to get the system to at least 300 micrometers Hg.
2. Faulty intrusion values.

If the poresizer registers intrusion values that either stay constant or increase as pressure increases there is undoubtedly a problem with the gold plated banana plug in the high pressure system. To rectify this problem, drain the high pressure system of high pressure fluid. This is accomplished with the use of a syringe. When all of the fluid is removed take the long handled needle-nosed pliers and **gently** unscrew the plug. Clean the plug and reinsert into the high pressure chamber. Do not turn the plug too tight. When resistance is felt on the pliers you have turned enough. Refill the chamber with fresh high pressure fluid.

If other problems occur consult the manual. Be safe with the machine and it will be safe with you.

APPENDIX B

RAW SAMPLE DATA AND STATISTICAL TABLES

This appendix contains all raw data generated from the mercury porosimetry study as well as data from physical measurement techniques for determining bulk density and water saturation techniques for determining porosity. Statistical tables are presented containing correlation coefficients for each individual borehole, each borehole set and for all borehole data.

Table B1: Preliminary summary of physical properties obtained from core segments at the Apache Leap Tuff Site. Columns labeled (med.) are results for medium core segments (2.5 cm diameter by 2.5 cm length) from mercury porosimetry. Columns labeled (large) are results for large core segments (6 cm diameter by 5 cm length) from water saturation method.

	Bulk Density (g/cm3)		Effective Porosity (%)		Grain Density (g/cm3)	
	med.	large	med.	large	med.	large
X Boreholes:						
Maximum	2.25	2.19	17.94	21.10	2.59	2.60
Minimum	1.94	1.97	9.80	14.30	2.21	2.34
Mean	2.13	2.10	14.06	17.58	2.48	2.55
Median	2.15	2.12	14.19	17.39	2.51	2.56
Coefficient of variation	0.03	0.03	0.13	0.10	0.04	0.02
Y Boreholes:						
Maximum	2.25	2.20	21.20	23.40	2.72	2.64
Minimum	1.94	1.90	11.22	14.49	2.28	2.51
Mean	2.13	2.10	15.04	17.72	2.51	2.56
Median	2.14	2.12	14.90	17.44	2.53	2.56
Coefficient of variation	0.03	0.03	0.14	0.12	0.03	0.01
Z Boreholes:						
Maximum	2.25	2.19	47.58	25.77	4.11	2.68
Minimum	1.95	1.86	9.18	14.77	2.22	2.37
Mean	2.13	2.10	14.75	17.72	2.52	2.55
Median	2.14	2.11	13.95	15.80	2.50	2.54
Coefficient of variation	0.03	0.03	0.40	0.15	0.11	0.02
All Boreholes:						
Maximum	2.25	2.20	47.58	25.77	4.11	2.68
Minimum	1.94	1.86	9.18	14.49	2.21	2.34
Mean	2.13	2.10	14.62	17.67	2.50	2.55
Median	2.14	2.12	14.31	17.39	2.51	2.56
Coefficient of variation	0.03	0.03	0.26	0.12	0.07	0.02

Table B2: Physical properties obtained from core segments at the Apache Leap Tuff Site. Columns labeled (med.) are results for medium core segments (2.5 cm diameter by 2.5 cm length) from mercury porosimetry. Columns labeled (large) are results for large core segments (6 cm diameter by 5 cm length) from water saturation method. Results are preliminary.

Borehole	Sample ID	Depth (m)	Bulk Density (g/cm3)		Effective Porosity (%)		Grain Density (g/cm3)	
			med.	large	med.	large	med.	large
X1	AA	2.10	2.11	2.11	10.91	17.36	2.37	2.55
	AB	2.90	2.13	2.13	11.84	16.23	2.42	2.55
	AC	3.80	2.15	2.13	13.50	17.40	2.48	2.58
	AD	6.90	2.18	2.12	12.40	16.48	2.49	2.54
	AE	10.00	2.18	1.99	12.80	14.99	2.50	2.34
	AF	12.70	2.16	2.18	15.10	16.11	2.54	2.60
	AG	15.80	2.16	2.18	14.10	15.98	2.52	2.60
X2	CA	1.90	2.08	1.97	14.20	21.10	2.43	2.50
	CB	2.90	2.04	2.06	9.80	18.76	2.26	2.54
	CC	3.60	2.04	2.04	10.50	18.80	2.27	2.51
	CD	6.60	2.14	2.12	13.50		2.47	
	CE	10.00	2.11	2.13	15.85	17.39	2.51	2.57
	CF	12.70	2.13	2.00	15.31	17.87	2.51	2.44
	CG	16.10	2.00	2.06	17.94	18.33	2.44	2.52
	CH	18.50	2.18	2.06	14.88	19.21	2.56	2.55
	CJ	21.70	2.17	2.15	14.19	16.89	2.53	2.59
	CK	24.70	2.15	2.06	16.13	20.44	2.56	2.59
	CM	27.90	2.10	2.09	16.33	18.98	2.51	2.58
	CN	30.80	2.15	2.09	15.91	19.46	2.55	2.59
X3	EA	1.80	1.94	2.04	12.20	20.61	2.21	2.57
	EB	2.70	2.01	1.97	14.36	20.15	2.34	2.47
	EC	3.80	2.07	2.00	15.40		2.45	
	ED	6.80	2.13	2.10	12.80		2.44	
	EE	9.90	2.15	2.16	13.20		2.47	
	EF	12.90	2.19	2.15	13.09		2.51	
	EG	15.80	2.23	2.14	13.23	15.68	2.57	2.54
	EH	18.80	2.16	2.19	14.31	14.30	2.53	2.56
	EJ	21.70	2.20	2.15	12.55	15.27	2.51	2.54
	EK	24.70	2.19	2.17	14.02	15.96	2.55	2.58
	EM	27.70	2.25	2.16	12.27	16.22	2.56	2.58
	EN	31.00	2.11	2.07	16.34	17.17	2.52	2.50
	EP	33.60	2.10	2.12	17.47	17.18	2.54	2.56
	ER	36.90	2.19	2.12	15.38	17.42	2.59	2.56
	ES	39.90	2.15	2.11	14.91	18.31	2.53	2.58
	ET	42.90	2.11	2.12	15.39	17.42	2.50	2.57

Table B2 (Continued)

Borehole	Sample ID	Depth (m)	Bulk Density (g/cm3)		Effective Porosity (%)		Grain Density (g/cm3)	
			med.	large	med.	large	med.	large
Y1	GB	1.90	2.12	2.17	13.70	16.71	2.46	2.60
	GC	3.30	2.15	2.14	11.90	16.62	2.44	2.56
	GD	4.10	2.14	2.13	13.33	16.69	2.47	2.56
	GA	6.70	2.10	2.13	13.93	17.05	2.43	2.56
	GF	9.90	2.11	2.09	16.61	18.82	2.53	2.57
	GG	12.20	2.13	2.13	15.99	15.96	2.54	2.53
	GH	15.70	2.17	2.17	11.22	15.65	2.45	2.57
Y2	JB	1.90	2.02	2.01	16.65	23.40	2.43	2.63
	JC	3.30	2.25	2.04	12.20	19.16	2.56	2.52
	JD	4.10	2.21	2.08	13.30	18.61	2.55	2.55
	JE	6.20	2.12	2.08	19.00	16.87	2.62	2.51
	JF	9.30	2.10	2.13	12.83	17.21	2.41	2.58
	JG	12.30	2.13	2.04	14.95	20.64	2.50	2.58
	JH	15.30	2.11	2.11	15.94	18.09	2.51	2.57
	JJ	18.50	2.17	2.00	13.76	20.82	2.52	2.53
	JK	21.40	2.14	2.11	16.03	16.81	2.54	2.54
	JM	24.50	2.07	2.08	17.37	17.48	2.50	2.52
	JN	27.30	2.15	2.09	16.60	17.44	2.57	2.53
	JP	30.30	2.19	2.12	12.38	18.67	2.50	2.61
Y3	MB	2.00	1.99	2.02	14.40	20.36	2.32	2.53
	MC	3.10	1.94	2.03	14.90		2.28	
	MD	4.10	2.15	2.05	21.20	22.43	2.72	2.64
	ME	6.20	2.15	2.01	14.64		2.52	
	MF	9.40	2.15	2.17	16.42		2.57	
	MG	12.40	2.02	1.90	17.37		2.44	
	MH	16.00	2.11	2.10	14.64	17.79	2.47	2.55
	MJ	18.20	2.23	2.18	12.63	14.55	2.55	2.55
	MK	21.30	2.25	2.20	11.96	14.49	2.55	2.57
	MM	24.20	2.23	2.15	13.68	14.70	2.59	2.52
	MN	27.40	2.20	2.15	14.85	16.15	2.58	2.56
	MP	30.30	2.16	2.14	15.50	17.56	2.56	2.59
	MR	33.30	2.19	2.17	15.70	16.48	2.59	2.59
	MS	36.50	2.10	2.12	17.21	18.18	2.54	2.59
	MT	39.30	2.09	2.13	18.10	17.11	2.55	2.57
	MU	42.20	2.15	2.15	15.61	16.94	2.55	2.59

Table B2 (Continued)

Borehole	Sample ID	Depth (m)	Bulk Density (g/cm3)		Effective Porosity (%)		Grain Density (g/cm3)	
			med.	large	med.	large	med.	large
Z1	PB	1.80	2.15	1.94	12.80	18.16	2.47	2.37
	PC	3.00	2.07	1.96	13.30		2.39	
	PD	4.10	2.05	2.07	15.70	22.56	2.44	2.68
	PE	6.00	2.10	2.11	11.61		2.37	
	PF	9.20	2.19	2.16	11.50		2.48	
	PG	12.50	2.13	2.09	11.68		2.41	
	PH	15.20	2.12	2.12	14.75		2.49	
Z2	SB	2.00	2.18	2.14	13.80	17.43	2.53	2.60
	SC	3.00	2.20	2.18	12.50	16.58	2.51	2.61
	SD	3.90	2.08	2.11	12.70	16.87	2.38	2.54
	SE	6.50	2.13	2.11	14.51	16.93	2.50	2.54
	SF	9.40	2.06	2.03	16.92	20.84	2.47	2.56
	SG	12.50	1.95	1.86	12.27	25.77	2.22	2.51
	SH	15.30	2.03	2.08	14.12	17.44	2.36	2.51
	SJ	18.60	2.10	2.13	13.95		2.44	
	SK	21.10	2.10	2.15	12.81		2.41	
	SM	24.50	2.17	2.17	13.34	14.77	2.50	2.54
	SN	27.40	2.15	2.15	47.58		4.11	
	SP	30.50	2.08	2.06	18.47		2.55	
Z3	UW	2.00	2.23	2.17	12.50	15.80	2.55	2.58
	UC	3.00	2.16	2.12	14.08	16.80	2.51	2.55
	UD	3.80	2.14	2.05	15.07	18.80	2.52	2.53
	UE	6.70	2.10	2.10	9.18	17.41	2.31	2.54
	UF	9.70	2.08	2.11	14.53	16.38	2.44	2.52
	UG	12.70	2.17	2.06	15.18	19.41	2.56	2.56
	UH	15.90	2.06	2.00	11.77	19.41	2.33	2.48
	UJ	18.80	2.19	2.16	13.12	14.98	2.52	2.54
	UK	21.70	2.25	2.18	12.13	14.94	2.56	2.57
	UM	24.70	2.18	2.16	14.83	15.71	2.56	2.57
	UN	27.70	2.23	2.19	15.19	15.31	2.63	2.59
	UP	30.70	2.22	2.18	11.16		2.50	
	UR	33.70	2.19	2.14	15.50	17.45	2.59	2.59
	US	36.80	2.13	2.11	16.65		2.56	
	UT	39.80	2.14	2.11	16.99		2.58	
	UU	42.80	2.19	2.12	14.32		2.56	

Table B3: Summary of pore area and pore size distribution properties at the Apache Leap Tuff Site. Columns labeled (upper) and (lower) refer to upper and lower peaks of the bimodal pore size distribution.

	Total Pore Area (m2/g)	Mode Pore Diameter (um)		Relative Porosity (%)		Relative Area (%)	
		upper	lower	upper	lower	upper	lower
X Boreholes:							
Maximum	4.939	4.59	0.1470	67.38	74.09	6.88	99.64
Minimum	2.207	1.72	0.0336	25.91	32.62	0.36	93.12
Mean	3.162	2.94	0.0674	50.91	49.09	3.09	96.91
Median	3.128	2.81	0.0702	54.30	45.96	3.17	97.09
Coef. Var.	0.141	0.25	0.3438	0.21	0.22	0.46	0.01
Y Boreholes:							
Maximum	16.510	4.59	0.1470	75.07	98.05	10.09	99.93
Minimum	2.054	0.09	0.0098	1.95	24.93	0.07	89.91
Mean	4.335	2.75	0.0609	52.00	48.00	4.29	95.71
Median	3.221	2.81	0.0549	60.47	42.53	4.57	6.20
Coef. Var.	0.845	0.43	0.4497	0.37	0.40	0.62	0.03
Z Boreholes:							
Maximum	4.015	4.59	0.1150	89.17	70.20	8.52	99.15
Minimum	1.960	1.72	0.0429	29.80	10.83	0.85	91.48
Mean	2.900	3.03	0.0701	55.30	44.70	3.77	96.23
Median	2.916	2.81	0.0702	55.44	24.80	3.74	96.44
Coef. Var.	0.169	0.26	0.2628	0.23	0.28	0.50	0.02
All Boreholes:							
Maximum	16.510	4.59	0.1470	89.17	98.05	10.09	99.93
Minimum	1.960	0.09	0.0098	1.95	10.83	0.07	89.91
Mean	3.466	2.91	0.0661	52.73	47.27	3.72	96.28
Median	2.999	2.81	0.0549	55.04	44.56	3.50	96.45
Coef. Var.	0.646	0.32	0.3568	0.28	0.31	0.57	0.02

Table B4: Pore area and pore size distribution properties at the Apache Leap Tuff Site. Columns labeled (up) and (low) refer to upper and lower peaks of the bimodal pore size distribution.

Borehole	ID	Depth (m)	Total Pore Area (m2/g)	Mode Pore Diameter (um)		Relative Porosity (%)		Relative Area (%)	
				up	low	up	low	up	low
X1	AA	2.10	3.008	2.81	0.0702	36.56	63.44	2.11	97.89
	AB	2.90	3.092	3.59	0.0702	49.82	50.18	2.13	97.87
	AC	3.80	3.163	3.59	0.0897	45.86	54.14	2.04	97.96
	AD	6.90	3.623	2.19	0.0702	33.14	66.86	2.08	97.92
	AE	10.00	2.999	2.81	0.0702	51.02	48.98	2.82	97.18
	AF	12.70	3.172	2.81	0.0549	50.50	49.50	2.82	97.18
	AG	15.80	3.241	2.81	0.0549	49.23	50.77	3.50	96.50
X2	CA	1.90	4.939	3.59	0.1150	30.25	69.75	0.36	99.64
	CB	2.90	2.666	3.59	0.0897	38.72	61.28	1.20	98.80
	CC	3.60	3.128	2.81	0.0897	33.20	66.80	1.21	98.79
	CD	6.60	2.961	4.59	0.0702	54.52	45.48	3.80	96.20
	CE	10.00	3.208	3.59	0.0702	47.74	52.26	1.78	98.22
	CF	12.70	3.072	3.59	0.0549	59.17	40.83	3.27	96.73
	CG	16.10	3.362	4.59	0.0702	63.35	36.65	5.24	94.76
	CH	18.50	3.158	2.81	0.0549	63.30	36.70	3.72	96.28
	CJ	21.70	2.938	1.72	0.0336	67.38	32.62	6.88	93.12
	CK	24.70	3.435	2.81	0.0549	56.80	43.20	3.17	96.83
	CM	27.90	3.594	2.81	0.0549	60.33	39.67	4.10	95.90
	CN	30.80	3.081	1.72	0.0429	61.00	39.00	5.77	94.23
X3	EA	1.80	3.202	2.81	0.1470	25.91	74.09	0.84	99.16
	EB	2.70	4.145	2.19	0.1150	29.09	70.91	1.30	98.70
	EC	3.80	3.232	3.59	0.0897	43.47	56.53	1.78	98.22
	ED	6.80	2.812	3.59	0.0702	46.42	53.58	2.26	97.74
	EE	9.90	2.934	3.59	0.0702	54.30	45.70	3.50	96.50
	EF	12.90	2.824	3.59	0.0702	54.59	45.41	2.85	97.15
	EG	15.80	2.963	2.81	0.0702	54.04	45.96	2.91	97.09
	EH	18.80	2.843	3.59	0.0549	63.24	36.76	3.80	96.20
	EJ	21.70	2.207	2.81	0.0549	54.29	45.71	3.67	96.33
	EK	24.70	2.813	2.19	0.0549	57.90	42.10	3.80	96.20
	EM	27.70	2.852	2.19	0.0429	55.86	44.14	3.08	96.92
	EN	31.00	3.492	2.19	0.0549	57.81	42.19	3.39	96.61
	EP	33.60	2.925	2.19	0.0549	64.78	35.22	5.08	94.92
	ER	36.90	2.877	2.19	0.0429	58.97	41.03	3.97	96.03
	ES	39.90	3.407	2.19	0.0429	57.37	42.63	5.09	94.91
	ET	42.90	3.318	2.19	0.0429	51.87	48.13	2.76	97.24

Table B4 (Continued):

Borehole	ID	Depth (m)	Total Pore Area (m2/g)	Mode Pore Diameter - (um) - up	Mode Pore Diameter - (um) - low	Relative Porosity - (%) - up	Relative Porosity - (%) - low	Relative Area - (%) - up	Relative Area - (%) - low
Y1	GB	1.90	3.258	3.59	0.0897	44.29	55.71	2.06	97.94
	GC	3.30	3.315	2.81	0.0702	43.24	56.76	2.11	97.89
	GD	4.10	3.673	2.81	0.0702	48.15	51.85	3.03	96.97
	GA	6.70	3.312	4.59	0.0549	53.84	46.16	3.35	96.65
	GF	9.90	2.776	4.59	0.0549	66.12	33.88	4.57	95.43
	GG	12.20	2.524	3.59	0.0549	75.07	24.93	10.09	89.91
	GH	15.70	2.667	3.59	0.0549	67.99	32.01	7.67	92.33
Y2	JB	1.90	4.051	4.59	0.1470	38.03	61.97	1.44	98.56
	JC	3.30	3.429	0.82	0.1150	27.99	72.01	1.89	98.11
	JD	4.10	5.364	3.59	0.0336	29.18	70.82	1.02	98.98
	JE	6.20	16.160	2.19	0.0125	14.73	85.27	0.52	99.48
	JF	9.30	2.291	4.59	0.0897	57.61	42.39	2.88	97.12
	JG	12.30	3.286	3.59	0.0702	57.47	42.53	3.90	96.10
	JH	15.30	3.077	3.59	0.0702	62.17	37.83	5.26	94.74
	JJ	18.50	2.916	3.59	0.0702	55.67	44.33	2.28	97.72
	JK	21.40	2.819	2.19	0.0549	68.13	31.87	4.80	95.20
	JM	24.50	3.570	2.81	0.0702	54.52	45.48	2.43	97.57
	JN	27.30	3.221	2.81	0.0549	64.99	35.01	5.18	94.82
	JP	30.30	2.500	2.81	0.0897	61.06	38.94	6.32	93.68
Y3	MB	2.00	10.070	0.82	0.0160	6.64	93.36	0.22	99.78
	MC	3.10	16.510	0.50	0.0098	1.95	98.05	0.07	99.93
	MD	4.10	13.740	0.09	0.0160	6.30	93.70	0.20	99.80
	ME	6.20	2.812	3.59	0.0897	52.79	47.21	3.80	96.20
	MF	9.40	3.301	2.19	0.0549	62.35	37.65	5.92	94.08
	MG	12.40	3.559	4.59	0.0897	51.98	48.02	3.14	96.86
	MH	16.00	3.282	2.81	0.0702	54.32	45.68	3.43	96.57
	MJ	18.20	2.401	2.81	0.0549	66.14	33.86	5.51	94.49
	MK	21.30	2.054	1.34	0.0429	69.04	30.96	8.15	91.85
	MM	24.20	2.728	2.19	0.0549	63.62	36.38	5.65	94.35
	MN	27.40	2.620	2.19	0.0549	67.16	32.84	7.09	92.91
	MP	30.30	2.890	2.19	0.0549	63.65	36.35	6.16	93.84
	MR	33.30	2.871	2.19	0.0429	64.76	35.24	6.32	93.68
	MS	36.50	2.851	2.19	0.0549	67.64	32.36	7.62	92.38
	MT	39.30	2.626	1.72	0.0549	70.82	29.18	9.66	90.34
	MU	42.20	3.209	2.19	0.0429	60.47	39.53	6.47	93.53

Table B4 (Continued):

Borehole	ID	Depth (m)	Total Pore Area (m2/g)	Mode Pore Diameter - (um) - up	low	Relative Porosity -(%)- up	low	Relative Area - (%) - up	low
Z1	PB	1.80	3.691	2.81	0.1150	29.80	70.20	0.96	99.04
	PC	3.00	3.765	3.59	0.1150	33.33	66.67	0.85	99.15
	PD	4.10	4.015	3.59	0.0897	37.20	62.80	1.51	98.49
	PE	6.00	2.599	3.59	0.0897	42.96	57.04	1.55	98.45
	PF	9.20	2.586	2.81	0.0897	55.55	44.45	4.70	95.30
	PG	12.50	2.491	3.59	0.0702	50.82	49.18	2.31	97.69
	PH	15.20	2.592	3.59	0.0702	64.60	35.40	4.83	95.17
Z2	SB	2.00	3.602	2.81	0.0897	38.33	61.67	1.56	98.44
	SC	3.00	3.010	2.81	0.0897	51.94	48.06	3.77	96.23
	SD	3.90	2.832	4.59	0.0702	60.56	39.44	3.74	96.26
	SE	6.50	3.572	4.59	0.0702	43.68	56.32	2.13	97.87
	SF	9.40	3.147	3.59	0.0897	51.64	48.36	3.86	96.14
	SG	12.50	3.697	2.81	0.0897	40.89	59.11	2.48	97.52
	SH	15.30	3.241	3.59	0.0897	47.06	52.94	2.18	97.82
	SJ	18.60	2.603	2.81	0.0702	65.81	34.19	5.67	94.33
	SK	21.10	2.430	2.19	0.0429	65.08	34.92	5.94	94.06
	SM	24.50	2.606	3.59	0.0549	64.43	35.57	5.54	94.46
	SN	27.40	2.627	2.19	0.0549	89.17	10.83	5.68	94.32
	SP	30.50	2.147	2.19	0.0549	75.20	24.80	8.52	91.48
Z3	UW	2.00	3.293	3.59	0.0702	42.40	57.60	1.62	98.38
	UC	3.00	3.207	3.59	0.0702	55.36	44.64	3.55	96.45
	UD	3.80	2.916	3.59	0.0549	49.28	50.72	1.17	98.83
	UE	6.70	2.407	4.59	0.0549	47.60	52.40	1.99	98.01
	UF	9.70	3.133	2.81	0.0702	55.44	44.56	2.73	97.27
	UG	12.70	2.858	3.59	0.0702	66.38	33.62	6.84	93.16
	UH	15.90	3.009	2.81	0.0702	49.82	50.18	3.64	96.36
	UJ	18.80	2.938	2.81	0.0702	57.83	42.17	3.56	96.44
	UK	21.70	2.389	2.19	0.0549	62.34	37.66	4.89	95.11
	UM	24.70	2.181	1.72	0.0549	73.86	26.14	7.00	93.00
	UN	27.70	2.483	2.19	0.0549	63.05	36.95	4.80	95.20
	UP	30.70	1.960	3.59	0.0429	53.28	46.72	3.10	96.90
	UR	33.70	2.679	2.19	0.0549	64.03	35.97	5.00	95.00
	US	36.80	2.686	1.72	0.0549	66.07	33.93	5.77	94.23
	UT	39.80	2.924	2.19	0.0549	65.62	34.38	5.00	95.00
	UU	42.80	3.181	1.72	0.0429	55.04	44.96	3.47	96.53

Table B5.1 X1 borehole regression statistics.

Correlation, Covariance, Cross-Product:

	ELEV	BULK	POROSITY	PAREA	LPD	SPD	LPDPER	LPSAPER
ELEV	1.000	-.650	-.780	-.169	.404	.743	-.459	-.935
	13.901	-.062	-4.105	-.134	.746	.033	-12.494	-1.952
	83.405	-.370	-24.627	-.805	4.478	.195	-74.963	-11.713
BULK	-.650	1.000	.530	.503	-.494	-.197	.165	.442
	-.062	.001	.019	.003	-.006	.000	.031	.006
	-.370	.004	.114	.016	-.037	.000	.184	.038
POROSITY	-.780	.530	1.000	.153	-.023	-.399	.560	.627
	-4.105	.019	1.994	.046	-.016	-.007	5.775	.496
	-24.627	.114	11.966	.276	-.096	-.040	34.650	2.974
PAREA	-.169	.503	.153	1.000	-.573	-.072	-.551	-.109
	-.134	.003	.046	.045	-.060	.000	-.854	-.013
	-.805	.016	.276	.270	-.362	-.001	-5.123	-.078
LPD	.404	-.494	-.023	-.573	1.000	.477	.535	-.232
	.746	-.006	-.016	-.060	.246	.003	1.939	-.064
	4.478	-.037	-.096	-.362	1.475	.017	11.632	-.387
SPD	.743	-.197	-.399	-.072	.477	1.000	-.253	-.738
	.033	.000	-.007	.000	.003	.000	-.022	-.005
	.195	.000	-.040	-.001	.017	.001	-.130	-.029
LPDPER	-.459	.165	.560	-.551	.535	-.253	1.000	.571
	-12.494	.031	5.775	-.854	1.939	-.022	53.344	2.335
	-74.963	.184	34.650	-5.123	11.632	-.130	320.066	14.010
LPSAPER	-.935	.442	.627	-.109	-.232	-.738	.571	1.000
	-1.952	.006	.496	-.013	-.064	-.005	2.335	.314
	-11.713	.038	2.974	-.078	-.387	-.029	14.010	1.882

Table B5.2 X2 borehole regression statistics.

Correlation, Covariance, Cross-Product:

	ELEV	BULK	POROSITY	PAREA	LPD	SPD	LPDPER	LPSAPER
ELEV	1.000	-.502	-.650	.138	.604	.828	-.783	-.757
	50.675	-.203	-10.959	.564	3.990	.134	-70.010	-10.708
	557.422	-2.229	-120.553	6.202	43.887	1.469	-770.112	-117.783
BULK	-.502	1.000	.255	-.111	-.521	-.652	.528	.429
	-.203	.003	.034	-.004	-.027	-.001	.375	.048
	-2.229	.035	.377	-.040	-.301	-.009	4.120	.532
POROSITY	-.650	.255	1.000	.264	.030	-.474	.659	.521
	-10.959	.034	5.609	.357	.066	-.025	19.589	2.450
	-120.553	.377	61.702	3.930	.727	-.280	215.477	26.953
PAREA	.138	-.111	.264	1.000	.119	.532	-.397	-.376
	.564	-.004	.357	.327	.063	.007	-2.853	-.428
	6.202	-.040	3.930	3.601	.696	.076	-31.378	-4.705
LPD	.604	-.521	.030	.119	1.000	.534	-.245	-.381
	3.990	-.027	.066	.063	.860	.011	-2.850	-.703
	43.887	-.301	.727	.696	9.459	.123	-31.349	-7.729
SPD	.828	-.652	-.474	.532	.534	1.000	-.911	-.858
	.134	-.001	-.025	.007	.011	.001	-.259	-.039
	1.469	-.009	-.280	.076	.123	.006	-2.852	-.425
LPDPER	-.783	.526	.659	-.397	-.245	-.911	1.000	.903
	-70.010	.375	19.589	-2.853	-2.850	-.259	157.612	22.533
	-770.112	4.120	215.477	-31.378	-31.349	-2.852	1733.729	247.858
LPSAPER	-.757	.429	.521	-.376	-.381	-.858	.903	1.000
	-10.708	.048	2.450	-.428	-.703	-.039	22.533	3.948
	-117.783	.532	26.953	-4.705	-7.729	-.425	247.859	43.430

Table B5.3 X3 borehole regression statistics.

Correlation, Covariance, Cross-Product:

	ELEV	BULK	POROSITY	PAREA	LPD	SPD	LPDPER	LPSAPER
ELEV	1.000	-.439	-.522	.101	.656	.806	-.687	-.747
	94.232	-.338	-7.807	.412	4.044	.224	-72.662	-8.619
	1413.481	-5.073	-117.107	6.183	60.658	3.362	-1089.93	-129.282
BULK	-.439	1.000	-.167	-.617	-.005	-.805	.767	.588
	-.338	.006	-.020	-.021	.000	-.002	.663	.055
	-5.073	.094	-.306	-.310	-.004	-.027	9.946	.832
POROSITY	-.522	-.167	1.000	.366	-.394	-.319	.373	.439
	-7.807	-.020	2.378	.238	-.386	-.014	6.264	.805
	-117.107	-.306	35.671	3.573	-5.789	-.212	93.953	12.073
PAREA	.101	-.617	.366	1.000	-.337	.399	-.508	-.368
	.412	-.021	.238	.178	-.090	.005	-2.338	-.184
	6.183	-.310	3.573	2.673	-1.355	.072	-35.073	-2.767
LPD	.656	-.005	-.394	-.337	1.000	.252	-.092	-.289
	4.044	.000	-.386	-.090	.403	.005	-.634	-.218
	60.658	-.004	-5.789	-1.355	6.047	.069	-9.506	-3.265
SPD	.806	-.805	-.319	.399	.252	1.000	-.902	-.806
	.224	-.002	-.014	.005	.005	.001	-.282	-.027
	3.362	-.027	-.212	.072	.069	.012	-4.223	-.412
LPDPER	-.687	.767	.373	-.508	-.092	-.902	1.000	.891
	-72.662	.663	6.264	-2.338	-.634	-.282	118.743	11.540
	-1089.93	9.946	93.953	-35.073	-9.506	-4.223	1781.151	173.106
LPSAPER	-.747	.588	.439	-.368	-.289	-.806	.891	1.000
	-8.619	.055	.805	-.184	-.218	-.027	11.540	1.412
	-129.282	.832	12.073	-2.767	-3.265	-.412	173.106	21.182

Table B5.4 All X series borehole regression statistics.

Correlation, Covariance, Cross-Product:

	ELEV	BULK	POROSITY	PAREA	LPD	SPD	LPDPER	LPSAPER
ELEV	1.000	-.389	-.564	.150	.574	.743	-.687	-.677
	72.859	-.217	-9.087	.580	3.594	.149	-64.663	-8.293
	2477.221	-7.364	-308.943	19.734	122.191	5.068	-2198.55	-281.962
BULK	-.389	1.000	-.027	-.378	-.266	-.702	.526	.388
	-.217	.004	-.003	-.011	-.013	-.001	.378	.036
	-7.364	.146	-.114	-.379	-.432	-.037	12.864	1.232
POROSITY	-.564	-.027	1.000	.281	-.088	-.361	.569	.525
	-9.087	-.003	3.560	.240	-.122	-.016	11.843	1.421
	-308.943	-.114	121.027	8.158	-4.151	-.544	402.674	48.323
PAREA	.150	-.378	.281	1.000	-.025	.404	-.418	-.329
	.580	-.011	.240	.204	-.008	.004	-2.085	-.214
	19.734	-.379	8.158	6.951	-.285	.146	-70.884	-7.262
LPD	.574	-.266	-.088	-.025	1.000	.352	-.096	-.299
	3.594	-.013	-.122	-.008	.539	.006	-.774	-.314
	122.191	-.432	-4.151	-.285	18.317	.207	-26.323	-10.687
SPD	.743	-.702	-.361	.404	.352	1.000	-.825	-.761
	.149	-.001	-.016	.004	.006	.001	-.214	-.026
	5.068	-.037	-.544	.146	.207	.019	-7.269	-.873
LPDPER	-.687	.526	.569	-.418	-.096	-.825	1.000	.868
	-64.663	.378	11.843	-2.085	-.774	-.214	121.542	13.718
	-2198.55	12.864	402.674	-70.884	-26.323	-7.269	4132.413	466.409
LPSAPER	-.677	.388	.525	-.329	-.299	-.761	.868	1.000
	-8.293	.036	1.421	-.214	-.314	-.026	13.718	2.057
	-281.962	1.232	48.323	-7.262	-10.687	-.873	466.409	69.931

Table B5.5 Y1 borehole regression statistics.

Correlation, Covariance, Cross-Product:

	ELEV	BULK	POROSITY	PAREA	LPD	SPD	LPDPER	LPSAPER
ELEV	1.000	-.337	-.097	.841	-.328	.793	-.922	-.504
	12.904	-.033	-.688	1.273	-.860	.038	-42.087	-4.313
	77.424	-.198	-4.127	7.637	-5.160	.228	-252.523	-25.879
BULK	-.337	1.000	-.705	-.166	-.702	.018	.081	.368
	-.033	.001	-.038	-.002	-.014	.000	.028	.024
	-.198	.004	-.227	-.011	-.084	.000	.168	.143
POROSITY	-.097	-.705	1.000	-.346	.556	-.257	.453	-.435
	-.688	-.038	3.868	-.286	.797	-.007	11.336	-2.036
	-4.127	-.227	23.205	-1.719	4.784	-.040	68.013	-12.215
PAREA	.841	-.166	-.346	1.000	-.388	.569	-.898	-.175
	1.273	-.002	-.286	.177	-.119	.003	-4.806	-.176
	7.637	-.011	-1.719	1.064	-.716	.019	-28.837	-1.056
LPD	-.328	-.702	.556	-.388	1.000	-.479	.425	.237
	-.860	-.014	.797	-.119	.532	-.005	3.936	.412
	-5.160	-.084	4.784	-.716	3.189	-.028	23.615	2.473
SPD	.793	.018	-.257	.569	-.479	1.000	-.772	-.333
	.038	.000	-.007	.003	-.005	.000	-.131	-.011
	.228	.000	-.040	.019	-.028	.001	-.785	-.063
LPDPER	-.922	.081	.453	-.898	.425	-.772	1.000	.198
	-42.087	.028	11.336	-4.806	3.936	-.131	161.609	5.993
	-252.523	.168	68.013	-28.837	23.615	-.785	969.656	35.961
LPSAPER	-.504	.368	-.435	-.175	.237	-.333	.198	1.000
	-4.313	.024	-2.036	-.176	.412	-.011	5.993	5.673
	-25.879	.143	-12.215	-1.056	2.473	-.063	35.961	34.036

Table B5.6 Y2 borehole regression statistics.

Correlation, Covariance, Cross-Product:

	ELEV	BULK	POROSITY	PAREA	LPD	SPD	LPDPER	LPSAPER
ELEV	1.000	-.039	-.051	.365	.127	.184	-.757	-.770
	48.673	-.017	-.778	9.661	.946	.045	-91.311	-10.147
	535.399	-.183	-8.538	106.274	10.404	.499	-1004.42	-111.617
BULK	-.039	1.000	-.655	-.074	-.587	-.221	-.167	.085
	-.017	.004	-.088	-.017	-.038	.000	-.177	.010
	-.183	.041	-.963	-.189	-.421	-.005	-1.947	.108
POROSITY	-.051	-.655	1.000	.573	-.014	-.358	-.123	-.169
	-.778	-.088	4.782	4.753	-.033	-.028	-4.653	-.696
	-8.538	-.963	52.602	52.279	-.362	-.304	-51.182	-7.656
PAREA	.365	-.074	.573	1.000	-.248	-.557	-.734	-.551
	9.661	-.017	4.753	14.375	-1.002	-.075	-48.124	-3.941
	106.274	-.189	52.279	158.120	-11.027	-.820	-529.367	-43.355
LPD	.127	-.587	-.014	-.248	1.000	.214	.259	-.025
	.946	-.038	-.033	-1.002	1.137	.008	4.782	-.050
	10.404	-.421	-.362	-11.027	12.507	.089	52.597	-.553
SPD	.184	-.221	-.358	-.557	.214	1.000	.115	.057
	.045	.000	-.028	-.075	.008	.001	.070	.004
	.499	-.005	-.304	-.820	.089	.014	.774	.042
LPDPER	-.757	-.167	-.123	-.734	.259	.115	1.000	.840
	-91.311	-.177	-4.653	-48.124	4.782	.070	299.031	27.440
	-1004.42	-1.947	-51.182	-529.367	52.597	.774	3289.338	301.836
LPSAPER	-.770	.085	-.169	-.551	-.025	.057	.840	1.000
	-10.147	.010	-.696	-3.941	-.050	.004	27.440	3.565
	-111.617	.108	-7.656	-43.355	-.553	.042	301.836	39.219

Table B5.7 Y3 borehole regression statistics.

Correlation, Covariance, Cross-Product:

	ELEV	BULK	POROSITY	PAREA	LPD	SPD	LPDPER	LPSAPER
ELEV	1.000	-.406	-.004	.618	-.159	-.186	-.726	-.826
	91.133	-.340	-.095	26.171	-1.687	-.041	-165.780	-22.935
	1366.989	-5.098	-1.423	392.560	-25.299	-.609	-2486.71	-344.020
BULK	-.406	1.000	-.304	-.637	.151	.261	.670	.593
	-.340	.008	-.059	-.248	.015	.001	1.407	.151
	-5.098	.115	-.890	-3.723	.220	.008	21.099	2.271
POROSITY	-.004	-.304	1.000	.336	-.179	-.115	-.284	-.181
	-.095	-.059	4.939	3.311	-.441	-.006	-15.092	-1.167
	-1.423	-.890	74.081	49.662	-6.619	-.087	-226.380	-17.507
PAREA	.618	-.637	.336	1.000	-.684	-.749	-.956	-.816
	26.171	-.248	3.311	19.707	-3.369	-.076	-101.583	-10.532
	392.560	-3.723	49.662	295.598	-50.530	-1.138	-1523.74	-157.977
LPD	-.159	.151	-.179	-.684	1.000	.939	.579	.273
	-1.687	.015	-.441	-3.369	1.229	.024	15.355	.881
	-25.299	.220	-6.619	-50.530	18.439	.356	230.318	13.215
SPD	-.186	.261	-.115	-.749	.939	1.000	.658	.394
	-.041	.001	-.006	-.076	.024	.001	.359	.026
	-.609	.008	-.087	-1.138	.356	.008	5.392	.392
LPDPER	-.726	.670	-.284	-.956	.579	.658	1.000	.918
	-165.780	1.407	-15.092	-101.583	15.355	.359	572.536	63.875
	-2486.71	21.099	-226.380	-1523.74	230.318	5.392	8588.035	958.127
LPSAPER	-.826	.593	-.181	-.816	.273	.394	.918	1.000
	-22.935	.151	-1.167	-10.532	.881	.026	63.875	8.450
	-344.020	2.271	-17.507	-157.977	13.215	.392	958.127	126.754

Table B5.8 All Y series borehole regression statistics.

Correlation, Covariance, Cross-Product:

	ELEV	BULK	POROSITY	PAREA	LPD	SPD	LPDPER	LPSAPER
ELEV	1.000	-.272	-.142	.406	.158	.118	-.638	-.774
	70.154	-.157	-2.623	12.655	1.571	.027	-104.903	-16.739
	2385.228	-5.329	-89.172	430.267	53.411	.933	-3566.710	-569.124
BULK	-.272	1.000	-.406	-.452	-.088	.057	.416	.403
	-.157	.005	-.062	-.116	-.007	.000	.563	.072
	-5.329	.161	-2.091	-3.934	-.244	.004	19.149	2.440
POROSITY	-.142	-.406	1.000	.414	-.170	-.260	-.173	-.123
	-2.623	-.062	4.843	3.390	-.444	-.016	-7.495	-.698
	-89.172	-2.091	164.650	115.256	-15.087	-.541	-254.823	-23.741
PAREA	.406	-.452	.414	1.000	-.501	-.582	-.858	-.578
	12.655	-.116	3.390	13.826	-2.215	-.060	-62.608	-5.550
	430.267	-3.934	115.256	470.098	-75.310	-2.047	-2128.674	-188.708
LPD	.158	-.088	-.170	-.501	1.000	.534	.413	-.028
	1.571	-.007	-.444	-2.215	1.413	.018	9.651	-.086
	53.411	-.244	-15.087	-75.310	48.048	.600	328.124	-2.908
SPD	.118	.057	-.260	-.582	.534	1.000	.276	.027
	.027	.000	-.016	-.060	.018	.001	.151	.002
	.933	.004	-.541	-2.047	.600	.026	5.123	.067
LPDPER	-.638	.416	-.173	-.858	.413	.276	1.000	.751
	-104.903	.563	-7.495	-62.608	9.651	.151	385.504	38.104
	-3566.710	19.149	-254.823	-2128.674	328.124	5.123	13107.143	1295.541
LPSAPER	-.774	.403	-.123	-.578	-.028	.027	.751	1.000
	-16.739	.072	-.698	-5.550	-.086	.002	38.104	6.670
	-569.124	2.440	-23.741	-188.708	-2.908	.067	1295.541	226.775

Table B5.9 Z1 borehole regression statistics.

Correlation, Covariance, Cross-Product:

	ELEV	BULK	POROSITY	PAREA	LPD	SPD	LPDPER	LPSAPER
ELEV	1.000	-.338	.059	.802	-.257	.906	-.954	-.810
	12.795	-.058	.347	1.949	-.350	.059	-43.181	-4.904
	76.768	-.350	2.084	11.695	-2.098	.357	-259.084	-29.424
BULK	-.338	1.000	-.591	-.549	-.796	-.128	.425	.588
	-.058	.002	-.047	-.018	-.015	.000	.261	.048
	-.350	.014	-.283	-.108	-.088	-.001	1.563	.289
POROSITY	.059	-.591	1.000	.583	.371	-.035	-.063	-.028
	.347	-.047	2.732	.655	.234	-.001	-1.309	-.079
	2.084	-.283	16.390	3.932	1.402	-.006	-7.857	-.473
PAREA	.802	-.549	.583	1.000	-.033	.715	-.809	-.671
	1.949	-.018	.655	.462	-.009	.009	-6.963	-.772
	11.695	-.108	3.932	2.773	-.051	.053	-41.778	-4.632
LPD	-.257	-.796	.371	-.033	1.000	-.409	.120	-.179
	-.350	-.015	.234	-.009	.145	-.003	.577	-.115
	-2.098	-.088	1.402	-.051	.869	-.017	3.462	-.691
SPD	.906	-.128	-.035	.715	-.409	1.000	-.842	-.650
	.059	.000	-.001	.009	-.003	.000	-.196	-.020
	.357	-.001	-.006	.053	-.017	.002	-1.174	-.121
LPDPER	-.954	.425	-.063	-.809	.120	-.842	1.000	.933
	-43.181	.261	-1.309	-6.963	.577	-.196	160.248	20.002
	-259.084	1.563	-7.857	-41.778	3.462	-1.174	961.487	120.012
LPSAPER	-.810	.588	-.028	-.671	-.179	-.650	.933	1.000
	-4.904	.048	-.079	-.772	-.115	-.020	20.002	2.865
	-29.424	.289	-.473	-4.632	-.691	-.121	120.012	17.193

Table B5.10 Z2 borehole regression statistics.

Correlation, Covariance, Cross-Product:

	ELEV	BULK	POROSITY	PAREA	LPD	SPD	LPDPER	LPSAPER
ELEV	1.000	.072	-.469	.736	.552	.728	-.779	-.813
	49.184	.036	-32.381	2.591	3.290	.088	-82.495	-11.733
	541.019	.399	-356.188	28.497	36.186	.973	-907.440	-129.059
BULK	.072	1.000	.208	-.236	-.069	-.260	.243	.135
	.036	.005	.148	-.009	-.004	.000	.265	.020
	.399	.057	1.623	-.094	-.047	-.004	2.913	.221
POROSITY	-.469	.208	1.000	-.264	-.372	-.329	.691	.298
	-32.381	.148	96.731	-1.300	-3.111	-.056	102.582	6.032
	-356.188	1.623	1064.041	-14.301	-34.221	-.616	1128.401	66.355
PAREA	.736	-.236	-.264	1.000	.424	.779	-.865	-.946
	2.591	-.009	-1.300	.252	.181	.007	-6.552	-.977
	28.497	-.094	-14.301	2.768	1.992	.074	-72.077	-10.749
LPD	.552	-.069	-.372	.424	1.000	.285	-.446	-.530
	3.290	-.004	-3.111	.181	.723	.004	-5.731	-.927
	36.186	-.047	-34.221	1.992	7.955	.046	-63.046	-10.199
SPD	.728	-.260	-.329	.779	.285	1.000	-.765	-.759
	.088	.000	-.056	.007	.004	.000	-.200	-.027
	.973	-.004	-.616	.074	.046	.003	-2.200	-.298
LPDPER	-.779	.243	.691	-.865	-.446	-.765	1.000	.847
	-82.495	.265	102.582	-6.552	-5.731	-.200	227.964	26.333
	-907.440	2.913	1128.401	-72.077	-63.046	-2.200	2507.603	289.665
LPSAPER	-.813	.135	.298	-.946	-.530	-.759	.847	1.000
	-11.733	.020	6.032	-.977	-.927	-.027	26.333	4.237
	-129.059	.221	66.355	-10.749	-10.199	-.298	289.665	46.605

Table B5.11 Z3 borehole regression statistics.

Correlation, Covariance, Cross-Product:

	ELEV	BULK	POROSITY	PAREA	LPD	SPD	LPDPER	LPSAPER
ELEV	1.000	-.224	-.421	.305	.763	.671	-.565	-.511
	93.450	-.119	-8.524	1.151	6.401	.063	-46.029	-8.514
	1401.745	-1.778	-127.862	17.268	96.017	.942	-690.441	-127.714
BULK	-.224	1.000	.013	-.294	-.191	-.320	.186	.175
	-.119	.003	.002	-.006	-.009	.000	.086	.017
	-1.778	.045	.023	-.094	-.136	-.003	1.291	.248
POROSITY	-.421	.013	1.000	.259	-.610	-.017	.633	.506
	-8.524	.002	4.389	.212	-1.111	.000	11.171	1.828
	-127.862	.023	65.834	3.179	-16.659	-.005	167.571	27.421
PAREA	.305	-.294	.259	1.000	.062	.582	-.383	-.338
	1.151	-.006	.212	.152	.021	.002	-1.259	-.227
	17.268	-.094	3.179	2.281	.314	.033	-18.880	-3.406
LPD	.763	-.191	-.610	.062	1.000	.316	-.673	-.596
	6.401	-.009	-1.111	.021	.754	.003	-4.922	-.893
	96.017	-.136	-16.659	.314	11.312	.040	-73.831	-13.388
SPD	.671	-.320	-.017	.582	.316	1.000	-.182	-.060
	.063	.000	.000	.002	.003	.000	-.015	-.001
	.942	-.003	-.005	.033	.040	.001	-.223	-.015
LPDPER	-.565	.186	.633	-.383	-.673	-.182	1.000	.933
	-46.029	.086	11.171	-1.259	-4.922	-.015	70.980	13.547
	-690.441	1.291	167.571	-18.880	-73.831	-.223	1064.693	203.206
LPSAPER	-.511	.175	.506	-.338	-.596	-.060	.933	1.000
	-8.514	.017	1.828	-.227	-.893	-.001	13.547	2.971
	-127.714	.248	27.421	-3.406	-13.388	-.015	203.206	44.572

Table B5.12 All Z series borehole regression statistics.

Correlation, Covariance, Cross-Product:

	ELEV	BULK	POROSITY	PAREA	LPD	SPD	LPDPER	LPSAPER
ELEV	1.000	-.238	-.277	.513	.679	.699	-.656	-.633
	72.463	-.133	-14.209	2.177	4.637	.111	-70.882	-10.346
	2463.740	-4.527	-483.108	74.023	157.666	3.780	-2410.00	-351.777
BULK	-.238	1.000	.023	-.371	-.263	-.378	.262	.201
	-.133	.004	.009	-.012	-.014	.000	.219	.025
	-4.527	.147	.312	-.413	-.470	-.016	7.435	.864
POROSITY	-.277	.023	1.000	-.061	-.288	-.176	.554	.303
	-14.209	.009	36.300	-.184	-1.394	-.020	42.364	3.502
	-483.108	.312	1234.203	-6.240	-47.380	-.675	1440.390	119.056
PAREA	.513	-.371	-.061	1.000	.243	.684	-.705	-.643
	2.177	-.012	-.184	.249	.097	.006	-4.460	-.616
	74.023	-.413	-6.240	8.450	3.306	.217	-151.653	-20.943
LPD	.679	-.263	-.288	.243	1.000	.317	-.473	-.529
	4.637	-.014	-1.394	.097	.644	.005	-4.824	-.815
	157.666	-.470	-47.380	3.306	21.900	.161	-164.008	-27.717
SPD	.699	-.378	-.176	.684	.317	1.000	-.688	-.548
	.111	.000	-.020	.006	.005	.000	-.163	-.020
	3.780	-.016	-.675	.217	.161	.012	-5.549	-.669
LPDPER	-.656	.262	.554	-.705	-.473	-.688	1.000	.890
	-70.882	.219	42.364	-4.460	-4.824	-.163	161.209	21.718
	-2410.00	7.435	1440.390	-151.653	-164.008	-5.549	5481.111	738.422
LPSAPER	-.633	.201	.303	-.643	-.529	-.548	.890	1.000
	-10.346	.025	3.502	-.616	-.815	-.020	21.718	3.691
	-351.777	.864	119.056	-20.943	-27.717	-.669	738.422	125.496

Table B5.13 All borehole data regression statistics.

Correlation, Covariance, Cross-Product:

	ELEV	BULK	POROSITY	PAREA	LPD	SPD	LPDPER	LPSAPER
ELEV	1.000	-.299	-.262	.268	.411	.472	-.628	-.635
	70.448	-.165	-8.446	5.067	3.200	.094	-78.564	-11.287
	7326.638	-17.209	-878.407	526.928	332.841	9.766	-8170.622	-1173.808
BULK	-.299	1.000	-.069	-.305	-.180	-.299	.389	.317
	-.165	.004	-.018	-.045	-.011	.000	.382	.044
	-17.209	.453	-1.822	-4.714	-1.145	-.049	39.762	4.604
POROSITY	-.262	-.069	1.000	.148	-.185	-.194	.273	.208
	-8.446	-.018	14.786	1.282	-.662	-.018	15.627	1.674
	-878.407	-1.822	1537.736	133.318	-68.851	-1.844	1625.165	174.131
PAREA	.268	-.305	.148	1.000	-.367	-.349	-.690	-.428
	5.067	-.045	1.282	5.061	-.767	-.019	-23.126	-2.039
	526.928	-4.714	133.318	526.385	-79.818	-1.934	-2405.064	-212.025
LPD	.411	-.180	-.185	-.367	1.000	.443	.105	-.178
	3.200	-.011	-.662	-.767	.862	.010	1.456	-.350
	332.841	-1.145	-68.851	-79.818	89.699	1.015	151.456	-36.401
SPD	.472	-.299	-.194	-.349	.443	1.000	-.198	-.318
	.094	.000	-.018	-.019	.010	.001	-.070	-.016
	9.766	-.049	-1.844	-1.934	1.015	.058	-7.289	-1.661
LPDPER	-.628	.389	.273	-.690	.105	-.198	1.000	.841
	-78.564	.382	15.627	-23.126	1.456	-.070	221.986	26.552
	-8170.622	39.762	1625.165	-2405.064	151.456	-7.289	23086.522	2761.448
LPSAPER	-.635	.317	.206	-.428	-.178	-.318	.841	1.000
	-11.287	.044	1.674	-2.039	-.350	-.016	26.552	4.486
	-1173.808	4.604	174.131	-212.025	-36.401	-1.661	2761.448	466.567

APPENDIX C

CALIBRATION RESULTS FROM PORESIZER

An explanation of calibration techniques and instrument performance is included in this appendix.

C.1 Poresizer Calibration

Over the course of this study, several penetrometers were used in the testing procedure. Each new penetrometer was inspected visually and by the poresizer before it was used for intrusion testing. Blank penetrometers were sealed, evacuated and filled with mercury to check manufacturer supplied penetrometer volumes.

Silica-alumina pellets were obtained from the manufacturer for instrument calibration purposes. The poresizer is checked after every 50 intrusion tests to ensure proper performance. Table C.1 shows the results of the latest test with those from the manufacturer. All parameters are within acceptable limits. The underestimation of pore area and over estimation of median pore diameter probably stems from the fact that intrusion pressures only reached 187 MPa instead of the listed 207 MPa.

TABLE C.1 Calibration results of Poresizer 9310 using silica-alumina pellets.

	MANUFACTURER	STUDY
TOTAL INTRUSION VOLUME (cm^3/gm)	0.33 ± .05	0.353
TOTAL PORE AREA (m^2/gm)	75 ± 10	61.2
MEDIAN PORE DIAMETER (VOLUME) (um)	0.03 ± .005	0.112
MEDIAN PORE DIAMETER (AREA) (um)	0.01 ± .002	0.009

C.2 Sample Variability

Because of the destructive nature of intrusion testing it is near impossible to retest the same sample. Samples from the same core location, only adjacent to each other, were tested for comparison and as

a variability indicator for the poresizer. Duplicate results were not expected nor obtained . Table C.2 shows results from a sample of densely welded tuff.

No significant differences between the two samples exist. This may be a function of the particular sample location more than it is a function of the poresizer. If it is assumed that the samples were "identical", then the poresizer variation is minimal and within the deviation suggested by the calibration pellets.

Nevertheless, poresizer variation should be considered during sample analysis but with a minimal degree of weighting.

TABLE C.2 Comparison of two densely welded tuff samples from the same location.

	ORIGINAL	"DUPLICATE"
TOTAL INTRUSION VOLUME (cm^3/gm)	.0363	.0375
TOTAL PORE AREA (m^2/gm)	5.630	5.204
MEDIAN PORE DIAMETER (VOLUME) (um)	.0353	.0474
MEDIAN PORE DIAMETER (AREA) (um)	.0156	.0159
BULK DENSITY (gm/cm^3)	2.356	2.314

REFERENCES

De Boer, J.H., The Shapes of Capillaries, in The Structure and properties of Porous Materials, ed., Everett, D.H., and F. S. Stone, Colston Research Society, Butterworths Scientific Publications, London, pp. 68 - 94, 1958.

Evans, D.D., Unsaturated Flow and Transport Through Fractured Rock Related to High-Level Waste Repositories, Progress Report to U.S. Nuclear Regulatory Commission, 1988.

Geomath, Variogram Computation Program, GAM3D and variogram plotting program, VPLOT2, Lakewood, Colorado, 1987.

Good, R.J., and R.Sh. Mikhail, The Contact Angle in Mercury Intrusion Porosimetry, Powder Technology, pp. 53 - 62, Vol. 29, 1981.

Hillel, D., Fundamentals of Soil Physics, Academic Press, New York, 1980.

Journel, A.G., and CH. J. Huijbregts, Mining Geostatistics, Academic Press, New York, 1978.

Joyner, L.G., Barrett, E.P. and R.J. Skold, The Determination of Pore Volume and Area Distributions in Porous Substances. II Comparison between Nitrogen Isotherm and Mercury Porosimeter Methods, J.Am. Chem. Soc. 73., 3155-58 July (1951).

Kim, Y.C., Geostatistics in Ore Reserve Estimation and Mine Planning, Course Notes, Department of Mining and Geological Engineering, University of Arizona, Tucson, Arizona, December 1982.

Kim, Y.C., Department of Mining and Geological Engineering, University of Arizona, Tucson, Arizona, personal communication, 1988.

Klar, E., Relations between Pore Characteristics and Compacting Properties of Copper Powders, in H.H. Hausner, ed., Perspectives in Powder Metallurgy, Vol. 6, 1971.

Klavetter, E.A., and R.R. Peters, An Evaluation of the Use of Mercury Porosimetry in Calculating Hydrologic Properties of Tuffs From Yucca Mountain, Nevada, SAND86-0286, Sandia National Laboratories, Albuquerque, NM, 1987.

Kloubek, J., Hysteresis in Porosimetry, Powder Technology, pp. 63 - 73, Vol. 29, 1981.

Kloubek, J., A New Method for the Investigation of Porous Structures using Mercury Porosimetry, Powder Technology, pp. 89 - 97, Vol. 29, 1981.

Matheron, G., The Intrinsic Random Functions and Their Applications, Adv. App. Prob., pp. 239-465, Vol. 5, 1973.

Micromeritics Instruction Manual for Poresizer 9310, June 1986.

Miller, I., and J.E. Freund, Probability and Statistics for Engineers, Prentice-Hall, Inc., Englewood Cliffs, New Jersey, 1977.

Modry, S., Svata M. and J. Van Brakel, Thematic Bibliography of Mercury Porosimetry, Powder Technology, pp. 13 - 43, Vol 29, 1981.

Moscou, L., and S. Lub, Practical Use of Mercury Porosimetry in the Study of Porous Solids, Powder Technology, pp. 45 - 52, Vol. 29, 1981.

Peterson, D.W., Dacitic Ash-Flow Sheet near Superior and Globe, Arizona, Stanford Univ., Stanford, California, Ph. D. thesis, 130 p.; U.S. Geological Survey open-file report, 130 p., April 3, 1961.

Peterson, D.W., Zoned Ash-Flow Sheet in the Region Around Superior, Arizona, in S. Titley, ed., Arizona Geological Society, Southern Arizona Guidebook, III, Tucson, Arizona, April 11-13, 1968.

Pickell, J.J., Swanson, B.F., and W.B. Hickman, Application of Air-Mercury and Oil-Air Capillary Pressure Data In the Study of Pore Structure and Fluid Distribution, Society of Petroleum Engineers Journal, pp. 55 - 61, Vol. 237, 1966.

Rahi, K. A., Hydraulic Conductivity Assessment for a Variably- Saturated Rock Matrix, University of Arizona, Tucson Arizona, Masters Thesis, Department of Hydrology and Water Resources, 1986.

Rasmussen, T. C. and D. D. Evans, Unsaturated Flow and Transport Through Fractured Rock - Related to High-Level Waste Repositories - Phase II, NUREG/CR-4655, U. S. Nuclear Regulatory Commission, pp. 475, 1986.

Ritter, H.L., and L.C. Drake, Pore-Size Distribution in Porous Materials: Pressure Porosimeter and Determinations of Complete Macropore-Size Distribution, Ind. Eng. Chem. Anal. Ed., 17, 782 (1945).

Rootare, H.M., and C.F. Prenzlow, Surface Areas from Mercury Porosimeter Measurements, The Journel of Physical Chemistry, Vol. 71, No. 8, July 1967.

Ternan, M., and O.M. Fuller, A Comparison of Methods Used to Measure Pore Size in Solids, The Canadian Journel of Chemical Engineering, Vol. 57, pp. 750 - 757, December, 1979.

Van Brakel, J., Modry, S., and M. Svata, Mercury Porosimetry: State of the Art, Powder Technology, pp. 1 - 12, Vol. 29, 1981.

Wardlaw, N.C., and R.P. Taylor, Mercury Capillary Pressure Curves and the Interpretation of Pore Structure and Capillary Behavior in Reservoir Rocks, Bulletin of Canadian Petroleum Geology, Vol. 24, No. 2, pp. 225 - 262, 1976.

Warrick, A.W., Myers, D.E., and D.R. Nielsen, Geostatistical Methods Applied to Soil Science, pp. 53 - 81, in Methods of Soil Analysis, Part I. Physical and Mineralogical Methods, Am. Soc. of Agronomy, Inc., Soil Science Society of America, Inc., Madison, WI., 1986.

Washburn, E.W., Note on a Method of Determining the Distribution of Pore Sizes in a Porous Material, National Academy of Science Proceedings, Vol. 7, p. 115, 1921.

Weber, D.S., Stable Isotopes of Authigenic Minerals in Variably Saturated Fracturated Tuff, University of Arizona, Tucson Arizona, Masters Thesis, Department of Hydrology and Water Resources, 1986.

Whittemore, O.J., Mercury Porosimetry of Ceramics, Powder Technology, pp. 167 - 175, Vol. 29, 1981.

Winslow, D.N., and C.W. Lovell, Measurements of Pore Size Distributions in Cements, Aggregates and Soils, Powder Technology, pp. 151 - 165, Vol. 29, 1981.

Yeh, T. C., Rasmussen, T. C. and D. D. Evans, Simulation of Liquid and Vapor Movement in Unsaturated Fractured Rock at the Apache Leap Tuff Site - Models and Strategies, NUREG/CR-5097, U. S. Nuclear Regulatory Commission, pp. 73, 1988.